Chem Soc Rev

REVIEW ARTICLE

View Article Online
View Journal | View Issue

Cite this: *Chem. Soc. Rev.*, 2018, 47, 8403

Surface organometallic chemistry in heterogeneous catalysis

Manoja K. Samantaray,[a] Eva Pump,[a] Anissa Bendjeriou-Sedjerari,[a] Valerio D'Elia,[b] Jérémie D. A. Pelletier,[a] Matteo Guidotti,[c] Rinaldo Psaro[c] and Jean-Marie Basset*[a]

The broad challenges of energy and environment have become a main focus of research efforts to develop more active and selective catalytic systems for key chemical transformations. Surface organometallic chemistry (SOMC) is an established concept, associated with specific tools, for the design, preparation and characterization of well-defined single-site catalysts. The objective is to enter a catalytic cycle through a presumed catalytic intermediate prepared from organometallic or coordination compounds to generate well defined surface organometallic fragments (SOMFs) or surface coordination fragments (SCFs). These notions are the basis of the "catalysis by design" strategy ("structure–activity" relationship) in which a better understanding of the mechanistic aspects of the catalytic process led to the improvement of catalyst performances. In this review the application of SOMC strategy for the design and preparation of catalysts for industrially relevant processes that are crucial to the energy and environment is discussed. In particular, the focus will be on the conversion of energy-related feedstocks, such as methane and higher alkanes that are primary products of the oil and gas industry, and of their product of combustion, CO_2, whose efficient capture and conversion is currently indicated as a top priority for the environment. Among the main topics related to energy and environment, catalytic oxidation is also considered as a key subject of this review.

Received 2nd May 2018

DOI: 10.1039/c8cs00356d

rsc.li/chem-soc-rev

[a] *King Abdullah University of Science and Technology (KAUST), KAUST Catalysis Center (KCC), Thuwal, 23955-6900, Saudi Arabia. E-mail: jeanmarie.basset@kaust.edu.sa*

[b] *Department of Materials Science and Engineering, School of Molecular Science and Engineering, Vidyasirimedhi Institute of Science and Technology, 21210, Payupnai, WangChan, Rayong, Thailand*

[c] *CNR – Institute of Molecular Sciences and Technologies, via Golgi 19, 20133 Milano, Italy*

1. Introduction

A new area of heterogeneous catalysis has been introduced in the past few decades under the name of surface organometallic chemistry (SOMC), which progressively opened the way to surface organometallic catalysis.[1] New catalytic reactions have

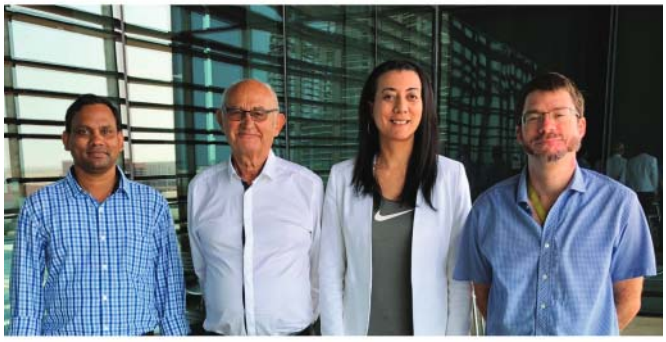

From left to right: Manoja K. Samantaray, Jean-Marie Basset, Anissa Bendjeriou-Sedjerari and Jérémie D. A. Pelletier

Professor Basset (middle) and his team at KAUST Catalysis Center (KCC, Saudi Arabia). He received his PhD in 1969 from the University of Lyon, France. He was funded by KCC for his work dedicated to catalysis by design. Dr Manoja Samantaray completed his PhD from IIT Bombay. In 2012 he moved to KCC as a research scientist following postdoctoral research at CPE Lyon. His research focuses on the design/synthesis of oxide supported well-defined single site catalysts for alkane metathesis. Jérémie D. A. Pelletier received his PhD in homogeneous catalysis in 2006 from the University of Leicester (UK). He is now the Laboratory Manager of KCC. His research focuses on SOMC (hydroaminalkylation, CO_2 valorization, etc.). Dr Anissa Bendjeriou-Sedjerari, Research Scientist at KCC, received her PhD in Materials Science from the University of Montpellier. She is strongly focused on the design of novel multifunctional materials, their advanced solid-state characterization and applications in heterogeneous catalysis.

been discovered (*e.g.* Ziegler Natta depolymerisation, alkane metathesis, non-oxidative coupling of methane to ethane and hydrogen, *etc.*)[2] or known ones have been considerably improved in terms of activity, selectivity or lifetime.[3] Its methods, based on grafting organometallic transition metals onto highly dehydroxylated metal-oxide supports handled under a strict controlled atmosphere, allow generation of catalytic sites that are in principle identical (single-site or single complex). This strategy presents considerable advantages over traditional techniques for the preparation of heterogeneous catalysts such as impregnation that lead to the formation of a variety of active sites. In this framework, the coordination sphere of the grafted metal can be opportunely designed with high certainty (well-defined catalytic site) because all preparative steps are carefully controlled with the concepts and tools of organometallic and/or coordination chemistry. Another advantage of this chemistry is that the surface is considered as a rigid ligand preventing, in most cases, undesired interplay between the catalytic sites (*e.g.* bimolecular deactivation).

The synthesis and grafting of "surface organometallic fragments" (SOMFs) or "surface coordination fragments" (SCFs) in which one or several fragments of reaction intermediates are linked to a surface-supported metal (*e.g.* M–H, M–R, M=CR_2, M≡CR, M=O, M=NR, M–O–OR) has enabled the strategy of "predictive catalysis" or "catalysis by design" by providing direct access into the "presumed catalytic cycle".[2] Such a "presumed cycle" is based on the concepts of molecular chemistry (organic, organometallic, coordination chemistry, biochemistry *etc.*) which explains quite well how bonds can be broken and reformed.[2] According to this strategy, the following remarks are considered as valid:

– During the various steps of a catalytic reaction of hydrocarbon molecules, SOMFs or SCFs convert into each other by bond cleavage and/or bond formation (if one excludes electron transfer reactions, acid-based catalysis);

– Each SOMF or SCF has a specific reactivity toward the substrates;

– The same surface metal atom can display one or more SOMF or SCF simultaneously;

Eva Pump

Eva Pump has been working at KAUST, Saudi Arabia, with Prof. Jean-Marie Basset since 2015. Her research focuses on surface organometallic chemistry (SOMC), more precisely on "Catalysis by Design". Her interests are related to the selective transformation of paraffins into higher valuable products through alkane metathesis and the elucidation of the mechanism. She received her PhD in 2014 at TU Graz (Austria) with Prof. Christian Slugovc studying olefin metathesis reactions.

Valerio D'Elia

Valerio D'Elia (from Avezzano, Italy) received his Master's degree in chemistry from the University of Perugia (2001). Following a period in pharmaceutical industry (Dompe, L Aquila), he received his PhD (2009) in organic chemistry from the University of Regensburg (Supervisor: O. Reiser). After postdoctoral research at LMU Munich (Supervisor: H. Zipse) he moved to Kaust Catalysis Center in Saudi Arabia as a research scientist in the group of J.-M. Basset. Since 2015 he has been a faculty member at the Vidyasirimedhi Institute of Science and Technology (VISTEC) in Thailand. His research interests include catalysis, CO_2 conversion and cyclic carbonate synthesis.

From left to right: Rinaldo Psaro and Matteo Guidotti

Dr Rinaldo PSARO, Director of CNR-ISTM (Milan, Italy) since 2008, was awarded the Federchimica prize (1990) and the Memorial Chini Lecture of the Italian Society of Chemistry (SCI, 2014). He served as a Coordinator of the Italian Group in Catalysis in 2006–2008 and 2012–2014 and as a Member of the Advisory Board of the International Association of Catalysis Societies in 2013–2017. He has co-authored 4 international patents and 220 papers in international journals focused on SOMC and nanostructured heterogeneous catalysts. Dr Matteo GUIDOTTI has been a Research Scientist at ISTM-CNR since 2001. He was a visiting researcher at the University of Poitiers, France (2003), Zaragoza, Spain (2010) and Delft, the Netherlands (2012). He has been a Fellow of the Academy of Sciences of the Institute of Bologna since 2013. He has co-authored 113 scientific publications and book chapters, 170 congress communications and 1 patent. He was awarded the Marotta Gold Medal Award, SCI, in 2017; Chiusoli Gold Medal Award, Industrial Chemistry Division, SCI, in 2014; and IX National Federchimica Prize in 1996.

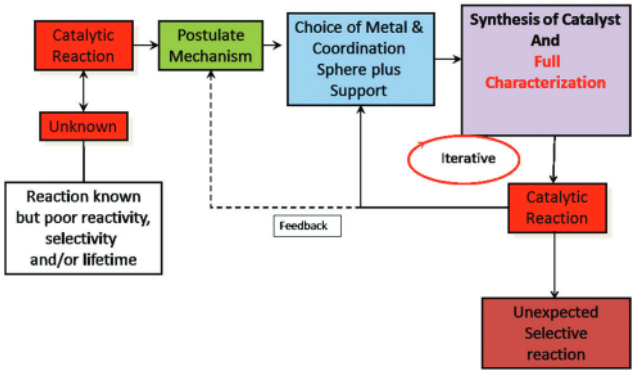

Scheme 1 Flowchart showing how the catalysis-by-design approach of SOMC can be applied to improve or discover catalytic reactions.

– The rules (structure and reactivity) of molecular chemistry can be applied easily to these fragments, although the surface brings additional properties.

According to these hypotheses, the concepts and elementary steps of molecular chemistry textbooks can be transposed to surfaces and employed to "reinvent" and/or rationalize heterogeneous catalysis. This model does not take into account reaction parameters specific to surfaces that should also be considered (chemical: redox, acid–base; physical: semi-conductive, porosity, hydrophilicity, hydrophobicity *etc.*). A simple method to improve existing or discover new catalytic reactions by the SOMC approach is given in Scheme 1.

Once a catalyst is prepared as a single-site (*e.g.* all sites are mostly identical and isolated from each other), its coordination sphere can be fully characterized by combining modern techniques: surface microanalysis, *in situ* IR, UV, and solid-state (SS) NMR spectroscopy,[4–7] DNP-SENS (dynamic nuclear polarization-surface enhanced NMR spectroscopy)[8] and several X-ray absorption-based technique such as *ex situ* or *in operando* XAS (X-ray absorption spectroscopy), EXAFS (extended X-ray absorption fine structure) and XANES (X-ray absorption near edge structure).[9–11] This means that all ligands coordinated to the metal and all atoms in its close proximity can be identified. The fact that each site is identical makes its characterization easier. Recent advances demonstrate that the best tools to characterize SOMFs are SS NMR,[12–15] DNP-SENS[16–19] and EXAFS.[20–23] Establishing a relationship between the structure and activity becomes then possible by knowing the structure of the SOMF or SCF.

In parallel to the latest advances in SOMC, the younger field of single atom catalysis (SAC), in which isolated single atoms are often dispersed on metal oxide supports,[24–29] is gaining momentum in heterogeneous catalysis.[30–33] The concept at the base of SAC is that the progressive decrease of the metal nanoparticle size toward the limit of the single atom leads to an increase of the so-called metal dispersion, activity and selectivity. It should be recognized that, whereas SAC is generally applied with noble metal atoms,[31] and SOMC is mostly concerned with early transition metals, in both cases, the active site consists of a "single metal atom". Yet, in SOMC, the metal atoms are coordinated by "ligands" that are specifically selected for the targeted reaction. In SAC the metallic atoms must adopt, with the reagents, the right coordination sphere to achieve the required reaction,[34,35] and the "spectator ligands" (oxo, halogen, N-heterocyclic carbene, amido, imido, nitrido, *etc.*), which are often crucial to tune the metal centre in SOMC, are lacking.[14,36,37]

Besides the nature of the metal centre, the outcome of catalytic reactions depends mostly on the SOMF structure. Each catalytic reaction requires a certain combination of the metal and ligands to achieve the desired reactivity. For example, metal hydrides are necessary for C–H bond activation as well as chain walking, whereas a metal carbene is essential for olefin metathesis.[21,38] Without them, these reactions may not proceed effectively even if some SOMFs can be regarded as precursors of other catalytically active species (*e.g.* a metal alkyl or a metal carbyne may be the precursor of a metal hydride).

Compared to focused[11,39–41] and comprehensive reviews[42] on SOMC and well-defined heterogeneous catalysts published in recent years, in this work the discovery of catalysts for reactions that are relevant to energy and environment is discussed with the main focus on the SOMF structure and design. Typical examples of SOMFs and of the catalytic reactions associated with some of these fragments are given in Scheme 2.

In this context, the first part of the review will be dedicated to C–H activation for the valorisation of alkanes by SOMC. Light alkanes contained in natural gas are key feedstock for energy generation and chemical industry and, at the same time, main sources of environmental concerns; their valorisation is regarded as a crucial topic for energy and environment.[43,44] Non-oxidative coupling of methane and alkane metathesis are key reactions in SOMC-based functionalization of alkanes and will be discussed in detail. To note, the (oxidative and non-oxidative) dehydrogenation of alkanes to olefins by SOMC-synthesized catalysts has become an emerging area of research in very recent years.[3,45–47] This field will likely be mature for review in the near future and will not be discussed here in detail. In the second part of the review, the focus will be on different transformations that are also crucial for energy and environment. Obviously, the activation and conversion of CO_2, the product of combustion of alkanes (flaring, energy production) and the main player in anthropogenic global warming, will be discussed as carried out using recently reported SOMC catalysts. Finally, emphasis will be given to the oxidation of hydrocarbons. Oxidation chemistry poses long-standing environmental challenges related to the use of hazardous and stoichiometric reagents, poorly selective catalysts and the generation of toxic wastes as highlighted by several authors.[48–52] Therefore, the progress in oxidation chemistry by well-defined catalysts will be discussed.

The most interesting aspect of SOMC in the context of catalysis is that the various steps of the catalytic cycle of well-defined systems allow rationalizing the deactivation, increasing activity and/or selectivity by modification of the support or ligand environment of the active site. The gap existing between heterogeneous and homogeneous catalysis can be bridged by a

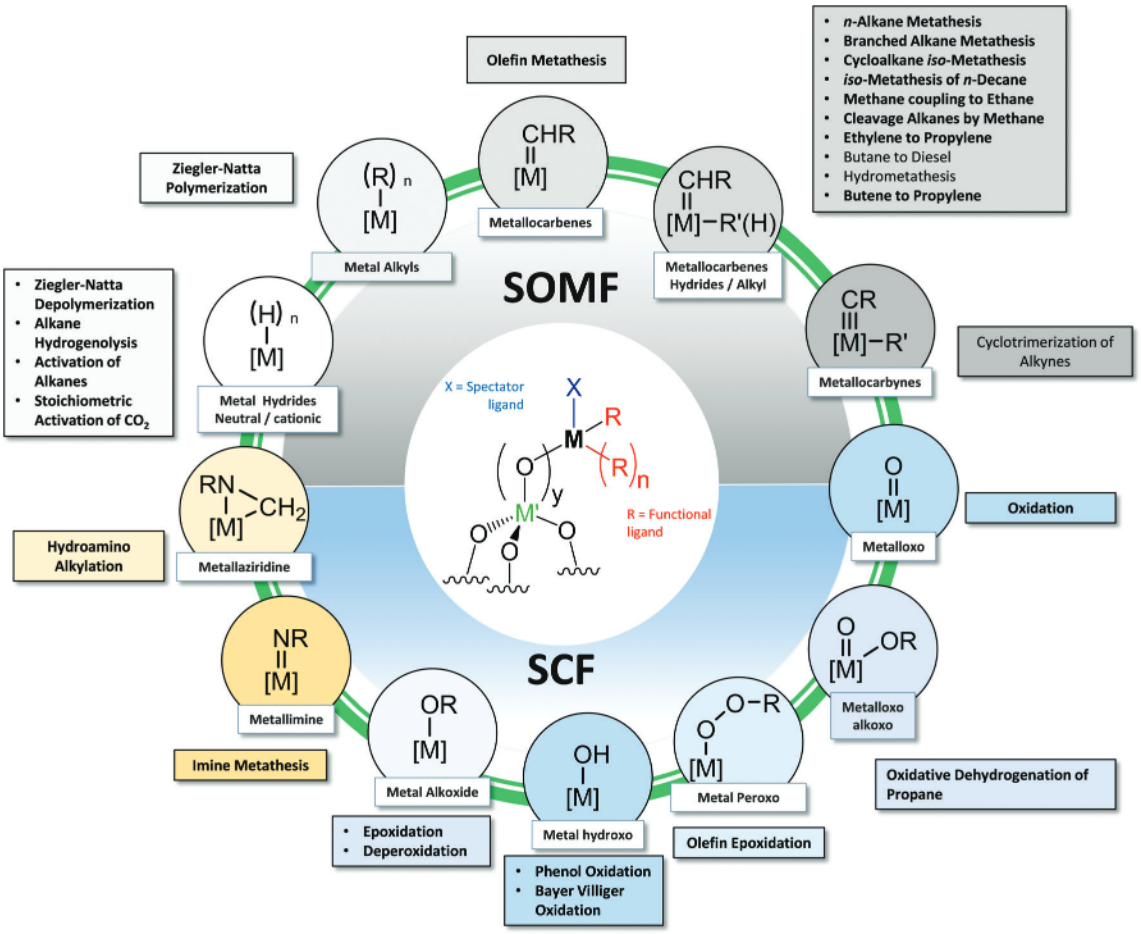

Scheme 2 Surface organometallic fragments (SOMFs) or surface coordination fragments (SCFs) and the corresponding catalytic reactions in which one fragment is part of the presumed catalytic mechanism.

methodology such as SOMC that uses a molecular approach to heterogeneous catalysis.

2. C–H bond activation by SOMC

The transformations of hydrocarbon to valuable products remain a challenge to the scientific community.[44,53] The primary reason is that C–C and C–H bonds are very unreactive towards most of the organometallic complexes because of their high bond dissociation energy (85 to 100 kcal mol^{-1}). The first C–H bond activation was reported by Joseph Chatt.[54] Since then, much effort has been made to understand and to expand this field by studying C–H bond activation of aromatics and alkanes.[55–58] Over the years, it has been discovered that particularly early transition metal hydrides are suitable candidates for the activation of alkanes at lower temperature. Nevertheless metal carbynes can also be considered as pre-catalysts for C–H bond activation because they react with alkanes to give M(alkyl)(carbene) which upon β-H elimination results in carbine hydrides which are efficient for alkane activation.[59] Herein, the synthesis and application of well-defined single-site oxide supported catalysts (as metal hydrides, metal alkyls, and metal carbene hydrides) for activation of alkanes are discussed.

2.1. Low-temperature catalytic hydrogenolysis of alkanes and polyolefins [M]–H, with M = Ti, Zr, Hf, Ta, W

In the following text, [M] refers to a transition metal linked to an oxide surface by one, two or three covalent bonds.

The first well-defined surface complex used in low temperature catalytic hydrogenolysis of alkanes was $[(\equiv SiO\text{-})_3ZrNp_3]$ (Np: neopentyl).[25] The single-site complex was prepared by the reaction of $ZrNp_4$ with dehydroxylated silica at 500 °C ($SiO_{2\text{-}500}$) and was fully characterized by SS NMR, IR and mass balance analysis.

During the hydrogenolysis of $[(\equiv Si\text{-}O\text{-})ZrNp_3]$, gaseous ethane and methane were produced in place of the expected neopentane. This discovery improved the understanding of the catalytic mechanism of the hydrogenolysis of hydrocarbons. Catalytic hydrogenolysis of the C–C bonds of alkanes[60,61] and even polyethylene and other polyolefins[62] to a mixture of methane and ethane was later reported. The first [Zr]–hydride was synthesized by hydrogen treatment at 150 °C of the well-defined $[(\equiv SiO\text{-})ZrNp_3]$, to obtain $[(\equiv Si\text{-}O\text{-})_{(4-x)}Zr(H)_x]$ (x = 1 or 2). Thanks to advances in solid-state NMR

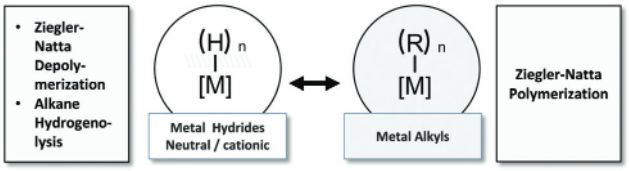

Fig. 1 Illustration of SOMFs for low-temperature catalytic hydrogenolysis of alkanes and polyolefins.

spectroscopy, two types of [Zr]–hydrides were identified after hydrogenolysis: (i) zirconium monohydride [(≡Si-O-)$_3$ZrH], **6** (70–80%) and (ii) zirconium bis-hydride [(≡Si-O-)$_2$ZrH$_2$], **8** (20–30%).[63]

It was understood that the hydrides of d^0 metal complexes may be very useful for exploring the catalytic activity of metal–neopentyl complexes as metal–hydrides are known to activate the alkane C–H bond effectively (Fig. 1).[64] Group IV metal hydrides cleave neopentane into ethane and methane, but do not cleave ethane. While [(≡SiO)$_{(4-x)}$Zr(H)$_x$] (x = 1 or 2) and [(≡SiO)$_{(4-x)}$Hf(H)$_x$] (x = 1 or 2) produce a 3 : 1 ratio of methane to ethane, in the case of [(≡SiO)$_{(4-x)}$Ti(H)$_x$] (x = 1 or 2) the observed ratio was 1 : 1.

High electron deficiency of the metal center is the key parameter to reach the required catalytic properties in alkane chemistry. The use of early transition metals as well as lanthanides with a d^0 configuration was proposed from molecular chemistry to lead to high efficiency in the hydrogenolysis of alkanes.[60]

The mechanism of such C–H bond activation is expected to occur through σ-bond metathesis with four center intermediates, as earlier proposed in homogeneous catalysis.[59,66,67] This indicates that the elementary steps on surface organometallic fragments should be similar or identical to those of molecular chemistry.

Using Ti–hydride as a catalyst precursor, the initial product distribution (propane to ethane 1 : 1) provides a clear understanding about the skeletal rearrangement of the surface neo-pentyl to the surface iso-pentyl fragment prior to product formation.[68] This field of catalytic hydrogenolysis is not only restricted to group IV metal hydrides, but also extends to group V [Ta]–H and VI [W]–H hydrides (Scheme 3).[65]

Tantalum–hydrides[69] catalyze the hydrogenolysis of acyclic alkanes such as propane, butane, iso-butane, and neopentane. [Ta]–H$_x$ can further cleave ethane, which was not possible with group IV metal–hydrides. For example, with [Ta]–H$_x$, propane is completely transformed into methane by successive C–C cleavage, unlike [Zr]–H$_x$[63] and [Hf]–H$_x$[70] (*vide supra*) (Scheme 4). All these studies outlined a simple picture for the elementary steps of C–C bond cleavage. In the case of group IV metal hydrides, the cleavage of the C–C bond occurs by a β-alkyl transfer leading to an olefin and a metal alkyl, while with [Ta] (group V) the cleavage occurs by a de-insertion mechanism[71] (Scheme 5).

Conversely, in the case of the tantalum hydride(s), [(≡SiO-)$_2$Ta(H)$_x$], which cleaves ethane, another mechanism

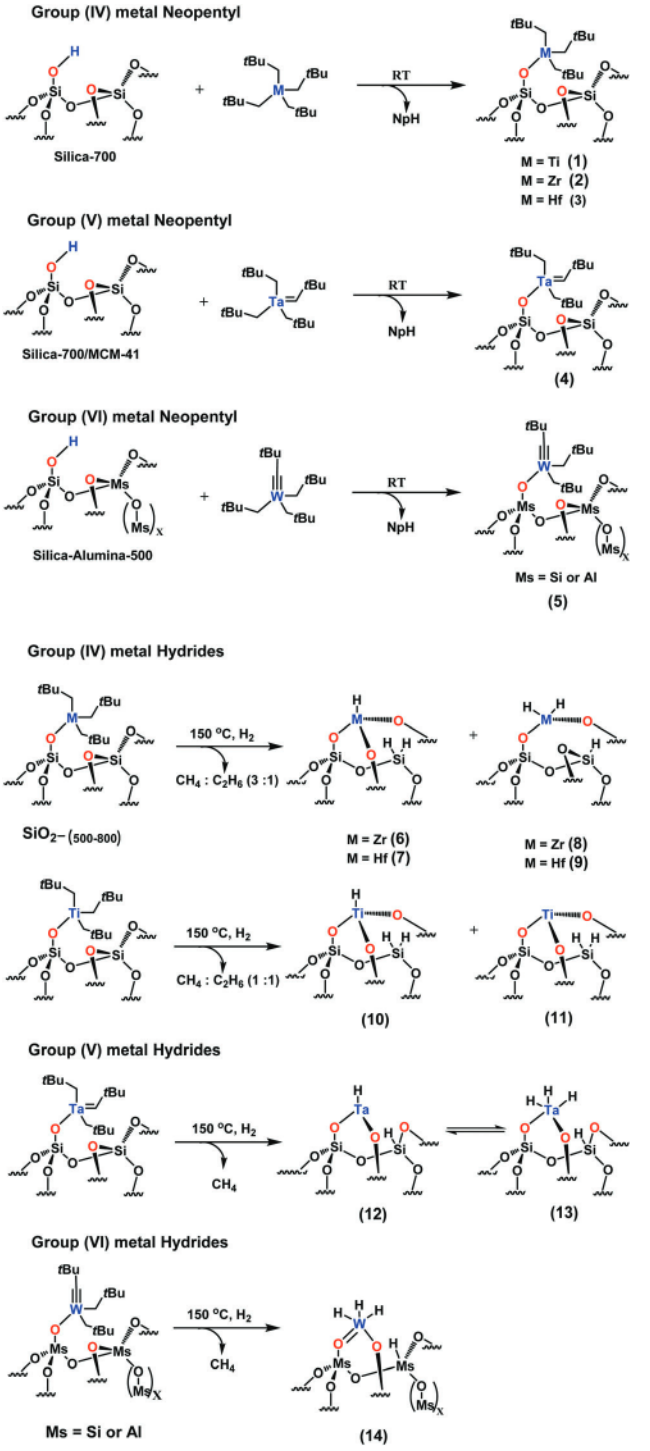

Scheme 3 Synthesis of group IV, V and VI neopentyl fragments and their hydride homologues used for low temperature hydrogenolysis of alkanes or polyolefins.[65]

must occur involving only one carbon atom at a time (Scheme 5). Among various reasonable possibilities, a [Ta]-methylidene de-insertion from a tantalum-ethyl species was assumed because the reverse step is known in organometallic chemistry.[72] Note that this reverse step has been postulated as the key step in Fischer–Tropsch synthesis.[73]

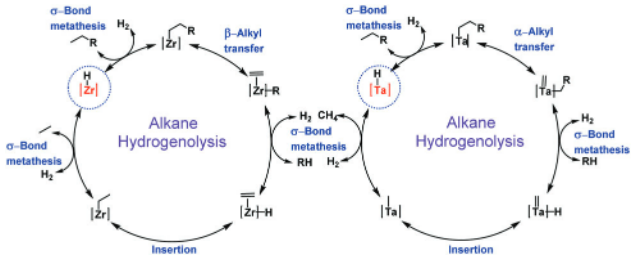

Scheme 4 Proposed mechanism for hydrogenolysis of alkanes, waxes and polyolefin by d^0 [Zr]–H_x (β-alkyl transfer) and by d^0 [Ta]–H_x (α-alkyl transfer). Note that a β-alkyl transfer is the reverse process of an olefin insertion into a metal–carbene bond (Scheme 5), which explains quite well the phenomenon of ethylene polymerization and polyethylene depolymerization on [Zr]–H.[62] In the case of ethane, this mechanism cannot occur since the resulting metal–ethyl intermediate does not possess any alkyl group in the β-position.[65]

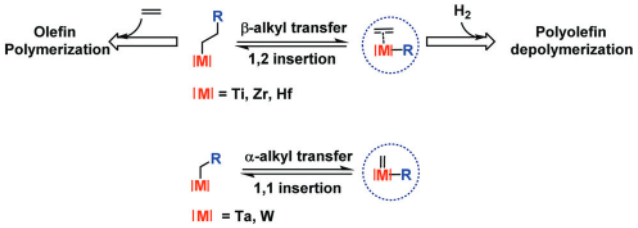

Scheme 5 β-Alkyl transfer and α alkyl transfer mechanisms are shown with group IV, group V and group V metal alkyl.[62,65]

2.2. Stoichiometric activation of C–H bonds by silica supported metal–hydrides [M]–H, with M = Zr, Ta

The transfer of the mechanistic concept of molecular organometallic chemistry to surface organometallic chemistry can only be achieved if the elementary steps are similar in both cases. This can only be possible if these elementary steps can be studied stepwise on SOMC. To study the elementary steps sequentially stoichiometric activation of reagents on the catalyst is necessary.

The SOMF [M]–H (Fig. 2) was first observed by reproducing stepwise the alkane hydrogenolysis.[60] This fragment has been shown to be the only one to activate alkane (until the recent discovery of C–H bond activation on [M]≡CR.[74–77] Nevertheless, metal–carbynes can also be considered as a pre-catalyst because they react with alkanes to give [M]-alkyl-carbenes which upon β-H elimination result in [M]-carbene-hydrides which is efficient for alkane activation). The first example of [M]–H was identified with the isolation of silica supported zirconium hydride.[60,61]

The silica-supported Zr(IV) mono-hydride **6** and bis-hydride **8**, obtained after controlled hydrogenolysis of [(≡SiO-)$ZrNp_3$]

Fig. 2 Illustration of SOMFs for C–H bond activation.

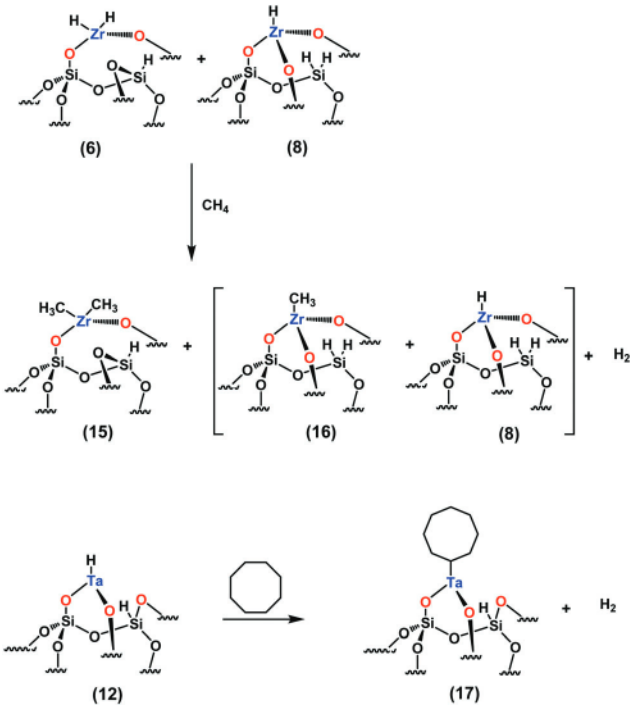

Scheme 6 Stoichiometric activation of methane and cyclooctane with hydride species 6, 8 and 12.[84]

(see the previous section), are well-known catalysts for hydrogen/deuterium exchange in saturated hydrocarbons,[78,79] olefin polymerization[80,81] as well as alkane or polyolefin hydrogenolysis.[62,82] The different reactivities of [(≡SiO-)$_3$Zr-H] **6** and [(≡SiO-)$_2$ZrH_2] **8** towards methane (to generate methylated zirconium, Scheme 6)[83,84] were investigated by *in situ* IR spectroscopy and solid-state ^{1}H and ^{13}C NMR spectroscopy using ^{13}C isotopically labeled methane. The bis-hydride [(≡SiO-)$_2$ZrH_2] **8** was identified by ^{1}H SS NMR and it was found to activate methane quantitatively at moderate temperature (150 °C) whereas the same reaction with the mono-hydride remains incomplete even after 48 hours in a batch reactor (Scheme 6).

The ^{1}H MAS NMR spectra of the reaction of [(≡SiO-)$_{(4-x)}$-Zr(H)$_x$] (x = 1 or 2) with methane showed a partial disappearance of the resonance of [(≡SiO-)$_3$ZrH] [δ(ZrH) = 10 ppm] whereas that of [(≡SiO)$_2$ZrH_2] [δ(ZrH_2) = 12 ppm] completely disappeared.[82,84] No other changes were observed as compared to the NMR spectra of the starting material. The different reactivities of both zirconium hydrides for methane incorporation were corroborated by *in situ* IR.

Similarly, when cycloalkane reacted with [Ta]–H at room temperature the evolution of one mole of hydrogen was observed, hence confirming a stoichiometric and not a catalytic reaction of cycloalkane with [Ta]–H at room temperature. The evolution of hydrogen is due to σ-bond metathesis which is already observed for group IV metal hydrides.[85,86]

2.3. Methane catalysis

Most commercial processes convert methane through an indirect route, for example, methane to syngas followed by its

transformation into hydrocarbons, alcohols, light olefins or gasoline.[87–89] Alternatively, methane can be directly converted through oxidative or non-oxidative routes. In the direct oxidative route,[90–92] methane is transformed into ethylene and water (thermodynamically favorable);[93] however, hydrocarbons are readily oxidized to form CO, CO_2 and water. Labinger has shown for the direct oxidative coupling of methane[94–96] there is an inherent limit for ethylene yield at around 30% due to the gas phase free radical reaction initiated on the surface.[92] Therefore, the selectivity of this process decreases dramatically, even at a high conversion of methane. In the direct non-oxidative coupling of methane, light alkanes and alkenes, aromatics, coke and the respective amount of hydrogen can be produced from methane. The thermodynamics towards ethane and ethylene are less favorable compared to the oxidative route,[94] yet no CO and CO_2 are generated.

2.3.1. Non-oxidative coupling of methane to ethane and hydrogen. The non-oxidative coupling of methane to ethane and hydrogen *via* SOMC was discovered in 2008,[96] using a silica supported single-site [Ta]–H catalyst. Methane can be converted over [Ta]–H in a continuous flow reactor (250 to 450 °C, 50 bar of CH_4 pressure) to hydrogen and ethane (selectivity ≥98%) with traces of other hydrocarbons (propane and ethylene) (TON = 40, 147 h, 475 °C, 50 bar).

This reaction was also tested using silica–alumina and alumina supported [W]–H systems.[97] Only ethane, traces of propane and hydrogen were observed, but no olefins. [W]–H catalysts are significantly more stable (up to 10 days with a constant conversion maintaining the high selectivity for ethane) than their [Ta]–H counterparts.

To understand the reaction mechanism, reaction intermediates of [Ta]–H and [W]–H were characterized by spectroscopic methods (IR, SS NMR) after $^{13}CH_4$ activation (150 °C for 24 h). For both metals, IR studies show a strong decrease of the ν(M–H) bands after bringing the [M]–H catalysts into contact with CH_4. ^{13}C CP MAS NM spectra show four distinct resonances corresponding to Si–CH_3, [M]–CH_3, [M]=CH_2 and [M]≡CH for both systems.[96,97]

Solid state characterization suggests that [Ta]–H and [W]–H follow a similar reaction mechanism which includes the aforementioned SOMFs (Fig. 3) [M]–hydride, [M]–CH_3, [M]=CH_2 and [M]≡CH. The proposed mechanism is shown in Scheme 7.

The initial elementary step is the activation of methane by [M]–H forming [M]–CH_3 and H_2 *via* σ-bond metathesis (i). [M](=CH_2)(H) is then generated by α-H transfer (ii). [M]≡CH is formed by further α-H abstraction followed by evolution of H_2 (iii). Another methane molecule reacts with the carbyne to form

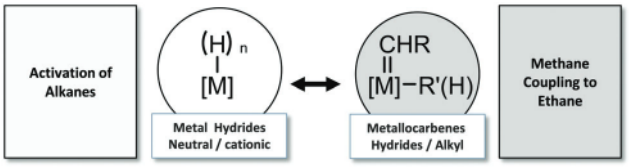

Fig. 3 Illustration of SOMFs for methane catalysis.

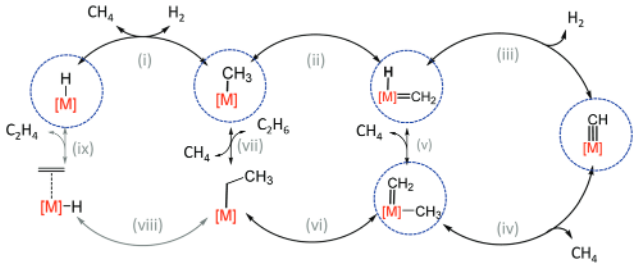

Scheme 7 A detailed mechanism of coupling of methane to ethane, ethylene and hydrogen using single site [M]–H catalysts. The structures in the blue circles have been characterized by spectroscopic methods.[98]

[M](=CH_2)(CH_3) (iv). This SOMF can be formed directly by activation of methane with [M](=CH_2)(H) (v). An insertion of the methylidene into the M–methyl bond leads to the formation of [M](-CH_2-CH_3) (vi). Ethane is then released by σ-bond metathesis with another molecule of methane (vii). For [Ta]–H, β-H elimination also occurs (viii), followed by the release of ethylene and [Ta]–H (ix).

The ageing of the catalyst is demonstrated by NMR: the Si–Me observed at −10 ppm is obtained by the transfer of one methyl of [M]–CH_3 to the adjacent silicon by opening a Si–O–Si bond (Scheme 8). This is a general mechanism that has been frequently observed on surfaces not only with hydrides, but also with methyl groups. The oxygen of the support reacts with [M], which is then deactivated as it becomes unable to produce the active site which should contain a methylidene and a hydride [M](=CH_2)(H).

2.3.2. Non-oxidative coupling of methane to ethane and hydrogen. The most efficient systems for the non-oxidative aromatization of methane are bifunctional Mo/ZSM-5 based on the pioneer work of Wang *et al.*[99] and the single-site iron catalyst Fe^{II} SiO_2 based on the work of Guo *et al.*[100] which are discussed in more detail below.

Bifunctional catalysts (Mo/ZSM5). Typical systems[94,99,101–104] are based on transition metals on zeolites according to the pioneer work of Wang *et al.* using Mo/ZSM5.[99] From a thermodynamic point of view, at around 730 °C and 1 bar pressure, a conversion of 15% of CH_4 is expected with high selectivity for benzene and naphthalene.[105] In reality, similar methane conversions of 15% can be reached.[106] However, the selectivity towards aromatics is much lower because of the concomitant coke formation which, consequently, leads to the deactivation of the catalyst with time on stream.[107]

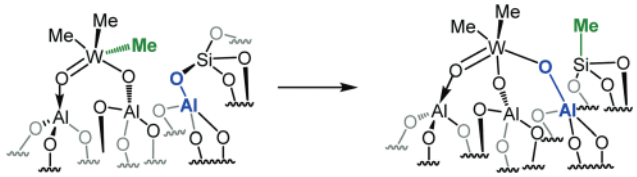

Scheme 8 A possible way for the ageing and deactivation of the catalyst on alumina after prolonged exposure to the reactant at 150 °C through the reaction of the metal with the oxygen atom of the framework.

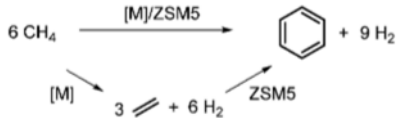

Scheme 9 Illustration of steps of non-oxidative aromatization of methane on bifunctional catalysts (formation of coke is not explained here).

Improving the understanding of the mechanism of non-oxidative coupling of methane might benefit the development of catalysts for methane dehydro-aromatization under non-oxidative conditions. A mechanism based on a bicomponent catalytic system (Scheme 9) has been proposed:[101,108,109] (I) the non-oxidative coupling of methane to ethane and ethylene over transition metals and (II) the oligomerization, cyclization and aromatization on Brønsted acidic sites of the zeolite; step I is the rate determining step in this reaction.

Molybdenum was found to be reduced to molybdenum carbide (Mo_2C_x (x = 1, 2, 3, 4, 6)[110] or MoO_xC_y)[107] nanoparticles which are produced during the activation phase.[111] This species first activates methane[112] to ethylene and hydrogen (we suspect that this occurs by non-oxidative coupling of methane to ethane followed by dehydrogenation of ethane to ethylene, which becomes more favorable at high temperature). The real structure of the molybdenum carbidic species has not yet been resolved, but the activation of methane has been postulated by DFT calculation using various models, such as $Mo_2(CH_2)_5^{2+}$, $Mo_2(CH_2)_4^{2+}$ and $Mo(CH_2)_2(CH_3)^+$.[111] Controlling the non-oxidative coupling of methane, *e.g.* with the help of SOMC, might be the key to improve the catalytic activity of methane dehydrogenative aromatization.

Once ethylene is formed, the Brønsted acidic sites of the zeolite become relevant for further transformations (Scheme 9).[108,113,114] A detailed mechanism has been proposed by DFT calculations[108] in which the chemisorbed light alkenes undergo acid-catalyzed chain growth within the zeolite channels (oligomerization). Once the olefinic cyclohexyl carbenium, $C_6H_{11}^+$, is formed, cyclization into a cyclic carbenium ion is assumed to occur prior to undergoing a series of desorption and protolysis steps to form an adsorbed cyclic unsaturated species which is converted instantaneously into benzene. Similarly, toluene, xylene, naphthalene, and other polyaromatics are formed in these aromatization steps.

Single-site Fer SiO_2. Single-site iron sites lattice-confined in nonacidic silica (Fer SiO_2)[100,115,116] were developed to optimize the performance of highly dispersed Fe cations on ZSM5,[117–120] which are active in MDA, however, with severe coke deposition induced on the Brønsted acidic sites of the zeolite. Guo *et al.*[100] reported that non-acidic silica as the support with "embedded" single-iron sites (Fig. 4) can activate methane and avoid intensive coke deposition.

Catalysis was performed at high working temperatures (≥950 °C). At 1090 °C (WHSV = 21 400 mL g_{cat}^{-1} h^{-1}), the reaction reached a maximum conversion of 48%. The selectivity towards hydrocarbons exceeded 99%, the selectivity for ethylene peaked at 48%, for benzene at ~ 20–30% and for naphthalene at ~ 25–30%. No deactivation of the catalyst was observed for 60 h of reaction time. The stability of the system has encouraged focusing on designing a single-site metal catalyst for conversion of methane into aromatics, which was verified by HAADF-STEM and XANES. The difficulty in avoiding carbon formation is related to an "ensemble" of atoms which favor the formation of graphite. It is well known that the formation of graphite, carbon nanotubes, graphenes, *etc.* involves a wide range of Fe-nanoparticles with exposed specific planes.[121]

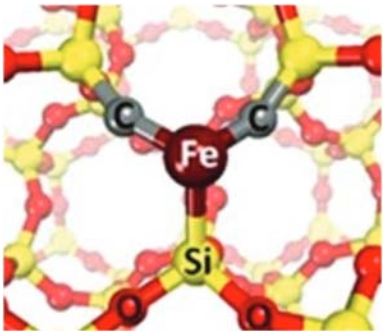

Fig. 4 A single site iron catalyst for methane activation is represented here. Reprinted with permission from ref. 100, Copyright 2014 American Association for the Advancement of Science.

A free radical mechanism is postulated to occur at >1000 °C in the gas phase generating $CH_3^\bullet$ radicals on the iron sites, which is followed by product formation in the gas phase.[100]

2.4. Metathesis of alkanes

In this section, we focus on metathesis of alkanes (light alkanes, branched alkanes, heavy alkanes, and cycloalkanes) through SOMC. Alkane metathesis represents a powerful tool which could be applied in various fields of chemistry and petrochemistry. Alkane metathesis might afford a solution for processing of fuels such as crude oil and natural gas; it also can lead from natural gas to ethane by non-oxidative coupling and then to liquid hydrocarbons by metathesis.[122]

Alkane metathesis is described by the following general equation:

$$2C_nH_{2n+2} \rightleftharpoons C_{n-i}H_{2(n-i)+2} + C_{n+i}H_{2(n+i)+2}$$

where i = 1, 2, .. n − 1; with i = 1, 2 favoured for n ≥ 4.

Consequently, this reaction was identified as a process where an alkyl fragment of one alkane molecule is transferred to another one. The methyl group is the smallest alkyl fragment and the easiest to be transferred. Also, ethyl and propyl groups can be transferred as known from cross-metathesis of olefins. Indeed, heavier alkanes result either (i) from successive reactions or (ii) from a heavier alkyl group transfer.

In 1968 Heckelsberg and Banks reported an unprecedented dual functional catalyst based on tungsten oxide on silica and chromia-alumina that could transform propane to heavier olefins and paraffins at 600 °C.[123] Along with the main product propylene, various cracking products were observed, which was understood to be due to high temperature. In 1973, Burnett and

Hughes reported a dual functional catalytic system for molecular redistribution of alkanes at lower temperature (E 400 °C), known at that time as "disproportionation of alkane".[124] In 1997, Basset *et al.* reported a single-site silica supported [Ta]–H catalyst which could perform an alkane disproportionation reaction at 150 °C under 1 atm.[86] This new reaction was named "alkane metathesis" due to its similarity with olefins metathesis.

2.4.1. 1st generation of catalysts [M]–H, with M: Ta, W. The first generation catalysts correspond to hydrides of [W] and [Ta] prepared from their metal neopentyl fragments. Tantalum hydride is the first well-defined surface organometallic catalyst used for alkane metathesis reactions. This Ta hydride is a precursor of the real coordination sphere of a single site [M](=CHR)(H) (*vide infra)* (Fig. 5 and 6). The surface complex, [(≡Si-O-)$_2$TaH], was synthesized by the reaction of [(≡Si-O-)$_x$Ta(=CHC^{t}Bu)(CH$_2$C^{t}Bu)$_{3-x}$] (x = 1 or 2) with hydrogen at 150 °C for 15 hours followed by a plateau of 200 °C for 2 hours.[125] The parent surface tantalum neopentyl complex was synthesized by the reaction of [Ta(=CHC^{t}Bu)(CH$_2$C^{t}Bu)$_3$] with silica dehydroxylated at 500 °C ($SiO_{2\text{-}500}$) (Scheme 10). It is worth noting that the reaction between $SiO_{2\text{-}500}$ and the tantalum precursor [Ta(=CHC^{t}Bu)(CH$_2$C^{t}Bu)$_3$] produces a mixture of monopodal (65%) and bipodal (35%) tantalum surface complexes. This is in sharp contrast to group IV metal precursors like Zr(Np)$_4$ and Ti(Np)$_4$ which are known to form exclusively monopodal surface complexes with $SiO_{2\text{-}500}$.[61,68] In contrast, Hf(Np)$_4$ follows the same pattern as [Ta] on $SiO_{2\text{-}500}$ generating a mixture of monopodal and bipodal species.[126]

The reaction of surface silanol with [Ta(=CHC^{t}Bu)(CH$_2$C^{t}Bu)$_3$] proceeds through the addition of [Si–OH] into the tantalum carbene bond (with formation of a monopodal tetra-neopentyl and a bipodal tantalum tris-neopentyl) (Scheme 10). The monopodal tetraneopentyl and the bipodal tris neopentyl undergo rearrangement by α-hydrogen transfer with formation of a neopentylidene followed by elimination of neo-pentane. This leads to the formation of one Ta–carbene ligand per tantalum center (Scheme 10). This observation was clearly demonstrated by using deuterated silanol as the silica source.[127]

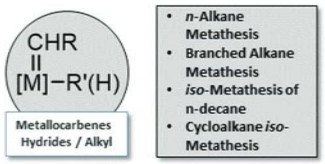

Fig. 5 Illustration of SOMFs for alkane metathesis.

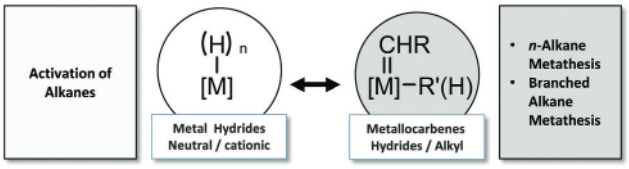

Fig. 6 Illustration of 1st generation SOMFs for alkane metathesis.

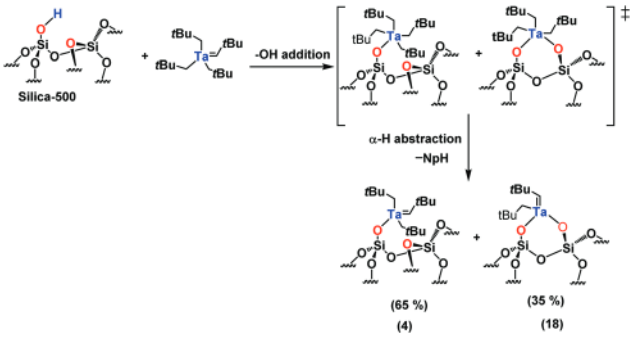

Scheme 10 The reactivity of [Ta(=CHC^{t}Bu)(CH$_2$C^{t}Bu)$_3$] towards $SiO_{2\text{-}500}$ which leads to a mixture of mono and bipodal complexes **4** and **18** is shown.[127]

Propane metathesis. Kinetic studies of propane metathesis were carried out using a continuous flow reactor. When [Ta]–H was brought into contact with propane, [Ta]–*n*-propyl and [Ta]–iso-propyl are formed by σ-bond metathesis with evolution of hydrogen. Subsequently, [Ta]–*n*-propylidene hydride or [Ta]–iso-propylidene hydride is formed by α-H abstraction. In parallel, propene is formed by β-H elimination from [Ta]–*n*-propyl or [Ta]–iso-propyl. Once the olefin is formed, it can coordinate to [Ta]=CRH, **19** or **20** in two different ways (*syn* or *anti*) resulting in four different metallacyclobutanes having methyl or ethyl in the 1,2 or 1,3 position (**21**, **22**, **23**, **24**) (Scheme 11). To avoid steric constraints, the most favorable metallacyclobutane has the substituent at the 1,3 position (conformer **21**, **23**) rather than the 1,2 position (conformer **22**, **24**).[128] Upon cycloreversion and subsequent reduction, methane, ethane, butane (*n*-butane, iso-butane) and pentane (*n*-pentane, iso-pentane) are formed.

It was observed that (i) the formation of butanes (*n*-butane, iso-butane) C(n + 1) is higher than the formation of pentanes (*n*-pentane, iso-pentane) C(n + 2). Similarly the formation of ethane C(n − 1) is higher as compared to methane C(n − 2) when n o 4 (ii). Furthermore, it was also observed that linear products are favored over branched products.[75] To understand the reaction mechanism, the flow rate in the continuous flow reactor was varied from 1 mL min^{-1} to 100 mL min^{-1}. At low contact time, the formation of hydrogen and olefin increases and the formation of alkane decreases. This confirms that the initial products of alkane metathesis are olefins and hydrogen. Subsequently, the newly generated olefins participate in olefin metathesis and new alkanes are formed after reduction with hydrogen. Based on the product distribution of alkanes and taking into account their selectivities, a mechanism was proposed for propane metathesis (Scheme 11).

Both the proposed reaction mechanism and the obtained product selectivities indicate that olefin metathesis is part of alkane metathesis.[129] To increase the reactivity in alkane metathesis reactions, the focus shifted from group V, [Ta], to group VI metals, specifically [W], as tungsten catalysts are well known for their improved performances for the olefin metathesis reaction over their tantalum counterparts.[130] During the reaction it was observed that [(≡Si-O-)W(≡C^{t}Bu)(CH$_2$^{t}Bu)$_2$] was not active

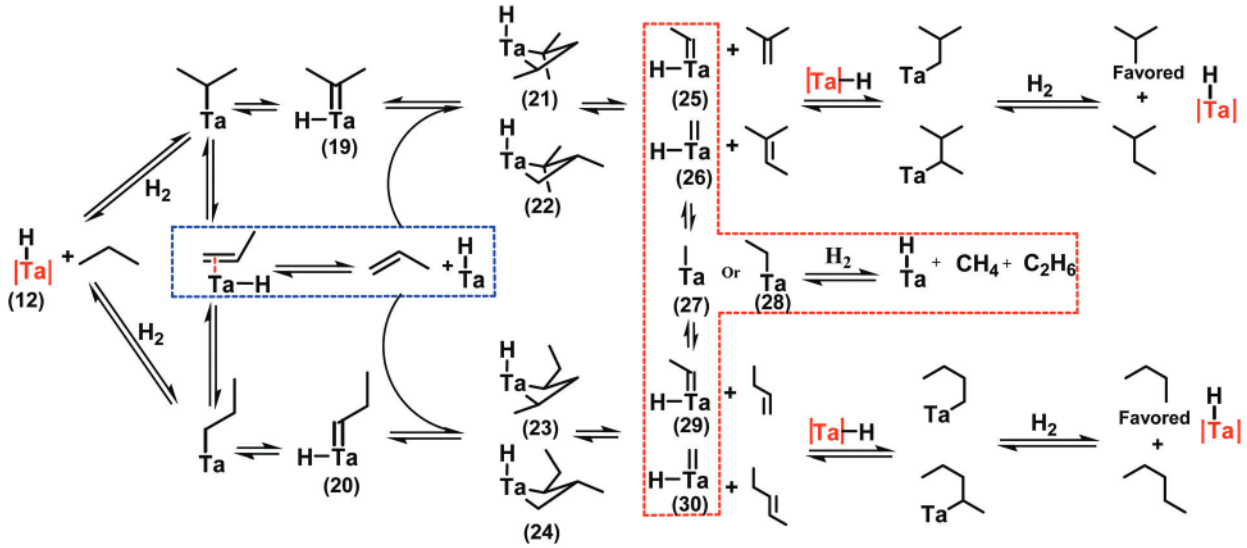

Scheme 11 Detailed pathway showing the formation of the metathesis products from propane using [Ta]–H as the catalyst precursor.[75]

in the alkane metathesis reaction whereas on silica–alumina [(≡Si-O-)$_{SiO_2\text{-}Al_2O_3}$W(≡C^{t}Bu)(CH$_2$^{t}Bu)$_2$] and on alumina supported [(Al$_S$-O-)W(≡C^{t}Bu)(CH$_2$^{t}Bu)$_2$] catalysts a TON of approximately 30 was achieved. The corresponding tungsten hydrides are much closer to the coordination sphere, which is necessary for the alkane metathesis reaction, than the carbyne alkyl. These [W]–hydrides, as catalyst **14**, were prepared and tested in the propane metathesis reaction reaching a TON of 129 (Fig. 7).

Mechanistic investigation in alkane metathesis clearly indicated that a metal carbene hydride is the active species influencing the reaction rate as well as the TON. To form a metal carbene hydride on the surface, the focus was shifted from the synthesis of metal neo-pentyl complexes to well-defined metal methyl of the active metals (W, Ta), which opens up the door for "2nd generation catalysts" in alkane metathesis reactions.

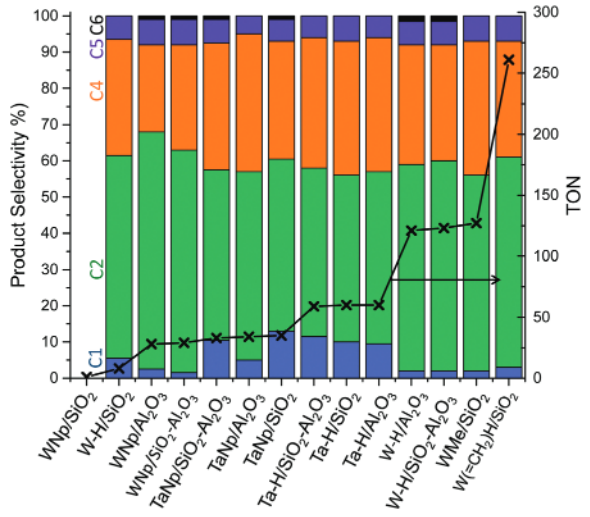

Fig. 7 Product distribution observed in propane metathesis with various supported metal carbene/carbyne and hydride catalysts. Note: WNp corresponds to [W](≡C^{t}Bu)(CH$_2$^{t}Bu)$_2$; TaNp corresponds to [Ta](≡C^{t}Bu)(CH$_2$^{t}Bu)$_2$; WMe corresponds to [–WMe$_5$] and W(=CH$_2$)H corresponds to [–W(CH$_2$)H$_3$].

2.5. Development of the 2nd generation catalysts

The first generation catalysts, neopentyl complexes and their corresponding hydrides, reached a maximum TON of 130 in propane metathesis. To increase the reactivity, the focus was laid on the synthesis of metal methyl complexes. The belief was that the generation of a metal carbene hydride from a metal methyl would be comparatively easy. The silica supported [(≡Si-O-)WMe$_5$] and [(≡Si-O-)TaMe$_3$] catalysts were prepared by the reaction of silica (Aerosil-200) dehydroxylated at 700 °C ($SiO_{2\text{-}700}$) and the corresponding molecular counterpart WMe$_6$ and TaMe$_4$ at −50 °C to −30 °C to obtain a golden yellow [(≡Si-O-)WMe$_5$][131] and a light grey colored [(≡Si-O-)TaMe$_3$][98] (Scheme 12). These compounds were fully characterized by SS NMR, IR, elemental analysis, and gas quantification methods and proved to be monopodal on $SiO_{2\text{-}700}$. These compounds are thermally stable at room temperature. Upon thermal exposure for a specific time period, complexes **31** and **34** transform into a mixture of monopodal and bipodal (i) metal carbyne in the case of [(≡Si-O-)WMe$_5$] and (ii) metal carbene in the case of [(≡Si-O-)TaMe$_4$] (Fig. 8). The [Ta]–carbene and [W]–carbyne species are fully characterized by SS NMR.

The primary goal was to design metal carbene hydride/carbene methyl on the surface to enhance the reactivity in alkane metathesis reactions.

In the case of [(≡Si-O-)WMe$_5$] the catalytic cycle can be entered *via* two separate paths: (i) [W]–carbene–hydride and (ii) [W(≡CH)Me]. (i) A [W]–carbene–hydride is formed after controlled hydrogenolysis treating [(≡Si-O-)WMe$_5$] with H$_2$ starting at −78 °C followed by a stepwise warming up to 150 °C (Scheme 13). The modification of the catalyst was monitored by FT-IR at various temperatures: −78 °C, room temperature and 150 °C.

The hydrogenolysis reaction at −78 °C gives a strong, sharp band at 1959 cm^{-1} corresponding to ν(W–H) stretching bands. With increasing temperature, the intensity of the sharp band at

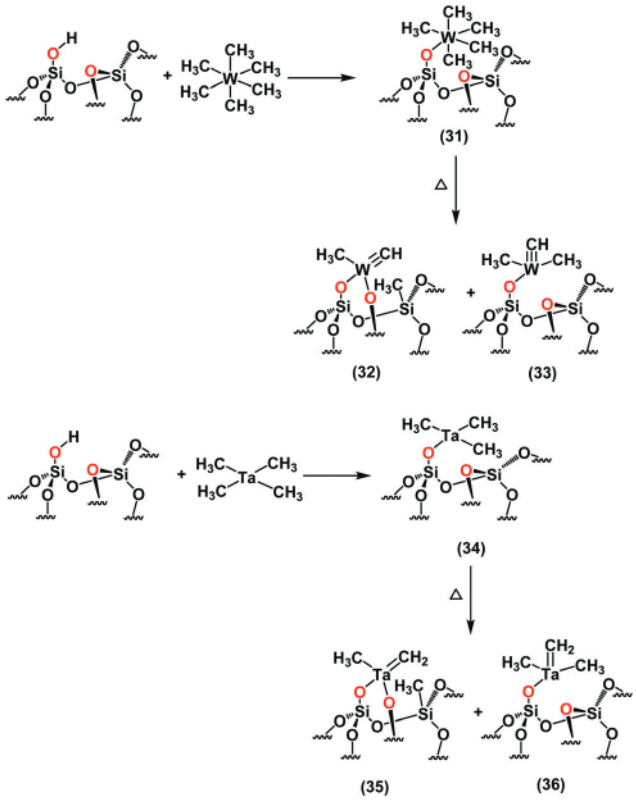

Scheme 12 General procedure for the synthesis of silica supported [(≡Si-O-)W(CH$_3$)$_5$][131] and [(≡Si-O-)Ta(CH$_3$)$_3$][98] and their corresponding carbyne and carbene complexes upon subsequent thermal treatment.

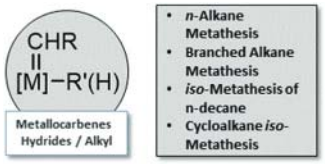

Fig. 8 Illustration of second generation SOMFs for alkane metathesis.

1959 cm^{-1} decreases and a new band at 1978 cm^{-1} is detected corresponding to another ν(W–H) vibration. The SS NMR of the hydrogenolysis product at −78 °C confirms the presence of a [W]–carbene–hydride with characteristic peaks at 231 ppm for carbene ^{13}C NMR and a [W]–H peak at 15 ppm in ^{1}H NMR.[132] Furthermore, DFT studies confirm [(≡Si-O-)W(H$_3$)(=CH$_2$)] to be the most stable species resulting after the hydrogenolysis of [(≡Si-O-)WMe$_5$]. For the first time, a coordination sphere that incorporates both functionalities, a [W]–carbene–hydride, was observed (Scheme 13). This [W]–carbene–hydride complex [(≡Si-O-)W(H$_3$)(=CH$_2$)] was tested in the propane metathesis reaction achieving a TON of 261 while with [(≡Si-O-)WMe$_5$], the TON was 130 (Fig. 7). (ii) A [W(≡CH)Me], which is formed after thermal treatment from [(≡Si-O-)WMe$_5$] activates alkanes through σ-bond metathesis with the metal methyl groups. After bringing [W(≡CH)Me] into contact with olefins, which are generated after β-H elimination, a [W]-bis-carbene might be formed, which can then undergo the olefin metathesis step.

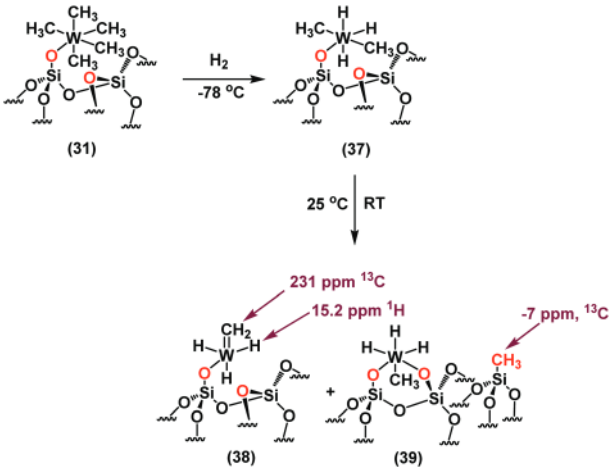

Scheme 13 Formation of [W]–carbene/hydride [(≡Si-O-)WH$_3$(=CH$_2$)] from [(≡Si-O-)W(Me)$_5$] with hydrogen at −78 °C.[132]

Indeed, by SS NMR it was found that upon the addition of cyclohexene, the [W]-carbyne methyl species [W(≡CH)Me] is in equilibrium with a bis-carbene [W(=CH$_2$)$_2$Me].[133] A more detailed mechanism is provided in the following paragraph.

In the case of [(≡Si-O-)TaMe$_4$] the elementary steps of ethane metathesis were considered starting from [Ta](=CH$_2$)Me (which is formed from [(≡Si-O-)TaMe$_4$])[98] (Scheme 14). The first step is a σ-bond metathesis between ethane and [Ta]–methyl generating a tantalum carbene ethyl which undergoes α-H abstraction leading to a [Ta] methyl ethylidene (evidenced by NMR spectroscopy). This clearly shows that alkane metathesis can be performed by a [Ta]–alkyl–carbene. All the other steps have been explained earlier.

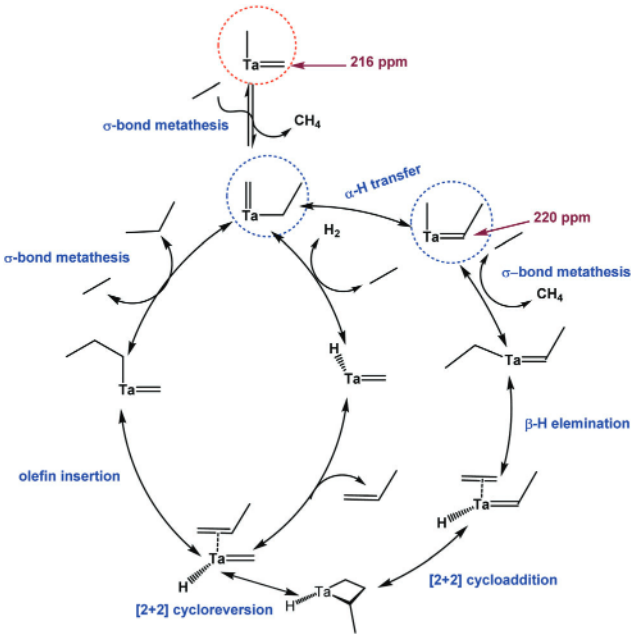

Scheme 14 Possible mechanistic steps of ethane metathesis using [(≡Si-O-)TaMe$_4$] as the catalyst precursor. Intermediates characterized (by SS NMR) are surrounded with a red or blue circle.[98]

2.5.1. Higher alkane iso-metathesis $C_n > C_5$. Higher alkane iso-metathesis is directly derived from alkane metathesis. Typical alkane metathesis is carried out with gaseous low molecular weight alkanes in fixed-bed reactors. With high molecular weight alkanes, which are liquid at low temperature (low saturation pressure), the reactions are carried out in a batch reactor. Using the same catalyst precursor [(≡Si-O-)W(CH_3)$_5$] a TON of 150 was found, together with a much higher proportion of lower alkane in the batch reactor using *n*-decane as the reactant.[134] The explanations are simple: (i) when the alkane is liquid, its concentration in a batch reactor is higher (contact time of catalyst to reactant) and (ii) C–H bonds are more abundant in the molecule and its rate of metathesis increased. For example, butane metathesis gives liquid products up to C_7, C_8, while *n*-decane metathesis gives a great variety of alkanes ranging from C_2 to C_{33} (Fig. 9) instead of C_{18} and ethane. This broad range of alkanes can be only observed if there is a sequential (i) isomerization of the alkenes resulting from the alkane. It occurs by insertion of the olefin into the metal hydride, then double bond migration takes place by β-H elimination. (ii) This is followed by olefin metathesis and (iii) reduction of the newly formed olefins to new alkanes or newly formed olefins undergo stepwise double bond migration which further broadens the product distribution as compared to the low molecular weight alkane metathesis reaction (Scheme 15 and Fig. 9).

Hence, a new term has been introduced to describe this phenomenon, alkane "iso-metathesis"[135,136] (Scheme 15 and Fig. 9), which was further generalized to a great variety of paraffins and to a great variety of catalysts (Scheme 16).

In *n*-decane metathesis using [(≡Si-O-)WMe_5], a TON of around 150 was reached.[134] To improve the reactivity of this SOMF, the support was changed from conventional silica to silica–alumina, a more acidic support.[138] WMe_6 was grafted on silica–alumina (dehydroxylated at 500 °C) to form a mixture of mono- and bipodal complexes, while on silica (dehydroxylated at 700 °C) a monopodal complex is exclusively formed. The bipodal complex originates from the migration of a [W]–methyl to the alumina center (Scheme 17). To generate [W]–carbyne species the sample was heated to 120 °C for 12 hours resulting

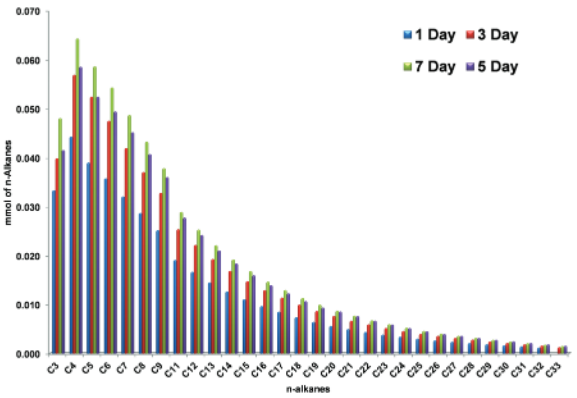

Fig. 9 Distribution of n-alkanes observed during the metathesis on n-decane using catalyst precursor [(≡Si-O-)W$(Me)_5$]. Reprinted with permission from ref. 134, Copyright 2015 John Wiley and Sons.

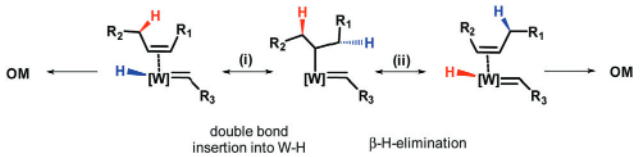

Scheme 15 Schematic representation of double bond migration as a combination of double bond insertion and β-H elimination.

in the formation of two sets of [W]–carbyne species: (i) one comes from the neutral [W] center and (ii) the other comes from the cationic [W] center (Scheme 17). The formation of the cationic [W]-species suggests that a methyl group from the W center was abstracted by an adjacent Al-center resulting in a Al–Me and a cationic W (Scheme 17). The *n*-decane metathesis reaction attained a TON of 350 using this complex.[134]

2.5.2. Metathesis of cyclic alkanes. Metathesis of cycloalkanes follows a similar mechanistic sequence to that of the metathesis of linear alkanes. It leads to their corresponding lower and higher homologues, *viz.* dehydrogenation to olefin, olefin metathesis and hydrogenation of the metathesized olefins. Using cycloalkanes as feedstock (primary class of compounds found in petroleum products) offers a valuable access to the synthesis of a broad range of saturated macrocycles which are important building blocks for pharmaceutical intermediates (*i.e.* macrolides), fragrance (*i.e.* musk) and as a biomarker for b. Braunii (biotechnology).[139,140]

After the synthesis of the well-defined precursor [(≡Si-O-)WMe_5] and its successful use in propane[131] and *n*-decane metathesis,[134] [(≡Si-O-)WMe_5] was tested for the metathesis of cyclic alkanes, using cyclooctane as the benchmark.[133] A maximum TON of around 450 was found after 190 hours using [(≡Si-O-)WMe_5]; only cycloalkanes were observed without olefins and polymeric products. The overall selectivity is limited to macrocyclic alkanes of carbon numbers cC_{12}–cC_{40} and ring contracted products (cC_5–cC_7). By contrast, homogeneous tandem systems have displayed a good selectivity for products with a carbon number of a multiple of 8, yet generating significant amounts of oligomers and polymers which is very different from our single site system.

The activation mechanism has been proposed by DFT calculations, rationalizing all elementary steps of alkane metathesis: (i) CH-bond activation of cyclo-octane followed by β-H elimination forming an olefin, (ii) olefin metathesis and (iii) hydrogenation of the new olefin.

The broad distribution range of resulting cycloalkanes using [(≡Si-O-)WMe_5] is due to the competition of olefin metathesis *vs.* double bond migration (DBM) (Scheme 18) as expected from a multifunctional catalyst.[74] Theoretical calculations have shown that DBM is favored under the applied reaction conditions. Therefore, mainly ring contracted products, such as cC_7, cC_6 and cC_5 (having beneficial ring strain), are observed when using [(≡Si-O-)WMe_5] on silica nanoparticles.

To improve the selectivity for cyclooctane metathesis, a new strategy was adopted to take advantage of confinement effects.[74] Instead of conventional spherical silica nanoparticles ($d_{particle}$ = 15 nm), mesoporous silicas with various pore diameters

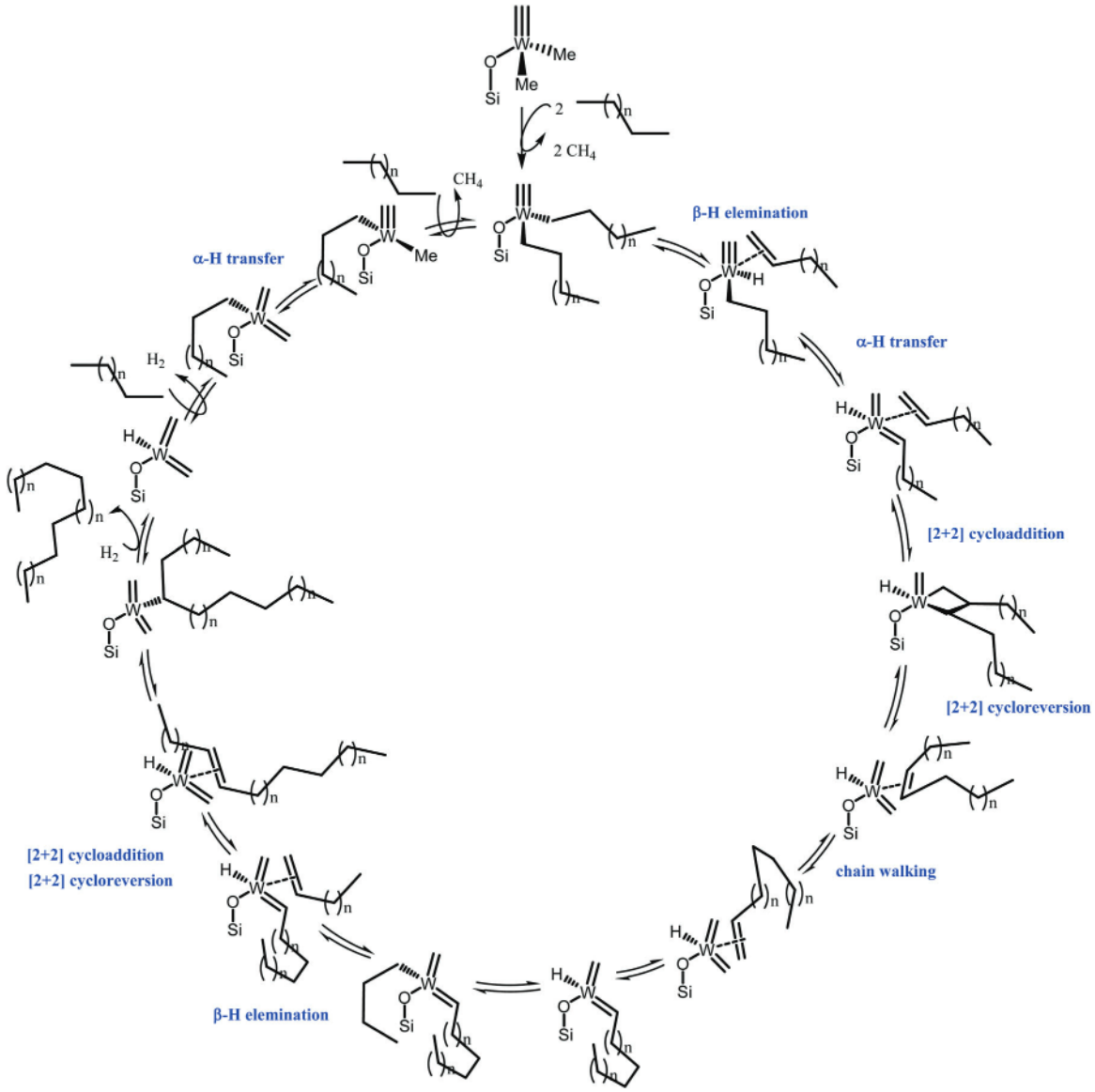

Scheme 16 General schematic representation of how isomerization of olefin occurs during the metathesis of alkanes using the [(≡Si-O-)W(≡CH)$(CH_3)_2$] catalyst precursor.[137]

[SBA15 (d_{pore} = 6.0 nm) and MCM41 (d_{pore} = 3.0 and 2.5 nm)] were used as grafting support. Deep solid state characterizations such as TEM, N_2 sorption and DNP-SENS confirmed the occurrence of the catalytic reaction inside the channel of the mesoporous silica support. Catalytic tests of cyclooctane metathesis showed clear correlations: (i) of improving selectivity toward the macrocyclic cC_{16} with decreasing pore size and (ii) of getting high selectivity for ring contracted products for large pore size. To understand this counterintuitive behavior, the pore size effect was investigated using detailed computational analyses (Sterimol parameter, effective volume). Calculations found that double bond migration is reduced using small pore sizes because intermediates and transition states are bulkier (transition state shape selectivity). In large pores, sizes significantly improve the TON due to better site accessibility.[141]

2.6. 3rd generation: invention of bi-metallic catalysts for better performance in alkane metathesis reactions

With the development of [(≡Si-O-)WMe_5], the most efficient catalyst for alkane metathesis reactions was discovered. This catalyst led to a TON of up to 260 for propane metathesis and even higher for *n*-decane metathesis (TON = 350) and cyclooctane metathesis (TON = 450).[132–134] Studying the elementary steps of alkane metathesis, C–H bond activation was understood to be the rate determining step.[74] With increasing concentration of olefins, the rate of the reaction, as well as its productivity and its lifetime, should increase as well. In the first attempt $Zr(Np)_4$ was introduced together with WMe_6 on silica to form a well-defined bi-metallic catalyst [(≡Si-O-)$W(CH_3)_5$/(≡Si-O-)$Zr(Np)_3$] on surface (Scheme 19).[142] By association with group IV metals which were found to activate the C–H

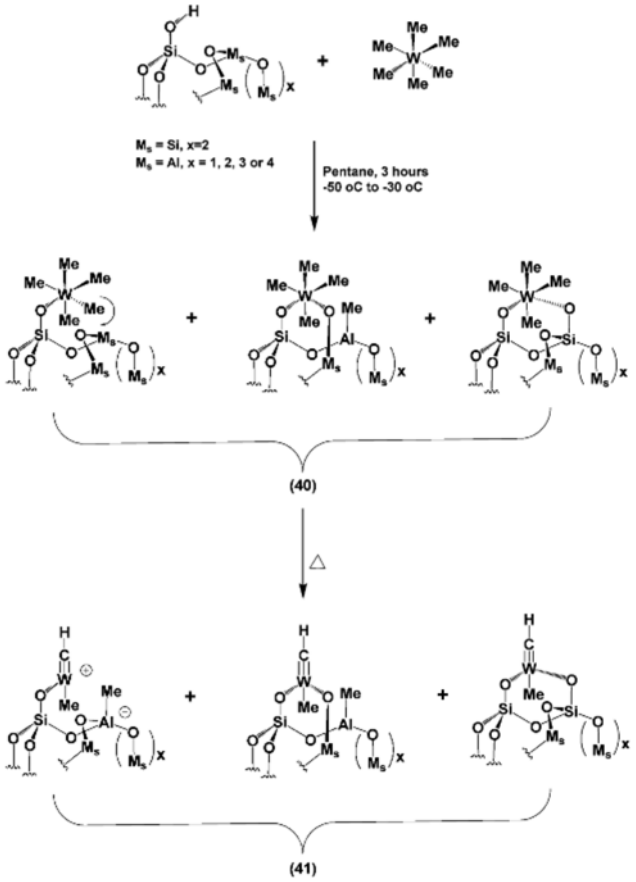

Scheme 17 Schematic representation showing the evolution of [W]–Me to [W]≡CH on silica–alumina.

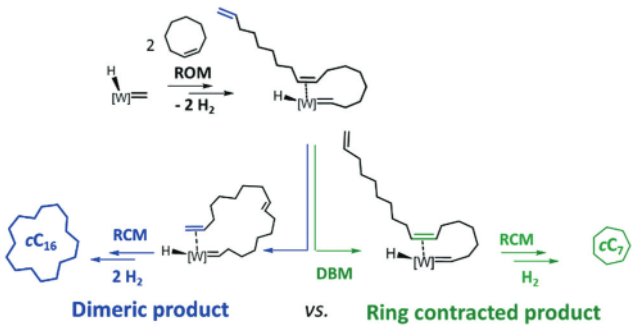

Scheme 18 Illustration of the formation of a broad product distribution (dimeric product vs. ring contracted product) in cyclooctane metathesis using [(≡Si-O-)WMe_5] as the pre-catalyst; ROM = ring opening metathesis, RCM = ring closing metathesis, DBM = double bond migration.[74]

bond of paraffin and produce olefin by β-H elimination with the original [W]-catalyst, the concentration of the olefin and its resulting metathesis rate could be increased. A new method was developed to synthesize bimetallic systems (Fig. 10) on surfaces keeping [W] intact and additionally introducing group IV metals. The reason was the following: as explained in the first section of this article, metals of group IV are very good candidates to activate C–H bonds of paraffins.

The sample was characterized by SS NMR spectroscopy (^{1}H, ^{13}C and HETCOR) (Fig. 11). Additionally, the NMR double-quantum (DQ) and triple quantum (TQ) study showed strong autocorrelation peaks for W–CH_3 groups and [Zr] neo-pentyl groups which confirms the grafting of WMe_6 and $Zr(Np)_4$ without rearrangement of their coordination sphere. Along with the expected original autocorrelation peaks, another cross-correlation peak (observed outside the diagonal) corresponds to the methyl peak of [Zr]–(CH_2–$C(CH_3)_3$) and that of [W]–CH_3 thus confirming that [W]–CH_3 and [Zr]–($CH_2C(CH_3)_3$) are in close vicinity to each other (Fig. 11). The hydrides were prepared by hydrogen treatment of [(≡Si-O-)$W(CH_3)_5$/(≡Si-O-)$Zr(Np)_3$] at room temperature for 15 hours or by heating at 100 °C with hydrogen for 12 hours.

This catalyst proved to be very efficient in alkane metathesis reactions with a TON of 1436 for the *n*-decane metathesis reaction. To further improve the reactivity of bimetallic systems, [Ti] was introduced in place of [Zr] as Ti is better than Zr for hydrogenolysis of alkanes.[65] It is known that hydrogenolysis begins by C–H bond activation, a common step between dehydrogenation and hydrogenolysis. A new, well-defined bi-metallic silica supported catalyst was prepared using [Ti] as the dehydrogenating source and [W] as the metathesis catalyst [(≡Si-O-)WMe_5/(≡Si-O-)$TiNp_3$] (Scheme 19). In the [W]/[Ti] bi-metallic catalyst, a similar SS NMR spectrum to that of [W]/[Zr] was observed, indicating that also [W]–CH_3 and [Ti]–($CH_2C(CH_3)_3$) are close by. The bimetallic system [(≡Si-O-)WMe_5/(≡Si-O-)$TiNp_3$] tested for the propane metathesis reaction in a continuous flow reactor resulted in the highest TON (10 000) obtained to date for any SOMC catalyst (Fig. 12).[143]

To understand the synergistic effect between both [W] and [Ti] catalysts, three catalytic beds were prepared. (i) One contained the bimetallic [W]/[Ti] system, (ii) the second one contained a layer of [(≡Si-O-)$W(CH_3)_5$] and [(≡Si-O-)$Ti(Np)_3$] separated by a layer of glass wool and (iii) the third one was a physical mixture of both [{(≡Si-O-)WMe_5} + {(≡Si-O-)$TiNp_3$}]. In all cases, the metal loading of the metathesis catalyst was kept constant. Comparing the results of all three combinations, it was observed

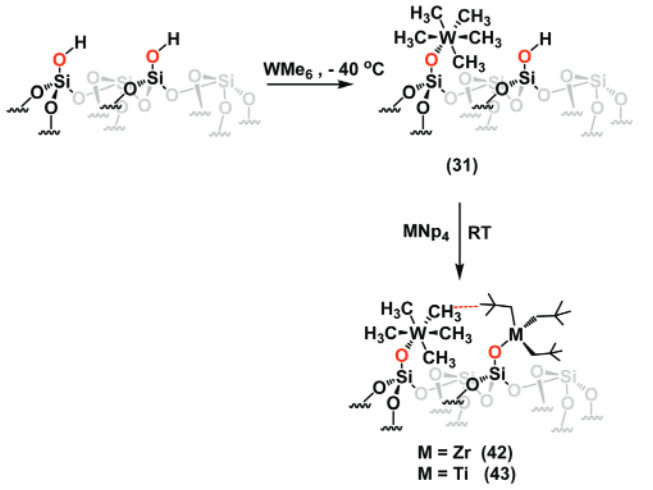

Scheme 19 Synthesis of a bi-metallic W/Zr precursor catalyst.[142]

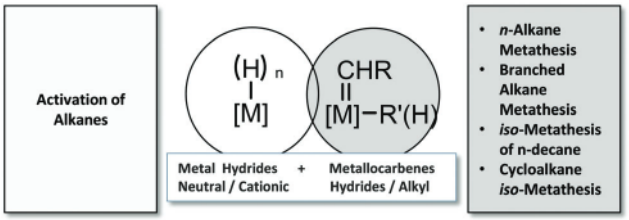

Fig. 10 Illustration of third generation SOMFs for alkane metathesis.

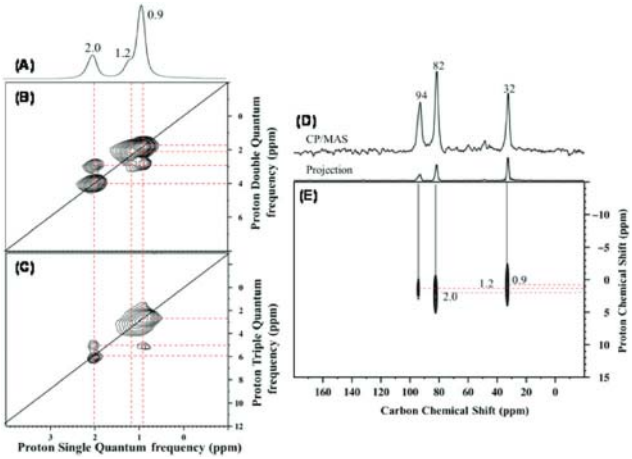

Fig. 11 One-dimensional ^{1}H MAS solid-state NMR spectrum of [≡Si-O-W(CH$_3$)$_5$ ≡Si-O-Zr(Np)$_3$] acquired at 600 MHz (14.1 T) with 22 kHz MAS frequency, a repetition delay of 5 s, and 8 scans. (B) Two-dimensional ^{1}H–^{1}H double-quantum/single-quantum (SQ) and (C) ^{1}H–^{1}H triple-quantum/SQ NMR spectra of 4 (both acquired with 32 scans per t_1 increment, 5 s repetition delay, 128 individual t_1 increments). (D) ^{13}C CP/MAS NMR spectrum of 4 (acquired at 9.4 T (f 0(^{1}H) = 400 MHz) with 10 kHz MAS frequency, 10 000 scans, 4 s repetition delay, and 2 ms contact time). Exponential line broadening of 80 Hz was applied prior to Fourier transformation. (E) 2D ^{1}H–^{13}C CP/MAS dipolar HETCOR spectrum of 4 (acquired at 9.4 T with 10 kHz MAS frequency, 3000 scans per t_1 increment, 4 s repetition delay, 64 individual t_1 increments, and 0.2 ms contact time). For all spectra depicted here, only W–Me in 4 was 50% ^{13}C labelled. Reprinted with permission from ref. 142, Copyright 2016 American Chemical Society.

that (i) [W]/[Ti] grafted on silica [(≡Si-O-)WMe$_5$/(≡Si-O-)Ti(Np)$_3$] yielded much higher TONs (up to 10 000) than either (ii) the mixed metal [{(≡Si-O-)WMe$_5$} + {(≡Si-O-)TiNp$_3$}] catalyst (TON 5204) or (iii) the layered [≡Si-O-Ti(Np)$_3$] and [(≡Si-O-)WMe$_5$] catalyst (TON 639). This study proved that the synergistic effect that comes from the proximity of the metals is the key for much better results than the other catalysts.

3. CO_2 chemistry by SOMC

The conversion of CO_2 to useful chemicals and fuels has become a main focus of industrial and academic research. Several efforts have targeted mitigation of CO_2 emissions by using it as a renewable C-1 feedstock as an alternative to the devalorizing geological dumping approach.[144–156] Several recent reviews have discussed the synthesis of industrially attractive compounds and intermediates from CO_2, such as dialkyl

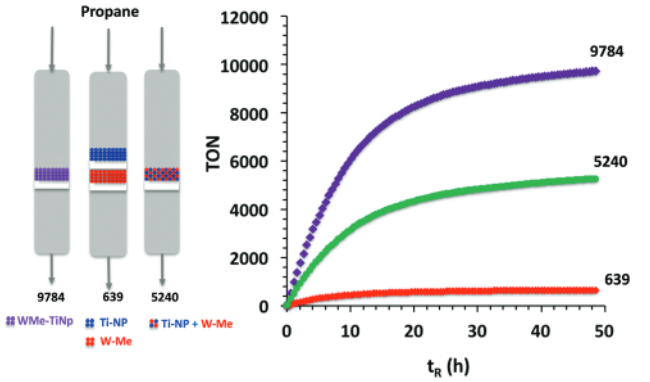

Fig. 12 Turnover number vs. time for pre-catalyst [(≡Si-O-)WMe$_5$/(≡Si-O-)TiNp$_3$] (4) (0.34 wt% W and 1.02 wt% Ti) (violet color), the mixture of [(≡Si-O-)W(Me)$_5$] and [(≡Si-O-)Ti(Np)$_3$] (0.27 wt% W, 1.05 wt% Ti) (green color), and a layer of [(≡Si-O-)TiNp$_3$] (1.1 wt% Ti) followed by a layer of [(≡Si-O-)WMe$_5$] (0.34 wt% W) (red color). TON is expressed in moles of propane transformed per mole of W. Reprinted with permission from ref. 143, Copyright 2017 American Chemical Society.

carbonates,[151] cyclic organic carbonates,[154,155] syngas,[149,151] formic acid,[148,151,157] methanol,[148,149,151,157–159] methylamines,[148,151,160] methane,[151] Fischer–Tropsch fuels,[151] ethers,[151] and CO,[147,149] by heterogeneous and immobilized catalysts along with the challenges and intricacies of such an approach. This section will cover exclusively those studies reporting the reactions of well-defined single site surface species with CO_2 and will provide insights into the pathways of CO_2 activation by such compounds. To note, several chemical processes that are of relevance for industry and academia involve the reduction of CO_2, *i.e.*, CO_2 to methane and methanol and the dry reforming of methane (reaction of CO_2 plus CH_4).[145,151,158] In the heterogeneous phase, these processes are generally catalyzed by transition metals in the form of highly active nanoparticles.[149,158,161,162] Surface-supported complexes (*e.g.* Cu, Ni, Au, *etc.*) prepared by surface organometallic chemistry can serve as precursors of metal nanoparticles upon reduction with H_2 leading to the formation of tiny, uniformly dispersed, well-defined and narrowly distributed nanoparticles on the support surface.[163–165] Catalysts prepared by such a methodology have been recently applied for the dry reforming of methane[166] and for the reduction of CO_2 to methanol;[167] however, as they do not involve the direct participation of surface organometallic fragments (SOMFs), they will not be described here in detail.

3.1. Stoichiometric activation of CO_2 by zirconium hydride

Until recent years, the only SOMC approach to CO_2 conversion was the stoichiometric reaction with supported metal hydrides (Fig. 13). The first example of CO_2 activation by surface organometallic complexes was with zirconium hydride supported onto silica in 2004.[63] CO_2 was used as a molecular probe to investigate the nature and the reactivity of supported tripodal monohydride (**44**) and bipodal bis-hydride (**45**) zirconium complexes. One molecule of CO_2 could be inserted per Zr–H bond to produce the corresponding formate complexes (**46**, **47**).

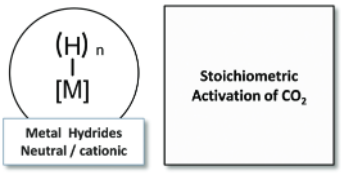

Fig. 13 Illustration of SOMFs for the stoichiometric activation of CO_2.

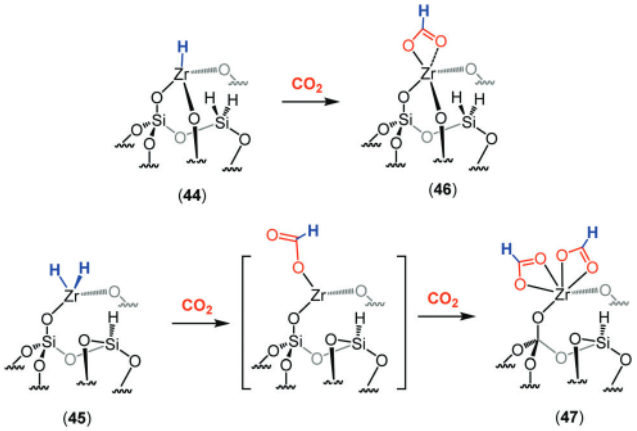

Scheme 20 Reactivity of zirconium mono- and bis-hydrides with carbon dioxide.[63]

Both mono- or bis-formate were detected by ^{13}C CP/MAS NMR according to the podality of the initial hydride (Scheme 20).[168]

Several years after this seminal paper, the insertion of CO_2 in zirconium hydrides was the subject of further theoretical and experimental studies, and DFT calculations using models of a supported tripodal zirconium monohydride [(≡Si-O-)$_3$ZrH] and bipodal zirconium bis-hydrides [(≡Si-O-)$_2$ZrH$_2$] were published.[169] It was shown that the reaction of CO_2 with both complexes is initiated by the formation of a weak adduct [O=C=O···Zr] leading to a η^1 and later to a more stable η^2-coordinated formate. The insertion of CO_2 into [(≡Si-O-)$_3$Zr-H] is virtually barrier-less and highly exothermic releasing about 10 kcal mol^{-1} with respect to the reagents. The insertion of each CO_2 molecule into [(≡Si-O-)$_2$Zr(H)$_2$] is similarly highly exothermic and barrier-less with the exception of the steps of rearrangement from the η^1 to the η^2 coordination of the first formate that has a small barrier of about 1.5 kcal mol^{-1}.

In a combined experimental and theoretical study, the formation of [Zr]–formates was investigated starting from [Zr]–hydrides supported on amino-modified silica.[170] According to the preparative method, the modified silica surface displays either bis-silylamino [(≡SiNH$_2$)$_2$] or silanol/silylamine [(≡SiOH)(≡SiNH$_2$)] ligands. Using the latter kind of surface, a mixture of three [Zr]–hydride complexes was prepared: [Zr]–mono-hydride ((≡Si-O-)$_2$(≡Si-NH-)[Zr]H); [Zr]–bis-hydride ((≡Si-O-)(≡Si-NH-)[Zr](H)$_2$) and an unprecedented complex presenting a π-bond between the surface and the metal ((≡Si-O-)(≡Si-N=)[Zr]H) (Scheme 21) (**48**). To unambiguously prove the formation of the latter compound, the insertion of CO_2 into the different metal hydrides was

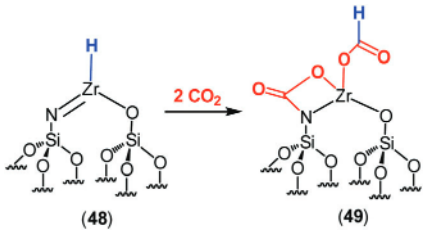

Scheme 21 Reaction of two molecules of CO_2 with ((≡Si-O-)(≡Si-N=)[Zr]H) by insertion into the Zr–H bond and addition to the N=Zr bond.[170]

studied. As previously observed, the formate formation was in all cases highly exothermic and facile, involving small reaction barriers (not higher than 10–12 kcal mol^{-1}) although generally higher than what was previously calculated for an unfunctionalized silica support.[169] Interestingly, the reaction of ((≡Si-O-)(≡Si-N=)[Zr](H)) with CO_2 (Scheme 21) was found to proceed through two nearly equivalent pathways; (i) the insertion of a first molecule of CO_2 into the [Zr]–H bond followed by addition of CO_2 to the N=Zr bond or (ii) the addition of CO_2 to the N=Zr bond followed by insertion of another molecule of CO_2 into the [Zr]–H bond. Consistently, when the mixture of surface hydrides was exposed to $^{13}CO_2$, a carbonyl signal at 161 ppm appeared in the ^{13}C CP-MAS spectrum that was readily assigned to a new cyclic zirconium formate carbimato complex (**49**). Additionally, [Zr]-mono-formate and [Zr]-bis-formate were detected at 181 ppm and 168 ppm, respectively.

The above-discussed literature demonstrates that the insertion of CO_2 into the zirconium hydride complexes prepared by SOMC is facile. In the case of homogeneous Ru,[171,172] Rh,[173] and Ir[174] complexes, the catalytic cycle for the synthesis of formic acid is completed by the reaction with H_2 that also restores the metal hydride catalyst. Nevertheless, no reports have surfaced on the isolation of formic acid from SOMC-prepared complexes.

3.2. Conversion of CO_2 to cyclic carbonate

Non-reductive processes have emerged as a valuable approach for the sustainable conversion of CO_2 including CO_2 from flue gas.[155,175,176] Processes such as the synthesis of polycarbonates,[177] mineral[178] or organic carbonates[155,179–181] and oxazolidinones[182] can proceed under very mild conditions without requiring high energy and potentially hazardous reagents such as hydrogen.[180] The synthesis of cyclic organic carbonates, in particular, represents a way to access commodity chemicals, solvents[183] and key intermediates with ramifications in the synthesis of polymers,[184,185] methanol,[186] diols,[184] *etc.* Differently from bulk chemicals such as urea (also produced from CO_2), cyclic carbonates and their derivatives afford a long-term storage of CO_2.[187]

Niobium halides and other coordination compounds have shown excellent catalytic activity for the conversion of CO_2 to cyclic organic carbonates under ambient conditions (Fig. 14).[188] DFT and kinetic studies on the cycloaddition of CO_2 to propylene oxide promoted by $NbCl_5$/DMAP (DMAP: *N*,*N*-dimethylamino pyridine) and $NbCl_5$/TBAB (TBAB: tetrabutylammonium bromide)

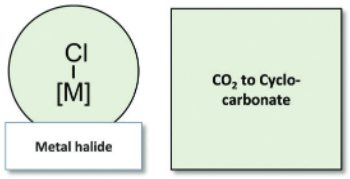

Fig. 14 Illustration of SCFs for conversion of CO_2 into cyclocarbonates.

have revealed the potential occurrence of a bimetallic cooperative mechanism in the homogeneous phase between two niobium centers for the activation of CO_2.[189] Indeed, the DFT-calculated barrier for CO_2 insertion into the ring-opened epoxide, generated upon nucleophilic attack of DMAP or Br^- (Nu), was found to be too high for a process occurring under ambient conditions (37.1 kcal mol^{-1}, Table 1, entry 1). Hence, a bimetallic mechanism was also considered in which a second niobium complex assists the insertion of CO_2. The calculated barrier for the latter process dropped to just 15.0 kcal mol^{-1} suggesting that the reaction can proceed under ambient conditions. The observed mechanistic features represent a potential obstacle for the synthesis of well-defined supported $NbCl_5$-based catalysts by SOMC as the isolated complexes (as generally prepared by SOMC) are supposed to be inactive under mild reaction conditions.

Bimetallic interactions have often been observed in homogeneous-phase catalysts,[190,191] but the creation of precise "bimetallic pockets" on metal oxide surfaces by grafting or impregnation strategies is extremely challenging.

A rare example of cooperative bimetallic catalysts was prepared by SOMC.[14] The silica supported counterparts of the homogeneous niobium $NbCl_5$ catalysts[192,193] were prepared using two silica supports treated at different dehydroxylation temperatures ($SiO_{2\text{-}200}$ and $SiO_{2\text{-}700}$, dehydroxylated at 200 °C and 700 °C, respectively). These supports differ by the density of silanol moieties (0.3 mmol g^{-1} for $SiO_{2\text{-}700}$; 0.78 mol g^{-1} for $SiO_{2\text{-}200}$)[3] and by their nature on the surface (isolated *vs.* vicinal silanols). Whereas the use of $SiO_{2\text{-}700}$ generally leads to isolated monopodal complexes (Fig. 15, **50**), the surface of $SiO_{2\text{-}200}$ displays a mixture of isolated and vicinal silanols and can, in principle, afford vicinal monopodal or bipodal complexes.

Table 1 Comparison of the reaction barriers for steps **II** and **III**[a] in the mechanism of cycloaddition of CO_2 to PO catalyzed by homogeneous and supported niobium and zirconium chlorides according to monometallic and bimetallic pathways[14]

Entry	Lewis acid catalyst	Pathway	Barriers of steps **II**, **III**[b]	Ref.
1	$NbCl_5$	Monometallic	37.1, 38.3	189
2	$NbCl_5$	Bimetallic	15.0, 29.3	189
3	$NbCl_5$@$SiO_{2\text{-}700}$	Monometallic	31.5, 35.2	14
4	$NbCl_5$@$SiO_{2\text{-}700}$	Bimetallic	15.9, 18.4	14
5	$ZrCl_4$ (**A**-*cis*)	Monometallic	20.2, 27.1	176
6	$ZrCl_4$ (**A**-*cis*)	Bimetallic	11.5, 27.3	176
7	$ZrCl_4$ (**A**-*trans*)	Monometallic	20.8, 30.9	176
8	$ZrCl_4$ (**A**-*trans*)	Bimetallic	14.5, 28.4	176

[a] The ring opening step (**I**) was found to be barrier-less in all instances. Step (**II**): CO_2 insertion in the metal–alkoxide bond. Step (**III**): cyclization. [b] Values are given in kcal mol^{-1}.

Treatment using two different $NbCl_5{\cdot}OEt_2$/silanol ratios (0.66 and 1.33) led to two different compounds **51** and **52** with nearly identical FTIR and ^1H and ^{13}C NMR spectra. However, the non-equivalence of these compounds could be unveiled by elemental analysis based on the grafted Nb/(initial silanols) ratio. Advanced ^{93}Nb NMR experiments, complemented with DFT models of the surface complexes, validated the prominent character (monopodal *vs.* bipodal) of both species. Replacement of the coordinated diethylether molecules with trimethyl phosphine followed by ^{31}P CP/MAS SSNMR spectrum showed the presence of two distinct phosphorous atoms for **51** and **52** in different proportions (Fig. 15a). Finally, double quantum ^{31}P CP/MAS SSNMR experiments showed that the monopodal species of **52** are in close proximity (Fig. 15b). By DFT calculations, the grafting of the precursor on a $SiO_{2\text{-}200}$ model was investigated (Fig. 15c). Results show that the first complex grafts exothermically in position **A**. The grafting of a second niobium complex in the vicinal silanol position **B** is also exothermic (ΔG E -21 kcal mol^{-1}) suggesting in principle a viable process. Similar, but less exothermic values, were observed for positions **C–F**.

Complexes **50–52** were tested for the cycloaddition of CO_2 to propylene oxide under relatively mild reaction conditions (60 °C, 10 bar initial CO_2 pressure). The presence of TBAB necessary as nucleophile (Nu) for the ring-opening of the epoxide. Results of the catalytic screening (using the same amount of niobium per system) are presented in Fig. 16. Compound **50** performed as a poor catalyst for the cycloaddition reaction confirming the hypothesis that isolated $NbCl_5$ complexes are non-efficient catalysts for the title reaction. The catalytic activity of **51** was lower than that of catalyst **52**. Based on these results, the catalytic activity increases with the density of grafted $NbCl_5$ complexes (0.9, 1.4 and 2 complexes per nm^2 for **50**, **51**, **52** respectively). A higher activity was found for catalyst **52** presenting vicinal or neighboring monopodal niobium complexes (Fig. 16).

DFT calculations were applied to study the mechanism of the cycloaddition of CO_2 to propylene oxide using complexes **50–52**. The proposed mechanism (Scheme 22) proceeds through the steps of epoxide ring-opening (**I**), CO_2 insertion into the metal–alkoxide bond (**II**) and carbonate ring closure (**III**).

The ring-opening (**I**) is generally barrier-less for strong Lewis acids and should be the same for mono- and bimetallic systems.[189] For the CO_2 insertion step (**II**) and the carbonate ring closure (**III**) monometallic and bimetallic mechanisms were considered (Table 1, entries 3, 4).

Results show that the occurrence of a bimetallic mechanism leads to a strong decrease (Table 1, entry 4) of the barriers for CO_2 insertion (**II**) and ring closure (**III**) compared to the monometallic mechanism (Table 1, entry 3). This again supports the conclusion that the presence of a neighboring niobium complex facilitates reaction under mild conditions.

Although it is extremely challenging to create precise and identical bimetallic sites on metal oxide surfaces by grafting strategies, the presented work shows that, by a judicious selection of the degree of dehydroxylation of the support and of the ratio between the amount of precursor and the initial number of silanols, it is possible to create a majority of

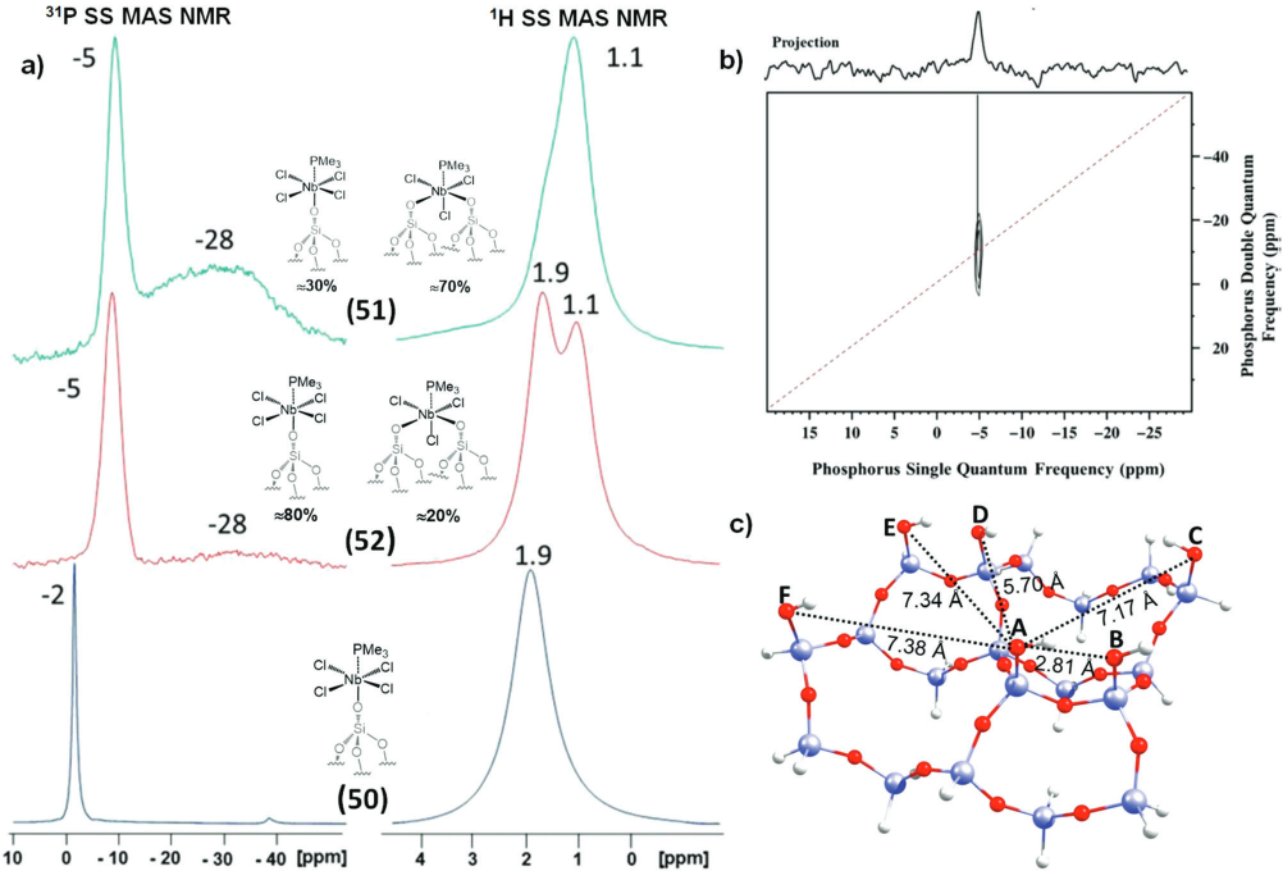

Fig. 15 (a) Comparison of ^{31}P SS NMR and ^{1}H SS NMR of **51** (top trace), **52** (middle trace) and **50** (bottom trace) showing the different proportions of monopodal and bipodal species in each compound. (b) Double quantum ^{31}P CP/MAS SS NMR of **52** and (c) model of $SiO_{2\text{-}200}$ with various possible anchoring positions used for the DFT study of the grafting process of neighboring niobium complexes. Adapted with permission from ref. 14, copyright 2015 American Chemical Society.

neighbouring monopodal complexes placed in a suitable arrangement to give rise to a cooperative catalytic effect. The extension of this method to other metals or to the combination of metals holds the potential to explore unprecedented cooperative effects in SOMC.

Besides several limitations concerning the economic costs, market size and durability of sequestration, main hurdles hindering the large-scale conversion of CO_2 to fuels and chemicals as a way to reduce the net anthropogenic emissions are represented by the need for energy intensive processes and reagents for CO_2 separation, purification, compression, transportation and conversion. The carbon costs associated with these processes could easily offset the environmental benefits of using CO_2 as a feedstock.[151,153] One possible way to bypass such a limitation would be the use of untreated flue gas as the source of CO_2 under ambient or very mild reaction conditions. This method would require the development of robust catalytic systems able to operate under challenging conditions (low CO_2 partial pressure, presence of moisture and impurities).

In 2016 Barthel *et al.*[175] reported a study using early transition metal halides as Lewis acids for the synthesis of cyclic carbonates prepared by bubbling a flow of diluted CO_2 or actual flue gas through a solution of epoxide and a catalyst. Whereas YCl_3/TBAB resulted as the most efficient catalyst after the initial screening using a flow of diluted CO_2 as simulated flue gas, and was later successfully tested using flows of actual flue gas, $ZrCl_4$/TBAB performed comparably well during the preliminary screening with diluted CO_2 (86% CO_2 conversion for $ZrCl_4$/TBAB *versus* 91% for YCl_3/TBAB at room temperature using a 50% v/v CO_2 flow in Ar as a carrier gas). Zirconium being an abundant metal, the authors selected $ZrCl_4$ for the preparation of a heterogeneous catalyst for the conversion of flue gas CO_2 and epoxides to cyclic carbonates.[176] The authors used $ZrCl_4{\cdot}(OEt_2)_2$ as the precursor that was reacted with $SiO_{2\text{-}700}$ and $SiO_{2\text{-}200}$ (**53**, Scheme 23). The reaction of the precursor with the highly dehydroxylated silica support ($SiO_{2\text{-}700}$) led to an isolated, monopodal Zr complex: $[(\equiv Si\text{-}O\text{-})ZrCl_3{\cdot}(OEt_2)_2]$ (**53′**) partly present as $[(\equiv Si\text{-}O\text{-})ZrCl_3{\cdot}OEt_2{\cdot}(O_s(\text{-}Si\equiv)_2)]$ (**53″**) because of the replacement of an ether ligand with an oxygen atom of the surface (O_s) as a ligand.

As observed for the case of $NbCl_5$ grafting, the grafting of $ZrCl_4{\cdot}(OEt_2)_2$ on $SiO_{2\text{-}200}$ using different amounts of precursor with respect to the initial number of surface silanols led to mixtures of monopodal and bipodal species in different proportions. When an excess of precursor (1.33 equiv.) was used (**54**), the main species found on the surface was $[(\equiv Si\text{-}O\text{-})ZrCl_3{\cdot}OEt_2{\cdot}(O_s(\text{-}Si\equiv)_2)]$

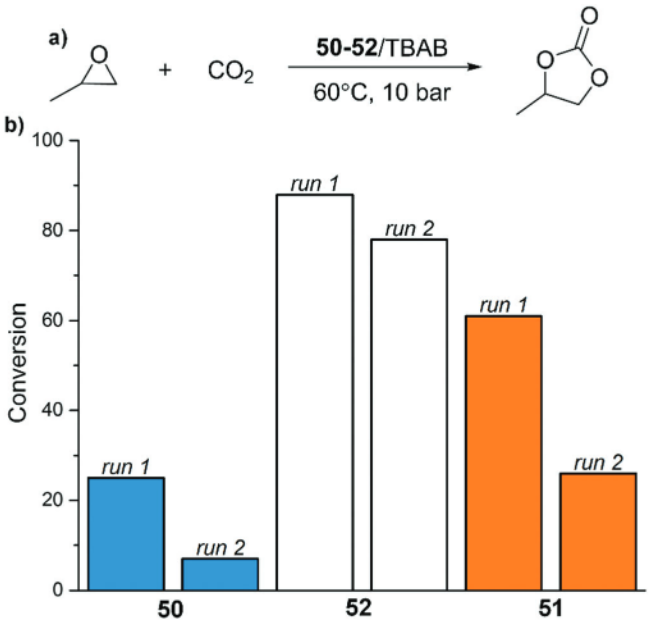

Fig. 16 Catalytic activity of compounds **50–52** in the cycloaddition of CO_2 to propylene oxide at 60 °C, 10 bar CO_2. Compound **52** is the most active at any catalytic run. The catalytic activity of the isolated complexes (**50**) is very low, mostly due to leached Nb species, as nearly no activity was detected when the catalyst was reused. Adapted with permission from ref. 14, copyright 2015 American Chemical Society.

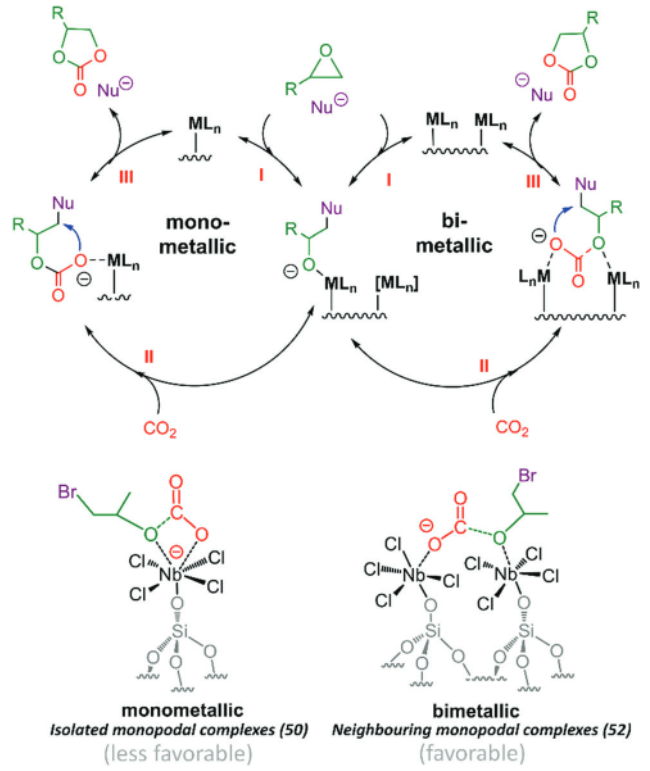

Scheme 22 (top) Three-step mechanism for the cycloaddition of CO_2 to epoxides catalyzed by a binary system composed of a Lewis acid ML_n (M: metal atom, L: ligand) and a nucleophile (Nu). The step of CO_2 insertion (**II**) might be monometallic or bimetallic. (bottom) Graphical representation of the transition state of CO_2 insertion for the isolated monopodal complexes of **50** (left) and for the neighbouring monopodal niobium complexes of **52** (right).[14]

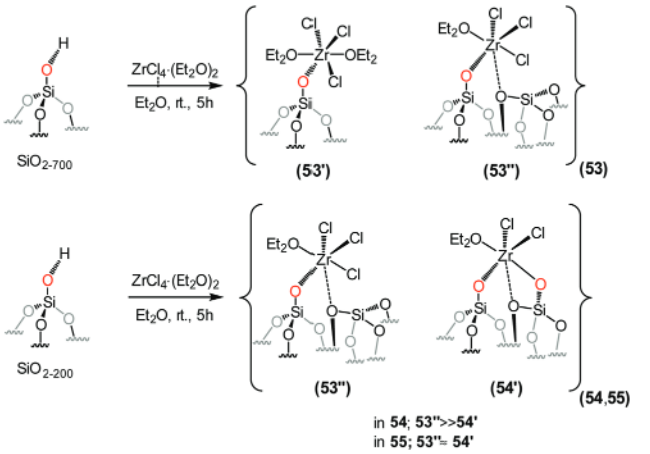

Scheme 23 [(≡Si-O-)$ZrCl_3$·$(OEt_2)_2$] and [(≡Si-O-)$ZrCl_3$·OEt_2·(Os(-Si≡)$_2$)] complexes in **53** and [(≡Si-O-)$ZrCl_3$·OEt_2·(Os(-Si≡)$_2$)] and [(≡Si-O-)$_2ZrCl_2$·OEt_2·(Os(-Si≡)$_2$)] complexes present in different proportions in **54** and **55**.[176]

(53″, 80%) with a minor component represented by bipodal complexes [(≡Si-O-)$_2ZrCl_2$·OEt_2·(Os(-Si≡)$_2$)] (20%) (**54′**). The same complexes were found on the surface of the compound prepared using a substoichiometric amount of precursor (0.66 equiv. with respect to the number of silanols of $SiO_{2\text{-}200}$, **55**) but the ratio of monopodal *versus* bipodal complexes was closer to one (Scheme 23).

Complex **54** presents a relatively high density of monopodal zirconium chloride complexes that could establish a cooperative catalytic effect as in the case of **52**. However, when **53–55** were tested for the cycloaddition of CO_2 to propylene oxide under mild conditions (60 °C, 10 bar CO_2) the best catalytic performance in the first run was by single-site complex **53** (Fig. 17). The activity of the catalysts was found to decrease through successive cycles or recovery and reuse as an effect of partial zirconium leaching, mostly after the first catalytic run, and likely, also as an effect of a change of the coordination environment at the zirconium center.

In order to explain the difference of activity between the niobium- and the zirconium-based catalysts, in terms of cooperativity between the neighboring monopodal complexes and activity of the isolated monopodal complexes, DFT calculations were carried out on homogeneous $ZrCl_4$·$(OEt_2)_2$ as a

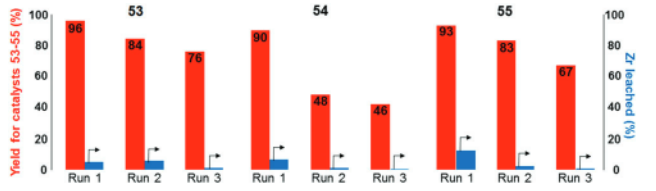

Fig. 17 Catalytic performance and zirconium leaching studies for the cycloaddition of CO_2 to PO catalyzed by **53–55** in the presence of TBAB. For each catalyst the PC yields for three consecutive catalytic cycles are shown (red columns). The percent fraction of zirconium leached (with regard to the initial amount on the catalyst) during the reaction is displayed (blue columns, right axis). Adapted with permission from ref. 176, copyright 2017, Elsevier.

cycloaddition catalyst considering the ether ligands in the *cis* or *trans* position with respect to each other (Table 1, entries 5–8). When analyzing the possible occurrence of monometallic or bimetallic processes, the authors observed that, although a bimetallic pathway of CO_2 insertion would proceed with a lower barrier than the monometallic route, the barrier of the rate-determining process (cyclization step, **III**) would not be affected. This is in good agreement with the outcome of the catalytic reactions showing nearly no dependency on the density of the zirconium complexes on the catalyst surface as observed in Fig. 17. Based on these results, supported $ZrCl_4$ can be considered as a single-site catalyst for the cycloaddition of CO_2 to epoxides.

4. Single-site catalytic oxidation

The oxidation of organic intermediates leads to a broad variety of industrially valuable products, such as alcohols, ketones, aldehydes, epoxides, carboxylic acids, esters, *etc.*[194,195] Oxidation reactions, aiming at the production of high added-value chemicals, are typically carried out using large amounts of over-stoichiometric oxidants (chromium$^{(VI)}$ compounds, permanganate, active chlorine-containing species or organic peroxoacids). In some cases, significant amounts of co-reactants, such as sacrificial reagents, or acid/base additives are required. Large quantities of hazardous wastes are produced and their disposal is economically burdensome and fosters an interest in developing greener and savvier catalytic processes.[196] The best oxidants in that regard are (i) molecular oxygen, a triplet biradical where a free radical chain autoxidation dominates, leading, however, to low selectivity.[197] (ii) Hydrogen peroxide (H_2O_2) that oxidizes organic compounds with an atom efficiency of 47% and is relatively cheap (o 0.5 EUR kg^{-1} for 100% H_2O_2) with respect to conventional lab-scale oxidants for fine chemistry applications (on a larger scale, H_2O_2 needs an attached production and poses safe transportation difficulties).[198,199] Nonetheless, H_2O_2 is not easily miscible with most of the organic non-polar solvents and cannot be used under controlled anhydrous conditions. (iii) Nitrous oxide (N_2O) is the 'optimal' mono-oxygen donor, just yielding molecular nitrogen as a co-product. Moreover, its high stability allows applications under a broad range of reaction conditions. On a large industrial scale, N_2O can be obtained as a cheap by-product from the synthesis process of adipic acid, but, for fine chemical applications, it is not suitable for standard batch liquid-phase reaction equipment as it is a gas.[200] (iv) Alkyl hydroperoxides (*e.g.* *tert*-butylhydroperoxide, TBHP, or cumyl hydroperoxide, CHP) are widely used for small-scale oxidations at both laboratory and industrial levels. They possess good thermal stability ($t_{1/2}$ = 520 h at 130 °C for a 0.2 M solution in benzene) and show fewer handling risks compared to 70% aqueous H_2O_2 or peroxoacetic acid.[201,202] Such hydroperoxides are quite versatile, due to their reasonable solubility in aqueous and in non-polar media. Yet, their atom efficiency remains low and they are rarely used in the presence of medium-pore zeolite supports, as they cannot be accommodated in micropore channels.

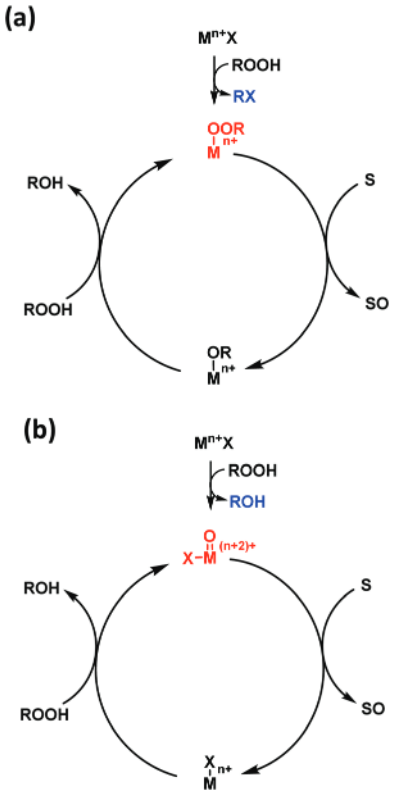

Scheme 24 Mechanism of oxygen transfer involving a (a) peroxometal and (b) an oxometal.[203]

The oxidation reaction generally follows either (i) one-electron free-radical oxidation (for instance on cobalt or manganese) involving the formation of alkoxy and alkylperoxy radicals (auto-oxidation) or (ii) oxygen transfer where an oxygen donor, such as ROOH or H_2O_2, heterolytically generates either a peroxometal (Scheme 24a) or an oxometal (Scheme 24b). Some other metals, such as $V^{(V)}$, can react through both routes depending on the substrate and on the reaction condition.[203]

In the peroxometal pathway the metal centre does not undergo any change in its oxidation state during the catalytic cycle. The oxygen-transfer ability of the coordinated peroxo moiety is due to its Lewis acid character. Early transition metals with a d^0 electronic configuration, such as $Ti^{(IV)}$, $Zr^{(IV)}$, $Nb^{(V)}$, $Mo^{(VI)}$, $W^{(VI)}$ or $Re^{(VII)}$, which are relatively poor oxidants generally react *via* the peroxometal pathway.

In the oxometal pathway the metal centre itself plays the role of the oxidising species: it undergoes a two-electron reduction and is eventually re-oxidised by the oxygen donor. Several first-row and/or late transition metals, such as $Mn^{(V)}$, $Cr^{(VI)}$ or $Os^{(VIII)}$, which are good oxidants in their highest oxidation state, operate *via* the oxometal pathway.

The challenge lies in the development of well-defined and more sustainable catalysts for oxidation reactions. This objective can be reached using the SOMC strategy to design SOMFs or SCFs having suitable active sites for a given catalytic oxidation. For this purpose, catalytically active redox metal centres should be used. Typical oxidation reactions in which single-site heterogeneous

catalysts and/or surface organometallic/coordination fragments are the catalysts are described below.

4.1. Epoxidation of alkenes

4.1.1. Single site titanosilicalite-1 zeotype catalysts. Titanium-containing microporous molecular sieves and, above all, titanosilicalite-1 zeotype, TS-1, have been shown to be the most promising and best-performing heterogeneous systems so far, displaying well-defined catalytically active sites in a crystalline zeolitic framework (Fig. 18). A huge variety of efficient and sustainable oxidation of commodities and fine chemicals, such as in alkene epoxidation, alcohol oxidation, ketone ammoxidation or oxidation of sulphur compounds or ethyl lactate,[204–211] can be catalysed using this system. Some processes based on the use of TS-1 have attained full maturity and an industrial exploitation level, such as the hydrogen peroxide propylene oxide, HPPO, processes by Degussa-Uhde BASF/Dow,[212,213] or the EniChem-Sumitomo cyclohexanone ammoximation process.[214] Although these zeotype catalysts were not obtained *via* SOMC, they are a milestone and a source of inspiration for the design and the optimisation of single-site oxidation catalysts featuring similar SCFs. Indeed, it demonstrates clearly that the presence of single well-defined metal atoms embedded in a tetrahedral silica matrix is required for a selective and efficient oxidation reaction.[215] These characteristics can be relatively easily reproduced and obtained thanks to the SOMC synthesis strategy and the rational construction of spatially isolated SCF moieties on the oxide surfaces, by considering the oxide surface as a rigid polydentate ligand.[216–219]

4.1.2. Titanosilicates through bifunctional templating. The bifunctional templating strategy is an intermediate approach according to which a metal precursor coordination complex may act simultaneously as a structure directing agent and as a precursor for the grafting of the chemically defined metal centre. The grafting of [Ti] species was optimized by using triethanolamine,[220,221] where the branched amine played the role of (i) a template for the mesoporous network and (ii) a ligand for the titanium complexes. Triethanolamine is prone to form complexes with titanium alkoxides to yield titanatrane complexes. In the presence of free triethanolamine, they give rise to meso-sized aggregates that act as templates for the final mesoporous titanosilicate catalyst (in this case a Ti-TUD-1 material). By high temperature treatment, all of the $Ti^{(IV)}$ coordination complexes are degraded and triethanolamine is removed, grafting titanium onto the internal surface of the mesopores.

In this way, the ''one-step'' grafted Ti-TUD-1 catalyst is about six times more active in oxidation reactions than in-framework substituted Ti-MCM-41 and has a similar activity to post-synthesis [Ti]-grafted MCM-41. Suitable oxidants, on this catalyst, are TBHP, H_2O_2 and, although with rather modest performance, molecular oxygen too.[222] This type of tetrahedral [Ti]-containing catalyst was also used to convert propene into propene epoxide in the presence of cyclohexylhydroperoxide (a co-product of the manufacture of cyclohexanol and cyclohexanone, see Section 4.3, hereafter) with high hydroperoxide conversion and interesting propene epoxide selectivities ($>50\%$).[223]

Chromium and molybdenum centres were incorporated into the framework of TUD-1 mesoporous silica by a fully comparable one-pot synthesis procedure, using triethanolamine as a bifunctional template.[224,225] Tetrahedrally coordinated $Cr^{(VI)}$-di-oxo sites incorporated into the TUD-1 silica framework were tested for the photo-oxidation of propane. High activity and selectivity towards acetone under blue visible light irradiation was observed. In contrast, [Mo]-containing TUD-1 silica was active in cyclohexene epoxidation with TBHP, leading to 88% selectivity towards cyclohexene oxide. However, this system suffered from active metal leaching into the reaction medium, especially during the first reaction runs.[225]

4.1.3. The development of SCFs for oxidation reactions. This section describes typical catalysts with a marked oxidation capability (in line with TS-1 zeotypes) and enhanced accessibility obtained by the SOMC strategy. The most relevant example for epoxidation of a large variety of alkenes is $Ti^{(IV)}$ supported onto silica or mesoporous silica (Fig. 19) even if other early transition metals also deserve increasing attention (see hereafter). Typical titanium-precursors are [Ti]–alkoxides (*e.g.* $Ti(OEt)_4$,[226] $Ti(OBu)_4$,[227–229] $Ti(O^iPr)_4$),[230–235] $[SiMe_2(\eta^5\text{-}C_5H_4)_2]TiCl_2$,[236] $[\{Ti(OiPr)_2(OMenth)\}_2]$, $[Ti(OMenth)_4]$ (OMenth = 1*R*,2*S*,5*R*-(−)-menthoxo),[237] Ti–calixarene chloride[238–240] or tris(*tert*-butoxy)siloxytitanium complex $(^iPrO)Ti\text{-}[OSi(O^tBu)_3]_3$.[241–244]

The first example of a single-site, surface coordination fragment is TiO_2/SiO_2 developed by Shell Oil in the late 1960s for the styrene monomer – propylene oxide process.[215,245] This catalyst is prepared by a gas-phase reaction of $TiCl_4$ onto

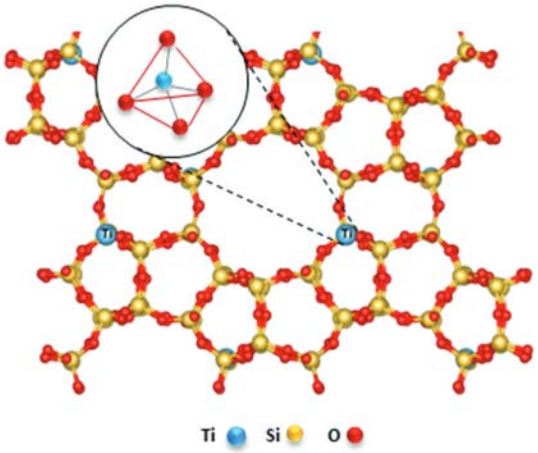

Fig. 18 Schematic illustration of titanosilicate-1 zeotype TS-1. In blue is [Ti], in red is O, and in yellow is Si.

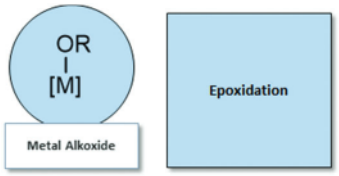

Fig. 19 Illustration of SCFs for epoxidation reactions.

a porous silica support and subsequent calcination, steam treatment and silylation. This synthesis was improved starting from [Ti]–H grafted on $SiO_{2\text{-}200}$, $SiO_{2\text{-}500}$ or $SiO_{2\text{-}700}$ using the SOMC strategy.[216] Starting from these well-defined SOMFs (already described in Sections 2 and 3), four different monopodal, bipodal and tripodal SOMC [Ti]–alkoxyl catalysts (OR = OH, ONp/OH, OMe and O^{t}Bu) were obtained (Scheme 25).

Four different SOMC [Ti]–alkoxyl catalysts (OR = OH, ONp/OH, OMe and O^{t}Bu) were prepared using $SiO_{2\text{-}200}$, $SiO_{2\text{-}500}$ or $SiO_{2\text{-}700}$ as the support to obtain monopodal, bipodal and tripodal surface species (Scheme 25).[1] Catalysts were tested in epoxidation of 1-octene using TBHP as an oxidant at 80 °C. The [Ti]–O^{t}Bu-catalyst was the most active catalyst reaching an initial activity of almost 1200 h^{-1}. Further, it was found that in all cases the tripodal catalyst was the most active one (Fig. 20).

Following this work, several studies have reported the synthesis of Ti$^{(IV)}$–silica based catalysts for the epoxidation of alkenes either in the presence of hydrogen peroxide (H_2O_2) or alkyl hydroperoxides (TBHP and CHP). The reaction with H_2O_2 occurs *via* an oxygen transfer leading to peroxometal complex [Ti]–hydroperoxide (Scheme 26). Then, the distal peroxidic oxygen, activated by its proximity to [Ti], is transferred to the double bond of the alkene, with parallel formation of a [Ti]–alkoxide. The latter can undergo a new catalytic cycle along with a water molecule.[1,246–248] A comparable mechanism in the presence of [Ti]–alkylhydroperoxide as an oxidant has been

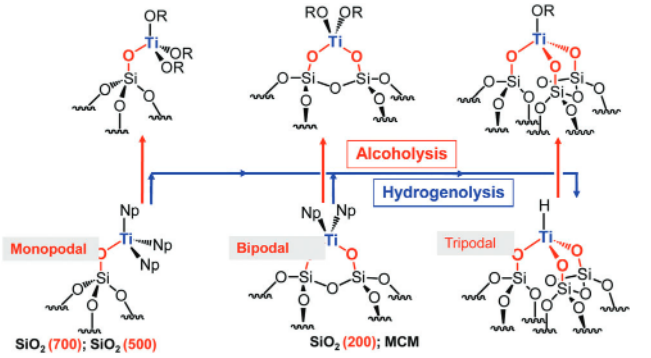

Scheme 25 Methods of preparation of mono-, di- and tripodal Ti alkoxides on silica surfaces.[216]

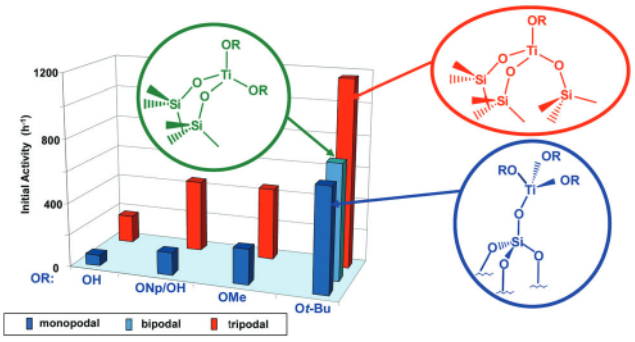

Fig. 20 Epoxidation of 1-octene in the presence of TBHP. Reaction conditions: 1-octene/[Ti] = 3000; TBHP/Ti = 150; T = 80 °C.[1]

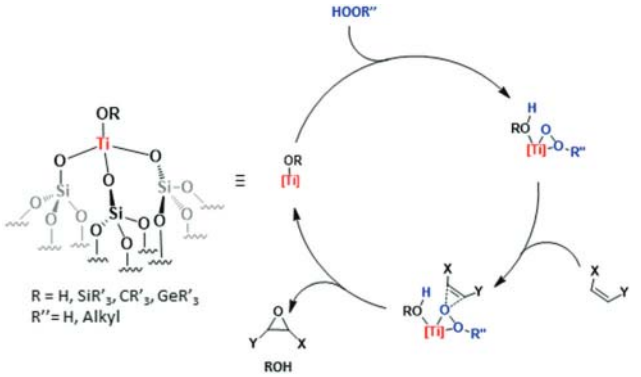

Scheme 26 Proposed mechanism of epoxidation of alkenes with hydrogen peroxide or alkyl hydroperoxides catalysed by Ti(IV) containing SCF sites.

validated by experimental and theoretical studies, yet the related alcohol is co-produced.[249] Consistently with a heterolytic pathway, the reaction retains the C=C bond configuration. An alkylperoxotitanium moiety, (≡Si-O-)$_3$Ti-OO-^{t}Bu, with a structure in agreement to the one of the intermediate depicted in the catalytic cycle of Scheme 26, has been synthesised by the reaction of an excess of TBHP on the surface hydride (≡Si–O)$_3$Ti–H. It proved to be an active species for the stoichiometric activation of alkenes.[1,216]

In addition, titanium hydroxyl mesoporous based catalysts, [(≡Si-O-)$_3$Ti-OH], are active and highly selective (>90%) for the epoxidation of cycloalkenes,[250–252] and their iso-propoxyl homologues Ti(O^{i}Pr)$_4$ showed good results in the epoxidation of non-functionalized alkenes, dienes and allylic alcohols using *tert*-butylhydroperoxide as an oxidant.[253] Interestingly, Ti(O^{i}Pr)$_4$-derived catalysts maintain their catalytic activity under mild conditions and in the presence of diluted aqueous hydrogen peroxide too (23% yield after 1 h of reaction).[234,251,254] By addition of chiral tartrates, namely, *R*-(+)-diethyl L-tartrate or *R*-(+)-diisopropyl L-tartrate, it was possible to induce enantioselectivity into the asymmetric epoxidation of styrene with TBHP.[255,256] Although modest enantiomeric excess values were attained, they were comparable to their homogeneous counterparts and, notably, better selectivity to styrene oxide was observed.[256]

Highly versatile tripodal [(≡Si-O-)$_3$Ti-OH] moieties were obtained by grafting titanocene dichloride onto a previously activated mesoporous MCM-41 $SiO_{2\text{-}500}$ support.[257,258] Following this approach, the bulky cyclopentadienyl ligands should inhibit the coalescence of Ti$^{(IV)}$ species on the surface of the support and control the formation of undesired large TiO_2-like domains. However, with high loadings of titanium species (higher than 5 wt%) a non-negligible contribution of DRS-UV bands, attributable to TiO_2-like moieties was also observed.[259,260] This shows that Ti contents around 2 wt% are the ideal compromise between titanium loading and active site isolation. Non-ordered or non-porous silica oxides, previously activated at 500 °C, have been used as supports as well.[261] Titanocene-grafted silicas revealed promising results in the epoxidation with TBHP of a wide variety of substrates, such as unsaturated cyclic terpenes

(*e.g.* limonene, carveol, isopulegol, carvotanacetol, terpinen-4-ol and α-terpineol).[262,263] By grafting $Ti^{(IV)}$ acetylacetonate, $Ti(acac)_4$, onto the surface of porous silica supports, TOF values six times higher than the ones obtained over embedded Ti–silica systems could be achieved.[264] In addition, thanks to the chemical environment surrounding the [Ti] SCF and to the role of the OH-function in directing the oxygen transfer from the oxidant to one specific side of the six-membered ring of the terpene, a complete diastereoselective epoxidation (100% d.e.) was achieved on homoallylic and bishomoallylic substrates, α-terpineol and terpinen-4-ol, respectively.[263] When the OH-group in α-terpineol was replaced by an acetyl moiety (α-terpinylacetate), the diastereoisomeric excess decreased from 100% down to 66%. Unfunctionalized terminal aliphatic alkenes, whose epoxidation over heterogeneous systems remains challenging due to the frequent undesired opening of the terminal oxirane ring, could be selectively converted into 1,2-epoxides by judiciously modifying the chemical environment around the [Ti]-centre, *e.g.* by silylation of the nearby silanols or by a fine tuning of the catalyst/oxidant/solvent combination as well as the surface polarity.[265–267]

Analogously, unsaturated fatty acid methyl esters (FAMEs), such as methyl oleate, methyl elaidate, methyl linoleate and mixtures of methyl esters obtained from high-oleic sunflower, castor, coriander and soy-bean oils, were successfully epoxidized over grafted [Ti]–OH SCFs.[261,268] The very high yields of *trans*-epoxystearate obtained using methyl oleate and methyl elaidate substrates (in *cis* and *trans* configurations, respectively) demonstrated the crucial role of the structural features of Ti-MCM-41 as an ordered solid. Very high yields of epoxidized FAMEs (up to 95% yield of epoxidized methyl linoleate or 96% yield of epoxidized castor oil methyl ester in 24 h) were obtained using Ti-MCM-41 with a relatively small excess of TBHP oxidant (only 10% over the stoichiometric amount).[269,270] By this method, unsaturated FAMEs could be epoxidized without the addition of peroxoacids (as in the widely-used Prilezhaev methodology).

The use of aqueous hydrogen peroxide is typically difficult over most mesoporous titanosilicates. Experiments on the interaction of TBHP and H_2O_2 with $Ti^{(IV)}$ centres have clarified that the addition of aqueous H_2O_2 leads to a rapid and irreversible transformation of the $Ti^{(IV)}$ centres into TiO_2-like domains that are catalytically inactive in epoxidation.[269] The role of the slow addition of H_2O_2 is thus crucial to avoid, or at least minimise, the decomposition of the oxidant and to keep the local water concentration as low as possible. Applying a controlled, drop-wise addition of aqueous H_2O_2 (4.17 mmol H_2O_2 h^{-1} $g_{cat}{}^{-1}$), excellent selectivity (>98%) and interesting yields (44% to 63%) were obtained in the epoxidation of cyclohexene.[259] Higher epoxide yields were found over Ti-MCM-48 compared to Ti-MCM-41 or Ti–SiO_2 and explained by the better site isolation, dispersion and stability of the $Ti^{(IV)}$ sites. The side production of allylic oxidation compounds (cyclohexenol and cyclohexenone) is negligible and the selectivity to the desired epoxide is very high.[251,254] Specific immersion calorimetry studies evaluating the interaction between the reactant and the catalyst indeed evidenced the very good affinity of cyclohexene towards titanosilicate, a crucial factor in the epoxidation reaction.[271] By optimizing the reaction conditions (especially, the catalyst to substrate ratio), high yields of up to 91% for the epoxide were obtained for Ti-MCM-41 with high stereoselectivity (80%) towards the *cis*-epoxide.

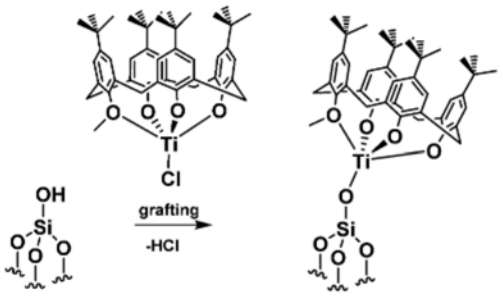

Scheme 27 Grafting of titano(IV)calixarene chloride onto an activated silica support. From ref. 238.

The use of bulky ligands at the [Ti] centre as 'spacers' to generate well-dispersed, isolated $Ti^{(IV)}$ sites has been explored by using multidentate calixarenes (Scheme 27).[238,239,272] $Ti^{(IV)}$–calixarene precursors were grafted onto activated $SiO_{2\text{-}500}$ at surface densities ranging from 0.1 to quasi-monolayer coverages (0.025–0.25 units nm^{-2}). Kinetic analyses during the epoxidation of cyclohexene confirmed that the calixarene-bound [Ti]-sites were significantly more active than their homogeneous analogues. The immobilisation on the silica surface, indeed, prevents the detrimental formation of aggregates and unselective Ti–O–Ti structures.

The bulky calixarene spacers could be removed by calcination at high temperature (550 °C under pure O_2) in order to afford highly dispersed [Ti]–OH SCFs, showing high activity towards cyclohexene and styrene epoxidation.[272,273] In addition, thanks to a specific *in situ* poisoning of the [Ti]–OH sites by means of phenylphosphonic acid, the $Ti^{(IV)}$ species available on the silica surface were titrated in order to determine the single-site intrinsic turnover frequency for *cis*-cyclooctene epoxidation from the surface density of active Ti sites.[274]

Other transition metals have been grafted onto activated mesoporous silica supports. Several examples employed chemically defined metallocene precursors of $Zr^{(IV)}$, $Mo^{(VI)}$, $Cr^{(VI)}$, $VO^{(IV)}$,[275–277] and $Nb^{(V)}$,[278] metallocalixarene species of $Zr^{(IV)}$, $Hf^{(IV)}$, $VO^{(IV)}$, $Ta^{(V)}$ and $Nb^{(V)}$,[272,279,280] tetraneopentylzirconium[252] as well as alkoxy and siloxy coordination complexes of $Ta^{(V)}$,[255,281–284] $W^{(VI)}$,[285] $Mo^{(VI)}$[284,286] and $Fe^{(III)}$.[287,288]

In particular, with regard to tantalum, a complementary approach has been pioneered by Tilley and co-workers.[281,282] An oxygen-rich metal precursor, such as $Ta(O^iPr)_2[OSi(O^tBu)_3]_3$, was grafted onto a metal oxide support *via* the thermolytic molecular precursor method at moderate temperature (ṙ 200 °C in air).[289] The [Ta] SCF underwent surface hydrophobization with $RMe_2Si\text{-}NMe_2$ species in order to obtain a more hydrophobic local environment, adequate to accommodate the apolar alkene substrate (Scheme 28).[282] Typical supports used were the high-area mesoporous silica solids MCM-41 and SBA-15, the latter being more thermally stable than the former, especially for this thermolytic purpose.

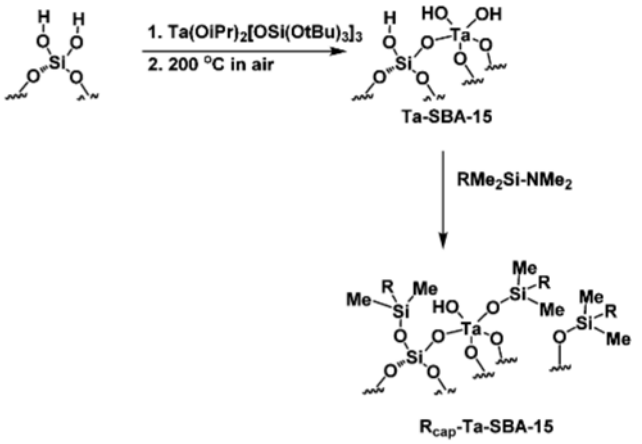

Scheme 28 Grafting of $Ta(OiPr)_2[OSi(O^tBu)_3]_3$ onto SBA-15 via a thermolytic molecular precursor approach, followed by surface modification by means of a silylating agent. R = Me, n-Bu. Adapted from ref. 282.

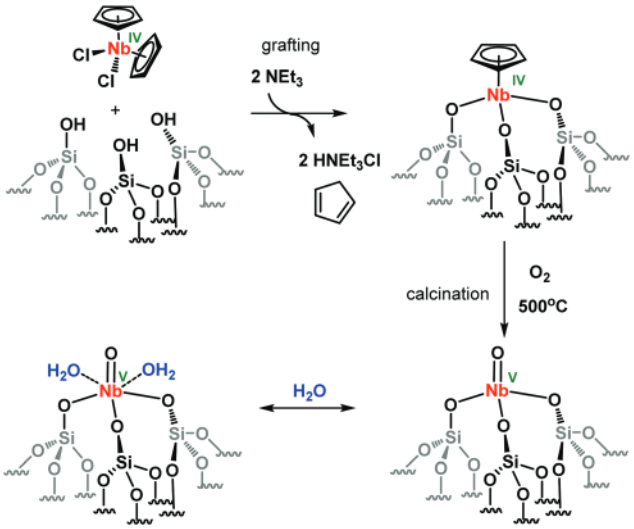

Scheme 29 Formation of single-site niobium(v) surface coordination fragments from niobocene(IV) dichloride.[280]

Trialkylsiloxy-modified $Ta^{(V)}$ centers obtained in this way exhibited excellent selectivity in epoxide formation (up to 98% after 2 h) in the oxidation of cyclohexene in the presence of aqueous H_2O_2 and an enhanced lifetime in aqueous media.[283] The remarkable stability and robustness of these [Ta] systems were later investigated by means of [Ta]-polysilsesquioxane model compounds. The presence of μ-oxo and μ-hydroxo bridges in surface dinuclear Ta–O–Ta moieties has been invoked as a possible key feature for the stabilization of Ta during the catalytic turnover.[290]

These studies paved the way to the use of analogous $Ta^{(V)}$ SCFs as catalytic sites for the epoxidation of alkenes and, in particular, [Ta] SCFs derived from grafted Ta(v)–calixarenes precursors proved to be not only up to 3 times more active in the epoxidation of cyclooctene than the corresponding $TaCl_5$-derived catalysts at high surface [Ta] densities, but also more selective (up to 95%) towards the direct, non-radical formation of the epoxide.[279,291] This class of catalysts demonstrates the utility of ligand-protected, supported [Ta] moieties for epoxidation when aqueous H_2O_2 is used as the oxidant and, according to this approach, ultra-high vacuum techniques were used to obtain supported monoatomic [Ta] species applied in the conversion of cyclohexene into cyclohexene epoxide and cyclohexanediol in moderate yields.[27]

Along group V metals, niobium-based SCFs also attract noteworthy attention. For example, niobocene$^{(IV)}$ dichloride can be first grafted and then calcined in dry air to give rise to tripodal $(Si\text{-}O)_3\text{-}Nb{=}O$ oxo-species (Scheme 29). This anhydrous tetracoordinated $Nb^{(V)}$ oxo-species undergoes hydration when exposed to water-containing reaction media forming a hexacoordinated diaquo-oxo $Nb^{(V)}$ moiety. A fully comparable [Nb]=O SCF can be obtained starting from a grafted $Nb^{(V)}$–calixarene moiety, after a calcination step, as for the case of [Ti] (Scheme 27).[292] These species constitute the catalytically-active site as confirmed by combined DR-UV-Vis, NIR, Raman, XRD, XANES and EXAFS analyses.[272,293]

[Nb]–silica catalysts showed excellent performance in the hydrogen peroxide-driven epoxidation of cyclic alkenes,[293,294] unsaturated fatty acid derivatives[295,296] and squalene.[297] High yields (up to 73%) and excellent chemoselectivity to the desired epoxides (up to 98%) were obtained in short reaction times (1 h) over Nb-grafted mesoporous silica catalysts. As observed for the analogous [Ta]-based systems, [Nb]-containing silica catalysts were very stable in water-containing media. Remarkably, aqueous H_2O_2 was an optimal oxidant for [Nb]-containing catalysts, whereas TBHP was the oxidant of choice in the presence of [Ti]–silica systems (Table 2). Additionally, Nb–SiO_2 catalysts showed an unexpected regioselectivity towards the epoxidation of electron-deficient C=C bonds, such as the ones in the exocyclic unsaturation of limonene[294] or α,β-unsaturated ketones.[297,298] Such unusual behaviour was explained by two factors: (i) invoking the rate-limiting oxidation of the solvent acetonitrile to generate peroxycarboximidic acid, which then reacts with electron-poor alkene bonds, and, (ii) on non-ordered amorphous silica supports for steric reasons.

4.2. Baeyer–Villiger oxidation

After TS-1, the only redox-active zeotype material which has shown a genuine heterogeneous character so far and remarkable stability and recyclability is a $Sn^{(IV)}$-substituted zeolite beta, Sn-BEA (Fig. 21).[299,300] In this solid, isolated tetrahedral tin sites are inserted and evenly dispersed into the zeolite BEA framework. They show noteworthy and enhanced activity for the Baeyer–Villiger oxidation of cyclic ketones, aromatic aldehydes and α,β-unsaturated aldehydes. The singular behaviour of [Sn]-BEA with hydrogen peroxide was first evidenced in comparison with [Ti]-BEA. These two zeolites were studied in the oxidation of dihydrocarvone under the same conditions. Major amounts of the corresponding cyclic lactone were observed over the former, whereas the latter formed large amounts of the epoxidised product. It is noteworthy that titanium-containing zeolites are practically inactive in the Baeyer–Villiger oxidation.[301] Detailed studies combining spectroscopic (IR spectroscopy of adsorbed acetonitrile),

Table 2 Comparison of the catalytic performance of grafted [Ti]–SiO_2 and [Nb]–SiO_2 catalysts in the liquid-phase epoxidation of limonene in the presence of TBHP and H_2O_2. Adapted from ref. 294

Catalyst	Oxidant	C[a] 1 h (%)	S[b] 1 h (%)	Endo/exo[c] 1 h	C[a] 3 h (%)	S[b] 3 h (%)	SAct[d] 1 h (h^{-1})
Nb/SiO_2-liq	H_2O_2	64	>98	24 : 76	74	>98	46
Nb/SiO_2-liq	TBHP	29	80	76 : 24	30	80	20
Ti/SiO_2-liq	H_2O_2	12	62	91 : 09	18	20	3
Ti/SiO_2-liq	TBHP	52	93	92 : 08	77	81	14

Conditions: dry CH_3CN solvent; 100 mg cat; 1.0 mmol limonene; 2.0 mmol aq. H_2O_2 or 1.1 mmol dry TBHP; solvent reflux temperature; glass batch reactor. [a] Limonene conversion. [b] Selectivity to limonene epoxide. [c] Endocyclic/exocyclic epoxide ratio. [d] Specific activity ($[mol_{converted\ limonene}]$ $[mol_{Nb}\ h]^{-1}$) after 1 h.

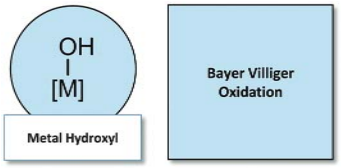

Fig. 21 Illustration of SCFs for Baeyer–Villiger oxidation.

mechanistic (DFT calculations) and kinetic experiments demonstrated that the active site is correlated with the presence of partially hydrolysed framework tin centres. In these systems, a Lewis acidic site and an adjacent basic site on the oxygen atom of the [Sn]–OH group formed upon hydrolysis are simultaneously present.[299] Such an acid–base pair is required to accomplish the following proposed catalytic mechanism (Scheme 30): (i) coordination of the cyclic ketone to the [Sn] center and of hydrogen peroxide to the [Sn]–OH "stannol" SCF; (ii) oxygen transfer from H_2O_2 to the coordinated ketone and (iii) desorption

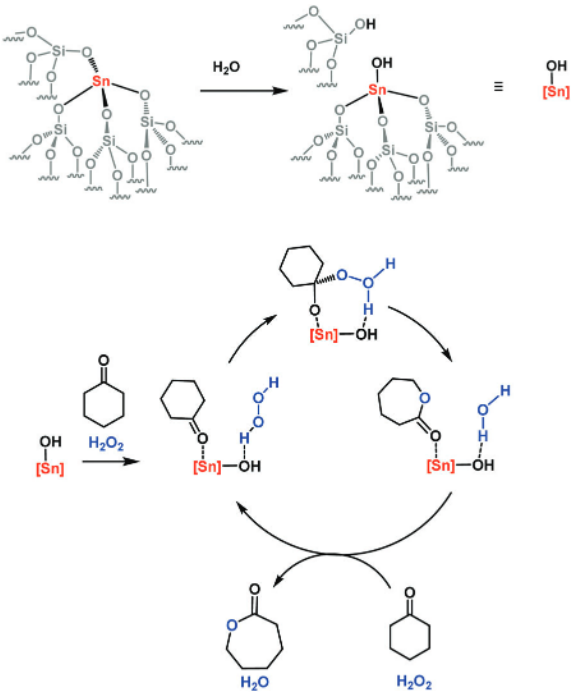

Scheme 30 Mechanism of the Baeyer–Villiger oxidation of cyclohexanone over Sn-BEA.[299]

of the lactone and water. The determining step for chemoselectivity towards Baeyer–Villiger oxidation products is the first one, the so-called "loaded complex", where the oxygen atom to be inserted from H_2O_2 is aligned for the nucleophilic attack of the activated carbonyl group of the coordinated ketone.

For Baeyer–Villiger transformations, Sn-BEA combined with hydrogen peroxide is a potential alternative to the use of conventional oxidants, such as peroxoacids, as the catalyst can be easily filtered from the reaction mixture and no detectable metal leaching is observed. In particular, Sn-BEA was successfully tested in the oxidation of delfone into δ-decalactone (an important creamy and fruity aroma for the flavours and fragrances industry) in a stirred reactor. The desired product was obtained in high yields (up to 86%), the zeolite remained active for a long time and turn-over numbers of *ca.* 10 000 were attained. Moreover, carrying out the reaction of the *R*-isomer of delfone (the most useful for flavouring purposes), the enantiomeric configuration of the migrating carbon atom was retained. This is an important feature when enantiopure ketone oxidization is carried out.

Sn-Containing Y zeolites were prepared by two-step post-synthetic methods, *via* hydrothermal dealumination and post-incorporation of the [Sn] centres by chemical vapor deposition or impregnation.[302] However, high [Sn]-content in the Sn–Y zeolite (up to 3.4 wt%) led to the formation of many inactive amorphous extra-framework [Sn] species, which also caused partial blockage of the zeolite pores and, hence, loss of catalytic efficiency.

[Sn]–OH SCFs were then obtained over mesoporous silica by grafting various R_nSnX_{4-n} precursors onto an activated MCM-41 surface.[303] In the presence of molecules with kinetic diameter smaller than the Sn-BEA pore openings (*ca.* 0.6–0.7 nm), mesoporous [Sn]-containing MCM-41 materials were less active than the zeotype counterpart. However, on bulkier cyclic ketones, such as adamantanone, cyclocitral, safranal, myrtenal, cinnamaldehyde, *para*-methoxycinnamaldehyde and piperonal, Sn-MCM-41 obtained from *n*-Bu_2SnCl_2 showed good conversions (up to 90%), high TONs and excellent selectivity.[303–306] Such higher conversions (compared to Sn-BEA) are attributed to large pore size and scarce hindering effects to diffusion. [Sn]-based silica catalysts proved to be robust towards leaching, although, catalyst deactivation was observed in some cases, likely due to the strong absorption of lactone derivatives onto the catalytically active sites. Interestingly, unsaturated ketones can be oxidised with good chemoselectivity to unsaturated lactones over [Sn]–OH sites, as they are practically inactive in the epoxidation reaction.[303]

4.3. Deperoxidation of cyclohexylhydroperoxide

The decomposition of cyclohexylhydroperoxide (chhp) into cyclohexanol and cyclohexanone is a key step in the broader oxidation process to obtain nylon-6 and nylon-6,6 polymers from cyclohexane. At the commercial level, the decomposition of chhp is performed over a homogeneous cobalt catalyst, leading to KA-oil with a quite high overall selectivity. However, the use of large amounts of alkaline species to neutralize the carboxylic acid by-products is the major drawback in such an approach.

Transition metals supported over inorganic oxides are suitable solid catalysts for the deperoxidation of chhp (Fig. 22).[218,307] Heterogeneous cobalt-containing catalysts were indeed able to promote this transformation, mainly when they are grafted on alumina, since the dimerization of the [Co]-species, leading to loss of catalytic activity, is inhibited when the metal centres are deposited on the oxide surface.[308] The system proved to be robust against Co leaching and full deperoxidation could be achieved in short reaction times (60 min), with no evident deactivation. On the other hand, when Co was embedded in a mesoporous silica matrix, as in Co-TUD-1, the deperoxidation activity of the metal sites was rather limited and the formation of some cyclohexanone due to uncatalyzed thermal propagation or termination reactions of the cyclohexylperoxo radical was invoked.[309–311] Transition metals capable of undergoing a one-electron switch, such as $Co^{(II)}$, $Mn^{(II)}$ or $Cr^{(II)}$, are able to catalyze the homolytic cleavage of chhp, then giving rise to the formation of cyclohexanol, cyclohexanone and other oxygenated side products (among which also molecular oxygen).[312]

Well-characterised surface-coordination species could be prepared with group 4 metals over $SiO_{2\text{-}700}$ using the SOMC approach.[218,307,313] In these systems, group IV centres, which are less prone to undergo a redox switch, promote the deperoxidation reaction *via* a heterolytic pathway. Accordingly, the [M]-OR SCF acts as a coordination site for the cyclohexylperoxo moiety, according to a mechanism that is fully consistent to the one observed for chhp deperoxidation over metal-free acid beta zeolites.[314]

Comparative deperoxidation tests showed that supported [Ti] was the most efficient catalyst amongst the metals of group 4 (Table 3).[214] However, its activity is lower than the corresponding molecular catalysts. It should also be mentioned that metal leaching was detected for the initial reaction time (*ca.* 30% of the overall amount), although specific heterogeinity tests confirmed that leached species were not responsible for the catalytic activity.[307] Furthermore, the co-presence of radical (uncatalyzed) pathways cannot be fully excluded.[315]

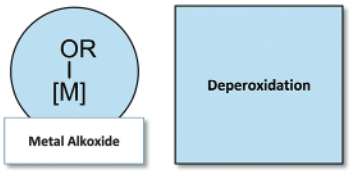

Fig. 22 Illustration of SCFs for the deperoxidation reaction.

Table 3 Comparison of group 4 metals in cyclohexylhydroperoxide deperoxidation

Catalyst	Ratio chhp/catal	Ratio chhp/catal (h)	Conv. (%)	TON	Init TOF[a] (h^{-1})
$(\equiv SiO)_3Ti(O^tBu)$	260	6	85	221	187
$(\equiv SiO)_3Zr(O^tBu)$	260	6	45	118	32
$(\equiv SiO)_3Hf(O^tBu)$	260	11	40	104	20

[a] TOF calculated at 0.5 h.

Group V metals (vanadium, niobium, tantalum) were studied with a focus on alkoxo-type derivatives. This was due to the difficulty to prepare alkyl or hydride-type compounds. Surface organometallic complexes were prepared (i) either by grafting an alkyl-complex in the presence of an alcohol or (ii) by starting directly from an alkoxy-compound on silica. In all cases, resulting complexes have been characterized by all surface organometallic chemistry techniques (EXAFS and solid NMR (1D and 2D with ^{13}C labeled compounds)). Several (mono-, bi- and tri-podal) compounds were reported.[313]

Group V compounds presented comparable catalytic performances to those obtained for Ti SCF. Remarkably, no metal leaching was detected in solution, a rare case in heterogeneous catalysis with such reactive media, indicating a true heterogeneous nature of the catalysts. As desired, two major reaction products, cyclohexanol and cyclohexanone, were identified (Schemes 31 and 32). Since relatively lower yields were achieved, with respect to the conventional homogeneous systems, Ta-based SOMC have not yet found full industrial exploitation.[316]

4.4. Phenol oxidation into quinones

The selective oxidation of substituted phenols plays a key role in several organic syntheses as well as in biochemical systems. TS-1 zeotype cannot be efficiently used as the average kinetic diameter of the substrate molecules are larger than the micropores of the catalyst itself.[317] For this reason [Ti]-containing mesoporous silica catalysts obtained by SOMC (Fig. 23) were

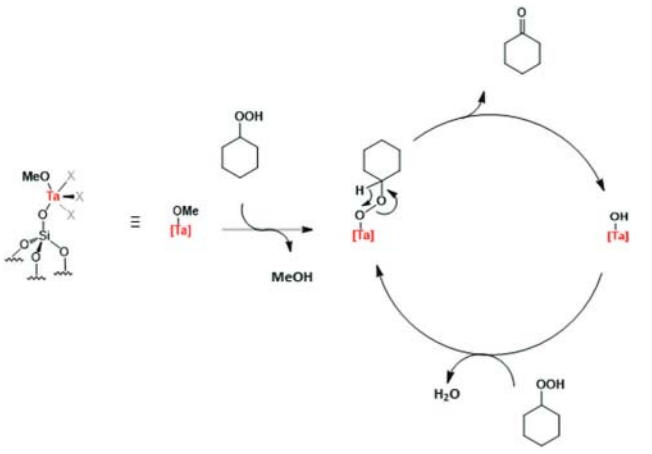

Scheme 31 Possible mechanism of deperoxidation of cyclohexylhydroperoxide using a monopodal [Ta]–methoxy catalyst.[218]

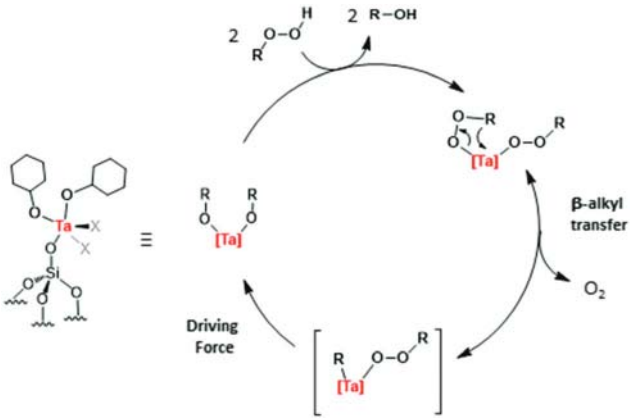

Scheme 32 Possible mechanism of deperoxidation of alkyl-hydroperoxide using a monopodal [Ta]–bis-alkoxy catalyst.[218]

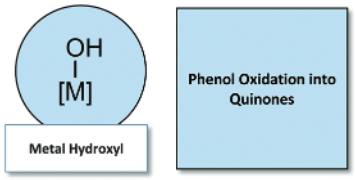

Fig. 23 Illustration of SCFs for phenol oxidation.

applied to the oxidation of 2,6-di-*tert*-butylphenol, DTBP, into *para*-benzoquinone in the presence of aqueous H_2O_2.

Nevertheless, it is worth highlighting that the use of [Ti]-catalysts with too large mesopore sizes or with a non-porous structure (using a pyrogenic silica as a support)[279] did not lead to any improvement in terms of catalytic performance either.

Mesoporous [Ti]–, [Zr]– and [V]–silica catalysts were prepared by grafting metallocene precursors onto the activated silica surface. Even though these complexes were active in phenol oxidation,[227,318,319,320] some of these systems suffered from leaching of active species in the reaction medium. In particular, this was observed for [V]-systems and, to a lesser extent, for [Zr]-based ones.[319]

A [Ti]-containing system, obtained by grafting titanocene dichloride onto commercial non-ordered activated silica,[321,322] was found to be the optimal catalyst, for the oxidation of 2,3,6-trimethylphenol, TMP, to trimethyl-*para*-benzoquinone, TMBQ, an important vitamin E intermediate. A quasi-quantitative yield of TMBQ (99% yield) was obtained after 1 h and no leaching of the homogeneous [Ti]-species was found, confirming the heterogeneous nature of the catalysis. To further enhance the catalyst performance (i) a polar aprotic solvent, such as acetonitrile, was used together with (ii) a slight excess of H_2O_2, (iii) a low phenol to [Ti] site ratio and, above all, (iv) an optimal [Ti]-concentration in the range of 0.7–1.0 sites per nm^2.[322] The plot of the chemoselectivity to TMBQ *vs.* [Ti] surface concentration displayed a clear bell-shaped trend (Fig. 24).[322] Indeed, lower [Ti] concentrations led to poorly selective mixtures of TMBQ and 2,2′,3,3′,5,5′-hexamethyl-4,4′-biphenol, while too

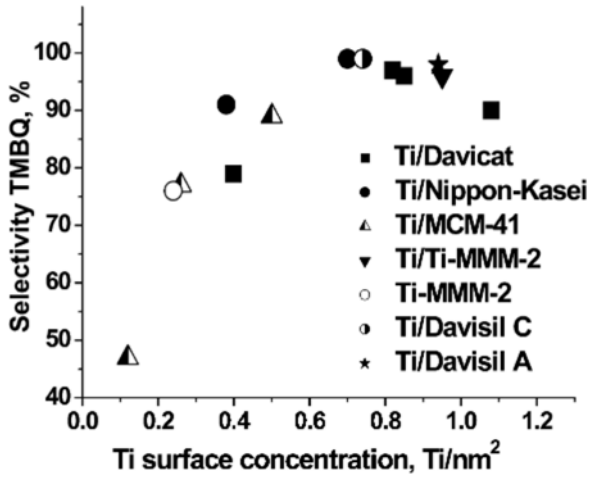

Fig. 24 Trend plot of TMBQ selectivity vs. [Ti] SCF surface density for a series of mesoporous Ti-grafted silica catalysts. Reaction conditions: 0.1 M TMP, 0.35 M H_2O_2, 0.006 mmol Ti sites, 1 mL acetonitrile, 80 °C, glass batch reactor. Adapted with permission from ref. 322, Copyright 2009, John Wiley and Sons.

high densities of [Ti] sites led to TiO_2-like nano-domains and consequently to an undesired disproportionation and decomposition of H_2O_2.[323]

From experimental and spectroscopic evidence (especially by DR-UV-vis and Raman spectroscopy), it was concluded that [Ti]–OH were distributed in close proximity across silica mesopores. This is a key feature in order to reach high TMBQ selectivity values. Moreover, the occurrence of a homolytic pathway, leading to the formation of active phenoxyl radicals during TMP oxidation over the [Ti]–silica catalyst, was confirmed by EPR techniques using the spin-trap agent, 3,5-dibromo-4-nitrosobenzene-sulfonic acid. Such evidence led to a mechanistic picture of the catalytic oxidation of substituted alkylphenols to quinones as reported (Scheme 33).[215,321,324]

A fine tuning of the surface concentration of [Ti] SCFs was confirmed on other thick-walled mesoporous Ti-SBA-15 systems too, when used for the oxidation of a wide series of di- and tri-substituted phenols.[325]

4.5. Considerations and future perspectives

Single-site heterogeneous catalysts containing redox-active centres can find an application as alternatives to stoichiometric non-catalytic processes, still largely used in oxidation reactions. In these transformations, hazardous or environmentally unfriendly reactants, also in over-stoichiometric ratios, are indeed still largely employed. Single-site catalysts, with defined SFCs, proved in some cases to be robust, easily recyclable and virtually ideal candidates for setting up innovative chemo- and regio-selective oxidation processes at the large-scale level. Furthermore, thanks to large mesopore silica supports, bulky substrates, typically used in fine chemical synthesis, can be easily accommodated and the high added-value of the obtained product can pay back the use of catalysts prepared by using expensive or unusual building blocks.

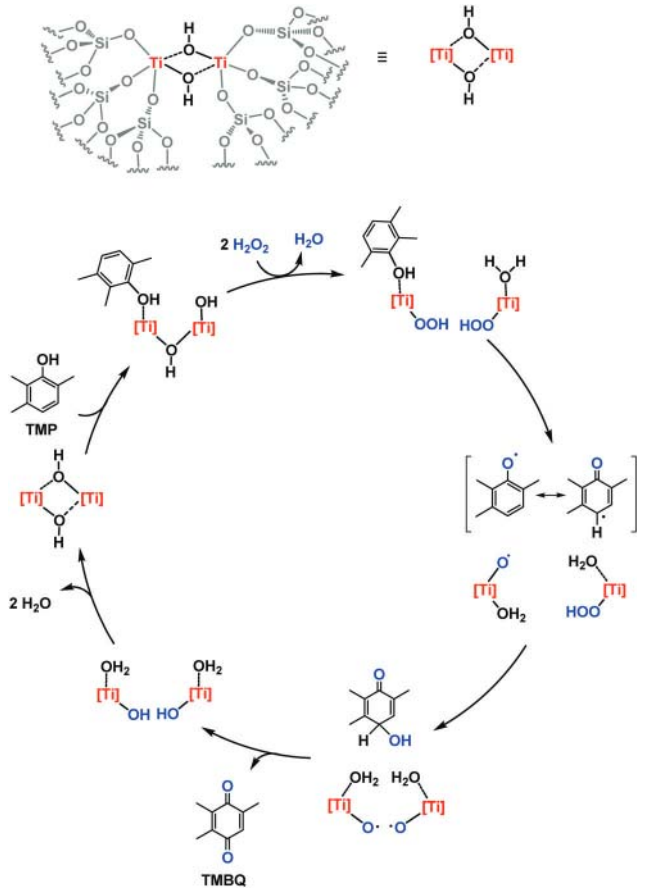

Scheme 33 Oxidation of substituted alkylphenols to related quinines in the presence of aqueous H_2O_2 over dinuclear [Ti]–OH SCFs. Adapted from ref. 322 and 324.

However, the development of bio-inspired truly inorganic equivalents of enzymes based on porous catalysts obtained *via* SOMC, which show comparable activity and selectivity, is still a challenge in most cases. The only notable exceptions are the successful examples of zeolites and zeotypes containing titanium (TS-1) and tin sites (Sn-BEA). This ends up in a major limitation to the efficient use of single metal site catalysts at the industrial level.

In this case too, a trans-disciplinary approach, based on the interlinked cooperation across chemists with different skills and backgrounds (in heterogeneous catalysis, organometallic chemistry, molecular modelling, biochemistry, organic synthesis, materials sciences, *etc.*) can be the only successful strategy to obtain durable results in this field in the following years.

5. Conclusion

Energy and environment are crucial challenges of our modern societies. Catalysis is at the centre of this paradigm. Among the most important catalytic transformations related to energy and environment, we have selected the activation functionalization of methane and paraffins, the activation and functionalization of CO_2 and the oxidation reactions. We have tried to show that when the active site is well defined, mostly, but not necessarily, by the SOMC strategy, the resulting single site approach leads to a rational understanding of the catalytic phenomenon. This rational understanding leads (i) to the discovery of new catalytic reactions which did not exist in homogeneous or heterogeneous catalysis, and (ii) to improved activities, selectivities and lifetimes of already existing reactions.

For almost each case, the mechanisms proposed are derived from the elementary steps postulated or demonstrated in molecular chemistry. By mechanism, we mean here the ways bonds are broken or formed to give the products and not the full range of steps going from the adsorption of reactants, their diffusion to the active site and the desorption of the products from the surface to the gas or liquid phase. In most cases, we have shown in this review article that the synthesis of the catalyst is starting from a "reaction intermediate" that was postulated in molecular chemistry and presumed to be part of the catalytic cycle. This reaction intermediate is either a surface organometallic fragment (SOMF) or a surface coordination fragment (SCF). In the case of the SOMF we have represented this reaction intermediate by [M](–R)(–R′), but we have added a spectator ligand X which may control the coordination, the electron density of the metal, along with the steric requirements. R and R′ can be identical or different. For example, in alkane metathesis one generation of catalyst contains R = H for C–H bond activation and R′ = CH_2 for olefin metathesis. We have thus introduced the concept of "cascade reactions" occurring on the same metal. The concept of cascade reactions may also be introduced by a combination of metal and support (as in the case of methane dehydro-aromatisation with Mo/ZSM-5). In the case of coordination fragments mostly used in oxidation they frequently employ alkoxides or oxygen containing ligands (hydroperoxy). Lewis acids belong to this category as explained in the mechanism of cyclic carbonate formation from CO_2 and epoxides.

Obviously other parameters than surface organometallic fragments or surface coordination fragments play a role such as (i) the rigidity of the surface which prevents bimolecular reactions responsible for deactivation, (ii) the chemical properties of the surface (*e.g.* acidity, redox, . . .), (iii) the physical properties of the surface (hydrophobic and hydrophilic, porosity, *etc.*). The "single site" approach is thus enriched by the superposition of the properties of the active metal/ligand associated with the properties of the support, which makes this field unique, outside classical homogeneous or classical heterogeneous catalysis.

Conflicts of interest

There are no conflicts to declare.

Acknowledgements

We thank KAUST for financial and human support and all our friends who helped us to develop the field in Europe, China, America, Japan, and Saudi Arabia. VDE thanks the Thailand Research Fund for generous support (Grant No. RSA6080059).

Notes and references

1 J.-M. Basset and R. Ugo, in *Modern Surface Organometallic Chemistry*, ed. R. Psaro, J.-M. Basset, D. Roberto and R. Ugo, Wiley-VCH Verlag GmbH & Co KGaA, Weinheim, 2009, ch. 1, pp. 1–21.

2 J. D. A. Pelletier and J. M. Basset, *Acc. Chem. Res.*, 2016, 49, 664–677.

3 S. Barman, N. Maity, K. Bhatte, S. Ould-Chikh, O. Dachwald, C. Haeßner, Y. Saih, E. Abou-Hamad, I. Llorens, J.-L. Hazemann, K. Köhler, V. D' Elia and J.-M. Basset, *ACS Catal.*, 2016, **6**, 5908–5921.

4 R. P. Saint-Arroman, M. Chabanas, A. Baudouin, C. Copéret, J.-M. Basset, A. Lesage and L. Emsley, *J. Am. Chem. Soc.*, 2001, **123**, 3820–3821.

5 D. D. Laws, H.-M. L. Bitter and A. Jerschow, *Angew. Chem., Int. Ed.*, 2002, **41**, 3096–3129.

6 S. E. Ashbrook and S. Sneddon, *J. Am. Chem. Soc.*, 2014, **136**, 15440–15456.

7 D. Grekov, T. Vancompernolle, M. Taoufik, L. Delevoye and R. M. Gauvin, *Chem. Soc. Rev.*, 2018, **47**, 2572–2590.

8 A. J. Rossini, A. Zagdoun, M. Lelli, A. Lesage, C. Copéret and L. Emsley, *Acc. Chem. Res.*, 2013, **46**, 1942–1951.

9 M. A. Newton and W. van Beek, *Chem. Soc. Rev.*, 2010, **39**, 4845–4863.

10 A. I. Frenkel, J. A. Rodriguez and J. G. Chen, *ACS Catal.*, 2012, **2**, 2269–2280.

11 P. Serna and B. C. Gates, *Acc. Chem. Res.*, 2014, **47**, 2612–2620.

12 F. Blanc, J.-M. Basset, C. Copéret, A. Sinha, Z. J. Tonzetich, R. R. Schrock, X. Solans-Monfort, E. Clot, O. Eisenstein, A. Lesage and L. Emsley, *J. Am. Chem. Soc.*, 2008, **130**, 5886–5900.

13 I. Romanenko, D. Gajan, R. Sayah, D. Crozet, E. Jeanneau, C. Lucas, L. Leroux, L. Veyre, A. Lesage, L. Emsley, E. Lacôte and C. Thieuleux, *Angew. Chem., Int. Ed.*, 2015, **54**, 12937–12941.

14 V. D'Elia, H. Dong, A. J. Rossini, C. M. Widdifield, S. V. C. Vummaleti, Y. Minenkov, A. Poater, E. Abou-Hamad, J. D. A. Pelletier, L. Cavallo, L. Emsley and J.-M. Basset, *J. Am. Chem. Soc.*, 2015, **137**, 7728–7739.

15 Z. S. Qureshi, A. Hamieh, S. Barman, N. Maity, M. K. Samantaray, S. Ould-Chikh, E. Abou-hamad, L. Falivene, V. D'Elia, A. Rothenberger, I. Llorens, J.-L. Hazemann and J.-M. Basset, *Inorg. Chem.*, 2017, **56**, 861–871.

16 P. Berruyer, M. Lelli, M. P. Conley, D. L. Silverio, C. M. Widdifield, G. Siddiqi, D. Gajan, A. Lesage, C. Copéret and L. Emsley, *J. Am. Chem. Soc.*, 2017, **139**, 849–855.

17 E. Pump, A. Bendjeriou-Sedjerari, J. Viger-Gravel, D. Gajan, B. Scotto, M. K. Samantaray, E. Abou-Hamad, A. Gurinov, W. Almaksoud, Z. Cao, A. Lesage, L. Cavallo, L. Emsley and J.-M. Basset, *Chem. Sci.*, 2018, **9**, 4866–4872.

18 E. Pump, J. Viger-Gravel, E. Abou-Hamad, M. K. Samantaray, B. Hamzaoui, A. Gurinov, D. H. Anjum, D. Gajan, A. Lesage, A. Bendjeriou-Sedjerari, L. Emsley and J.-M. Basset, *Chem. Sci.*, 2017, **8**, 284–290.

19 T.-C. Ong, W.-C. Liao, V. Mougel, D. Gajan, A. Lesage, L. Emsley and C. Copéret, *Angew. Chem., Int. Ed.*, 2016, **55**, 4743–4747.

20 F. Humblot, F. Lepeltier, J. P. Candy, J. Corker, O. Clause, F. Bayard and J. M. Basset, *J. Am. Chem. Soc.*, 1998, **120**, 137–146.

21 N. Maity, S. Barman, Y. Minenkov, S. Ould-Chikh, E. Abou-Hamad, T. Ma, Z. S. Qureshi, L. Cavallo, V. D'Elia, B. C. Gates and J.-M. Basset, *ACS Catal.*, 2018, **8**, 2715–2729.

22 D. Yang, S. O. Odoh, T. C. Wang, O. K. Farha, J. T. Hupp, C. J. Cramer, L. Gagliardi and B. C. Gates, *J. Am. Chem. Soc.*, 2015, **137**, 7391–7396.

23 N. Merle, F. Le Quéméner, Y. Bouhoute, K. C. Szeto, A. De Mallmann, S. Barman, M. K. Samantaray, L. Delevoye, R. M. Gauvin, M. Taoufik and J.-M. Basset, *J. Am. Chem. Soc.*, 2017, **139**, 2144–2147.

24 M. Yang, J. Liu, S. Lee, B. Zugic, J. Huang, L. F. Allard and M. Flytzani-Stephanopoulos, *J. Am. Chem. Soc.*, 2015, **137**, 3470–3473.

25 E. J. Peterson, A. T. DeLaRiva, S. Lin, R. S. Johnson, H. Guo, J. T. Miller, J. Hun Kwak, C. H. F. Peden, B. Kiefer, L. F. Allard, F. H. Ribeiro and A. K. Datye, *Nat. Commun.*, 2014, **5**, 4885.

26 H. Wei, X. Liu, A. Wang, L. Zhang, B. Qiao, X. Yang, Y. Huang, S. Miao, J. Liu and T. Zhang, *Nat. Commun.*, 2014, **5**, 5634.

27 G. Zwaschka, M. Rondelli, M. Krause, M. D. Rötzer, M. N. Hedhili, U. Heiz, J. M. Basset, F. F. Schweinberger and V. D'Elia, *New J. Chem.*, 2018, **42**, 3035–3041.

28 M. Rondelli, G. Zwaschka, M. Krause, M. D. Rötzer, M. N. Hedhili, M. P. Högerl, V. D'Elia, F. F. Schweinberger, J.-M. Basset and U. Heiz, *ACS Catal.*, 2017, **7**, 4152–4162.

29 B. Qiao, A. Wang, X. Yang, L. F. Allard, Z. Jiang, Y. Cui, J. Liu, J. Li and T. Zhang, *Nat. Chem.*, 2011, **3**, 634–641.

30 X.-F. Yang, A. Wang, B. Qiao, J. Li, J. Liu and T. Zhang, *Acc. Chem. Res.*, 2013, **46**, 1740–1748.

31 S. Liang, C. Hao and Y. Shi, *ChemCatChem*, 2015, **7**, 2559–2567.

32 A. Wang, J. Li and T. Zhang, *Nat. Rev. Chem.*, 2018, **2**, 65–81.

33 B. C. Gates, M. Flytzani-Stephanopoulos, D. A. Dixon and A. Katz, *Catal. Sci. Technol.*, 2017, **7**, 4259–4275.

34 H. Yan, H. Cheng, H. Yi, Y. Lin, T. Yao, C. Wang, J. Li, S. Wei and J. Lu, *J. Am. Chem. Soc.*, 2015, **137**, 10484–10487.

35 G. Kyriakou, M. B. Boucher, A. D. Jewell, E. A. Lewis, T. J. Lawton, A. E. Baber, H. L. Tierney, M. Flytzani-Stephanopoulos and E. C. H. Sykes, *Science*, 2012, **335**, 1209–1212.

36 N. Maity, S. Barman, Y. Minenkov, S. Ould-Chikh, E. Abou-Hamad, T. Ma, Z. S. Qureshi, L. Cavallo, V. D'Elia, B. C. Gates and J.-M. Basset, *ACS Catal.*, 2018, **8**, 2715–2729.

37 M. Pucino, V. Mougel, R. Schowner, A. Fedorov, M. R. Buchmeiser and C. Copéret, *Angew. Chem., Int. Ed.*, 2016, **55**, 4300–4302.

38 E. Díaz, A. Restrepo and F. Núñez-Zarur, *Organometallics*, 2018, **37**, 2023–2036.

39 Y. Liang and R. Anwander, *Dalton Trans.*, 2013, **42**, 12521–12545.
40 S. L. Wegener, T. J. Marks and P. C. Stair, *Acc. Chem. Res.*, 2011, **45**, 206–214.
41 C. Copéret, F. Allouche, K. W. Chan, M. P. Conley, M. F. Delley, A. Fedorov, I. B. Moroz, V. Mougel, M. Pucino, K. Searles, K. Yamamoto and P. A. Zhizhko, *Angew. Chem., Int. Ed.*, 2018, **57**, 6398–6440.
42 C. Copéret, A. Comas-Vives, M. P. Conley, D. P. Estes, A. Fedorov, V. Mougel, H. Nagae, F. Núñez-Zarur and P. A. Zhizhko, *Chem. Rev.*, 2016, **116**, 323–421.
43 C. Pratt and K. Tate, *Environ. Sci. Technol.*, 2018, **52**, 6084–6097.
44 A. I. Olivos-Suarez, À. Szécsényi, E. J. M. Hensen, J. Ruiz-Martinez, E. A. Pidko and J. Gascon, *ACS Catal.*, 2016, **6**, 2965–2981.
45 K. Searles, G. Siddiqi, O. V. Safonova and C. Copéret, *Chem. Sci.*, 2017, **8**, 2661–2666.
46 K. C. Szeto, Z. R. Jones, N. Merle, C. Rios, A. Gallo, F. Le Quemener, L. Delevoye, R. M. Gauvin, S. L. Scott and M. Taoufik, *ACS Catal.*, 2018, **8**, 7566–7577.
47 A. M. Love, C. A. Carrero, A. Chieregato, J. T. Grant, S. Conrad, R. Verel and I. Hermans, *Chem. Mater.*, 2016, **28**, 5495–5504.
48 I. Hermans, E. S. Spier, U. Neuenschwander, N. Turrà and A. Baiker, *Top. Catal.*, 2009, **52**, 1162–1174.
49 A. C. Lindhorst, S. Haslinger and F. E. Kühn, *Chem. Commun.*, 2015, **51**, 17193–17212.
50 O. A. Kholdeeva, *Catal. Sci. Technol.*, 2014, **4**, 1869–1889.
51 C. L. Hill, *Nature*, 1999, **401**, 436–437.
52 K. Weissermel and H.-J. Arpe, in *Industrial Organic Chemistry Fourth Edition*, ed. K. Weissermel and H.-J. Arpe, Wiley-VCH Verlag GmbH & Co KGaA, Weiheim, 2008, ch. 8, pp. 193–215.
53 K. I. Goldberg and A. S. Goldman, *Acc. Chem. Res.*, 2017, **50**, 620–626.
54 J. Chatt and J. M. Davidson, *J. Chem. Soc.*, 1965, 843–855.
55 Y. Fujiwara, I. Moritani, S. Danno, R. Asano and S. Teranishi, *J. Am. Chem. Soc.*, 1969, **91**, 7166–7169.
56 M. L. Green and P. J. Knowles, *J. Chem. Soc. D*, 1970, 1677.
57 P. Foley and G. M. Whitesides, *J. Am. Chem. Soc.*, 1979, **101**, 2732–2733.
58 G. E. Keller and M. M. Bhasin, *J. Catal.*, 1982, **73**, 9–19.
59 M. E. Thompson, S. M. Baxter, A. R. Bulls, B. J. Burger, M. C. Nolan, B. D. Santarsiero, W. P. Schaefer and J. E. Bercaw, *J. Am. Chem. Soc.*, 1987, **109**, 203–219.
60 C. Lecuyer, F. Quignard, A. Choplin, D. Olivier and J. M. Basset, *Angew. Chem., Int. Ed. Engl.*, 1991, **30**, 1660–1661.
61 F. Quignard, C. Lecuyer, A. Choplin, D. Olivier and J.-M. Basset, *J. Mol. Catal.*, 1992, **74**, 353–363.
62 V. R. Dufaud and J. M. Basset, *Angew. Chem., Int. Ed.*, 1998, **37**, 806–810.
63 F. Rataboul, A. Baudouin, C. Thieuleux, L. Veyre, C. Copéret, J. Thivolle-Cazat, J.-M. Basset, A. Lesage and L. Emsley, *J. Am. Chem. Soc.*, 2004, **126**, 12541–12550.
64 N. S. Radu and T. D. Tilley, *J. Am. Chem. Soc.*, 1995, **117**, 5863–5864.
65 S. Norsic, C. Larabi, M. Delgado, A. Garron, A. de Mallmann, C. Santini, K. C. Szeto, J.-M. Basset and M. Taoufik, *Catal. Sci. Technol.*, 2012, **2**, 215–219.
66 P. L. Watson, *J. Am. Chem. Soc.*, 1983, **105**, 6491–6493.
67 P. L. Watson, *J. Chem. Soc., Chem. Commun.*, 1983, 276–277.
68 C. Rosier, G. P. Niccolai and J. M. Basset, *J. Am. Chem. Soc.*, 1997, **119**, 12408–12409.
69 S. Soignier, M. Taoufik, E. Le Roux, G. Saggio, C. Dablemont, A. Baudouin, F. Lefebvre, A. de Mallmann, J. Thivolle-Cazat, J.-M. Basset, G. Sunley and B. M. Maunders, *Organometallics*, 2006, **25**, 1569–1577.
70 G. Tosin, C. C. Santini, A. Baudouin, A. De Mallman, S. Fiddy, C. Dablemont and J.-M. Basset, *Organometallics*, 2007, **26**, 4118–4127.
71 M. Chabanas, V. Vidal, C. Coperet, J. Thivolle-Cazat and J. M. Basset, *Angew. Chem., Int. Ed.*, 2000, **39**, 1962–1965.
72 G. Parkin, E. Bunel, B. J. Burger, M. S. Trimmer, A. Vanasselt and J. E. Bercaw, *J. Mol. Catal.*, 1987, **41**, 21–39.
73 M. Leconte, A. Theolier and J. M. Basset, *J. Mol. Catal.*, 1985, **28**, 217–231.
74 E. Pump, Z. Cao, M. K. Samantaray, A. Bendjeriou-Sedjerari, L. Cavallo and J.-M. Basset, *ACS Catal.*, 2017, **7**, 6581–6586.
75 J. M. Basset, C. Copéret, L. Lefort, B. M. Maunders, O. Maury, E. Le Roux, G. Saggio, S. Soignier, D. Soulivong, G. J. Sunley, M. Taoufik and J. Thivolle-Cazat, *J. Am. Chem. Soc.*, 2005, **127**, 8604–8605.
76 F. Rascon and C. Coperet, *J. Organomet. Chem.*, 2011, **696**, 4121–4131.
77 C. Coperet, O. Maury, J. Thivolle-Cazat and J. M. Basset, *Angew. Chem., Int. Ed.*, 2001, **40**, 2331–2334.
78 A. M. Pyle and K. J. Jens, *J. Mol. Catal.*, 1986, **38**, 337–339.
79 G. L. Casty, M. G. Matturro, G. R. Myers, R. P. Reynolds and R. B. Hall, *Organometallics*, 2001, **20**, 2246–2249.
80 V. A. Zakharov, V. K. Dudchenko, E. A. Paukshtis, L. G. Karakchiev and Y. I. Yermakov, *J. Mol. Catal.*, 1977, **2**, 421–435.
81 M. Jezequel, V. Dufaud, M. J. Ruiz-Garcia, F. Carrillo-Hermosilla, U. Neugebauer, G. P. Niccolai, F. Lefebvre, F. Bayard, J. Corker, S. Fiddy, J. Evans, J. P. Broyer, J. Malinge and J. M. Basset, *J. Am. Chem. Soc.*, 2001, **123**, 3520–3540.
82 C. Thieuleux, C. Coperet, V. Dufaud, C. Marangelli, E. Kuntz and J. M. Basset, *J. Mol. Catal. A: Chem.*, 2004, **213**, 47–57.
83 F. Quignard, A. Choplin and J. M. Basset, *J. Chem. Soc., Chem. Commun.*, 1991, 1589–1590.
84 C. Thieuleux, E. A. Quadrelli, J. M. Basset, J. Dobler and J. Sauer, *Chem. Commun.*, 2004, 1729–1731.
85 J. Corker, F. Lefebvre, C. Lecuyer, V. Dufaud, F. Quignard, A. Choplin, J. Evans and J. M. Basset, *Science*, 1996, **271**, 966–969.
86 V. Vidal, A. Theolier, J. Thivolle-Cazat and J. M. Basset, *Science*, 1997, **276**, 99–102.
87 T. Koerts, M. J. A. G. Deelen and R. A. van Santen, *J. Catal.*, 1992, **138**, 101–114.

88 T. Koerts and R. A. van Santen, *J. Mol. Catal.*, 1992, **74**, 185–191.
89 M. T. Portilla, F. J. Llopis and C. Martinez, *Catal. Sci. Technol.*, 2015, **5**, 3806–3821.
90 B. L. Farrell, V. O. Igenegbai and S. Linic, *ACS Catal.*, 2016, **6**, 4340–4346.
91 J. H. Lunsford, *Angew. Chem., Int. Ed.*, 1995, **34**, 970–980.
92 J. A. Labinger, *Catal. Lett.*, 1988, **1**, 371–375.
93 N. A. S. Amin and S. E. Peng, *Pertanika J. Sci. Technol.*, 2009, **17**, 363–370.
94 Y. Xu, X. Bao and L. Lin, *J. Catal.*, 2003, **216**, 386–395.
95 K. Sun, D. M. Ginosar, T. He, Y. Zhang, M. Fan and R. Chen, *Ind. Eng. Chem. Res.*, 2018, **57**, 1768–1789.
96 D. Soulivong, S. Norsic, M. Taoufik, C. Coperet, J. Thivolle-Cazat, S. Chakka and J.-M. Basset, *J. Am. Chem. Soc.*, 2008, **130**, 5044–5045.
97 K. C. Szeto, S. Norsic, L. Hardou, E. Le Roux, S. Chakka, J. Thivolle-Cazat, A. Baudouin, C. Papaioannou, J. M. Basset and M. Taoufik, *Chem. Commun.*, 2010, **46**, 3985–3987.
98 Y. Chen, E. Abou-hamad, A. Hamieh, B. Hamzaoui, L. Emsley and J. M. Basset, *J. Am. Chem. Soc.*, 2015, **137**, 588–591.
99 L. S. Wang, L. X. Tao, M. S. Xie, G. F. Xu, J. S. Huang and Y. D. Xu, *Catal. Lett.*, 1993, **21**, 35–41.
100 X. G. Guo, G. Z. Fang, G. Li, H. Ma, H. J. Fan, L. Yu, C. Ma, X. Wu, D. H. Deng, M. M. Wei, D. L. Tan, R. Si, S. Zhang, J. Q. Li, L. T. Sun, Z. C. Tang, X. L. Pan and X. H. Bao, *Science*, 2014, **344**, 616–619.
101 C. Karakaya, S. H. Morejudo, H. Zhu and R. J. Kee, *Ind. Eng. Chem. Res.*, 2016, **55**, 9895–9906.
102 B. M. Weckhuysen, D. Wang, M. P. Rosynek and J. H. Lunsford, *J. Catal.*, 1998, **175**, 347–351.
103 J. Yang, F. Deng, M. Zhang, Q. Luo and C. Ye, *J. Mol. Catal. A: Chem.*, 2003, **202**, 239–246.
104 Y. Shu, R. Ohnishi and M. Ichikawa, *Appl. Catal., A*, 2003, **252**, 315–329.
105 P. M. Bijani, M. Sohrabi and S. Sahebdelfar, *Chem. Eng. Technol.*, 2012, **35**, 1825–1832.
106 L. Su, L. Liu, J. Zhuang, H. Wang, Y. Li, W. Shen, Y. Xu and X. Bao, *Catal. Lett.*, 2003, **91**, 155–167.
107 R. Horn and R. Schlogl, *Catal. Lett.*, 2015, **145**, 23–39.
108 K. S. Wong, J. W. Thybaut, E. Tangstad, M. W. Stöcker and G. B. Marin, *Microporous Mesoporous Mater.*, 2012, **164**, 302–312.
109 N. Kosinov, F. J. A. G. Coumans, E. A. Uslamin, A. S. G. Wijpkema, B. Mezari and E. J. M. Hensen, *ACS Catal.*, 2017, **7**, 520–529.
110 K. Föttinger, in *Fuel Production with Heterogeneous Catalysis*, ed. J. Sa, CRC Press, Boca Raton, 2014, ch. 7, pp. 193–212.
111 D. Zhou, S. Zuo and S. Xing, *J. Phys. Chem. C*, 2012, **116**, 4060–4070.
112 S. Shetty, S. Sivakumar, S. K. Jana and G. Sreenivasarao, *Catal. Lett.*, 2018, **148**, 68–78.
113 J. P. van den Berg, J. P. Wolthuizen and J. H. C. van Hooff, *J. Catal.*, 1983, **80**, 139–144.
114 A. Corma and S. Iborra, in *Catalysts for Fine Chemical Synthesis*, ed. E. G. Derouane, Wiley & Sons, Chichester, 2006, ch. 6, pp. 125–140.
115 P. Schwach, X. Pan and X. Bao, *Chem. Rev.*, 2017, **117**, 8497–8520.
116 M. Sakbodin, Y. Wu, S. C. Oh, E. D. Wachsman and D. Liu, *Angew. Chem., Int. Ed.*, 2016, **55**, 16149–16152.
117 B. M. Weckhuysen, D. Wang, M. P. Rosynek and J. H. Lunsford, *J. Catal.*, 1998, **175**, 338–346.
118 B. M. Weckhuysen, D. Wang, M. P. Rosynek and J. H. Lunsford, *Angew. Chem., Int. Ed.*, 1997, **36**, 2374–2376.
119 P. Tan, *J. Catal.*, 2016, **338**, 21–29.
120 Y. Lai and G. Veser, *Catal. Sci. Technol.*, 2016, **6**, 5440–5452.
121 L. R. Enakonda, L. Zhou, Y. Saih, S. Ould-Chikh, S. Lopatin, D. Gary, P. Del-Gallo and J. M. Basset, *ChemSusChem*, 2016, **9**, 1911–1915.
122 J. M. Basset, S. Chakka, M. Taoufik and J. Thivolle-Cazat, *Eur. Pat.*, EP2022772A1, 2009.
123 L. F. Heckelsberg, R. L. Banks and G. C. Bailey, *Ind. Eng. Chem. Prod. Res. Dev.*, 1968, **7**, 29–31.
124 R. L. Burnett and T. R. Hughes, *J. Catal.*, 1973, **31**, 55–64.
125 V. Vidal, A. Théolier, J. Thivolle-Cazat, J.-M. Basset and J. Corker, *J. Am. Chem. Soc.*, 1996, **118**, 4595–4602.
126 E. Le Roux, M. Chabanas, A. Baudouin, A. de Mallmann, C. Copéret, E. A. Quadrelli, J. Thivolle-Cazat, J.-M. Basset, W. Lukens, A. Lesage, L. Emsley and G. J. Sunley, *J. Am. Chem. Soc.*, 2004, **126**, 13391–13399.
127 V. Dufaud, G. P. Niccolai, J. Thivolle-Cazat and J.-M. Basset, *J. Am. Chem. Soc.*, 1995, **117**, 4288–4294.
128 M. Leconte and J. M. Basset, *J. Am. Chem. Soc.*, 1979, **101**, 7296–7302.
129 J. L. Herisson and Y. Chauvin, *Makromol. Chem.*, 1971, **141**, 161–176.
130 E. Le Roux, M. Taoufik, M. Chabanas, D. Alcor, A. Baudouin, C. Coperet, J. Thivolle-Cazat, J. M. Basset, A. Lesage, S. Hediger and L. Emsley, *Organometallics*, 2005, **24**, 4274–4279.
131 M. K. Samantaray, E. Callens, E. Abou-Hamad, A. J. Rossini, C. M. Widdifield, R. Dey, L. Emsley and J. M. Basset, *J. Am. Chem. Soc.*, 2014, **136**, 1054–1061.
132 N. Maity, S. Barman, E. Callens, M. K. Samantaray, E. Abou-Hamad, Y. Minenkov, V. D'Elia, A. S. Hoffman, C. M. Widdifield, L. Cavallo, B. C. Gates and J. M. Basset, *Chem. Sci.*, 2016, **7**, 1558–1568.
133 E. Callens, E. Abou-Hamad, N. Riache and J. M. Basset, *Chem. Commun.*, 2014, **50**, 3982–3985.
134 M. K. Samantaray, R. Dey, E. Abou-Hamad, A. Hamieh and J. M. Basset, *Chem. – Eur. J.*, 2015, **21**, 6100–6106.
135 G. E. Dobereiner, G. Erdogan, C. R. Larsen, D. B. Grotjahn and R. R. Schrock, *ACS Catal.*, 2014, **4**, 3069–3076.
136 N. Riache, E. Callens, M. K. Samantaray, N. M. Kharbatia, M. Atiqullah and J. M. Basset, *Chem. – Eur. J.*, 2014, **20**, 15089–15094.
137 N. Riache, E. Callens, J. Espinas, A. Dery, M. K. Samantaray, R. Dey and J. M. Basset, *Catal. Sci. Technol.*, 2015, **5**, 280–285.
138 G. Crépeau, V. Montouillout, A. Vimont, L. Mariey, T. Cseri and F. Maugé, *J. Phys. Chem. B*, 2006, **110**, 15172–15185.
139 Y. Lisha, A. Rui, L. Kun, C. Bo and W. Xinhong, *Curr. Pharm. Des.*, 2016, **22**, 4086–4093.

140 T. Ogoshi and T.-a. Yamagishi, *Pillararenes*, The Royal Society of Chemistry, Cambridge, 2016, pp. 1–22.
141 B. Werghi, E. Pump, M. Tretiakov, E. Abou-Hamad, A. Gurinov, P. Doggali, D. H. Anjum, L. Cavallo, A. Bendjeriou-Sedjerari and J.-M. Basset, *Chem. Sci.*, 2018, **9**, 3531–3537.
142 M. K. Samantaray, R. Dey, S. Kavitake, E. Abou-Hamad, A. Bendjeriou-Sedjerari, A. Hamieh and J.-M. Basset, *J. Am. Chem. Soc.*, 2016, **138**, 8595–8602.
143 M. K. Samantaray, S. Kavitake, N. Morlanés, E. Abou-Hamad, A. Hamieh, R. Dey and J.-M. Basset, *J. Am. Chem. Soc.*, 2017, **139**, 3522–3527.
144 M. Cokoja, C. Bruckmeier, B. Rieger, W. A. Herrmann and F. E. Kühn, *Angew. Chem., Int. Ed.*, 2011, **50**, 8510–8537.
145 M. Aresta, A. Dibenedetto and A. Angelini, *Chem. Rev.*, 2014, **114**, 1709–1742.
146 H. Takeda, C. Cometto, O. Ishitani and M. Robert, *ACS Catal.*, 2016, **7**, 70–88.
147 J. Bonin, A. Maurin and M. Robert, *Coord. Chem. Rev.*, 2017, **334**, 184–198.
148 J. Klankermayer, S. Wesselbaum, K. Beydoun and W. Leitner, *Angew. Chem., Int. Ed.*, 2016, **55**, 7296–7343.
149 Y. Zheng, W. Zhang, Y. Li, J. Chen, B. Yu, J. Wang, L. Zhang and J. Zhang, *Nano Energy*, 2017, **40**, 512–539.
150 W. H. Bernskoetter and N. Hazari, *Acc. Chem. Res.*, 2017, **50**, 1049–1058.
151 J. Artz, T. E. Müller, K. Thenert, J. Kleinekorte, R. Meys, A. Sternberg, A. Bardow and W. Leitner, *Chem. Rev.*, 2017, **118**, 434–504.
152 A. Otto, T. Grube, S. Schiebahn and D. Stolten, *Energy Environ. Sci.*, 2015, **8**, 3283–3297.
153 N. von der Assen, J. Jung and A. Bardow, *Energy Environ. Sci.*, 2013, **6**, 2721–2734.
154 Q.-W. Song, Z.-H. Zhou and L.-N. He, *Green Chem.*, 2017, **19**, 3707–3728.
155 R. R. Shaikh, S. Pornpraprom and V. D'Elia, *ACS Catal.*, 2018, **8**, 419–450.
156 G. Centi, E. A. Quadrelli and S. Perathoner, *Energy Environ. Sci.*, 2013, **6**, 1711–1731.
157 Y. Li, S. H. Chan and Q. Sun, *Nanoscale*, 2015, **7**, 8663–8683.
158 A. Goeppert, M. Czaun, J.-P. Jones, G. K. Surya Prakash and G. A. Olah, *Chem. Soc. Rev.*, 2014, **43**, 7995–8048.
159 J. Albo, M. Alvarez-Guerra, P. Castaño and A. Irabien, *Green Chem.*, 2015, **17**, 2304–2324.
160 A. Tlili, E. Blondiaux, X. Frogneux and T. Cantat, *Green Chem.*, 2015, **17**, 157–168.
161 Z. W. Ulissi, M. T. Tang, J. Xiao, X. Liu, D. A. Torelli, M. Karamad, K. Cummins, C. Hahn, N. S. Lewis, T. F. Jaramillo, K. Chan and J. K. Nørskov, *ACS Catal.*, 2017, **7**, 6600–6608.
162 C. Rogers, W. S. Perkins, G. Veber, T. E. Williams, R. R. Cloke and F. R. Fischer, *J. Am. Chem. Soc.*, 2017, **139**, 4052–4061.
163 D. Gajan, K. Guillois, P. Delichère, J.-M. Basset, J.-P. Candy, V. Caps, C. Coperet, A. Lesage and L. Emsley, *J. Am. Chem. Soc.*, 2009, **131**, 14667–14669.
164 K. Pelzer, J.-P. Candy, G. Godard and J.-M. Basset, in *Nanoparticles and Catalysis*, ed. D. Astruc, Wiley-VCH Verlag GmbH & Co. KGaA, Weinheim, 2008, ch. 18, pp. 553–620.
165 Z. S. Qureshi, P. B. Sarawade, I. Hussain, H. Zhu, H. Al-Johani, D. H. Anjum, M. N. Hedhili, N. Maity, V. D'Elia and J.-M. Basset, *ChemCatChem*, 2016, **8**, 1671–1678.
166 L. Li, L. Zhou, S. Ould-Chikh, D. H. Anjum, M. B. Kanoun, J. Scaranto, M. N. Hedhili, S. Khalid, P. V. Laveille, L. D'Souza, A. Clo and J. M. Basset, *ChemCatChem*, 2015, **7**, 819–829.
167 K. Larmier, W. C. Liao, S. Tada, E. Lam, R. Verel, A. Bansode, A. Urakawa, A. Comas-Vives and C. Copéret, *Angew. Chem., Int. Ed.*, 2017, **56**, 2318–2323.
168 N. E. Schlörer, E. J. Cabrita and S. Berger, *Angew. Chem., Int. Ed.*, 2002, **41**, 107–109.
169 M. P. Kalhor, R. Wischert, C. Copéret and H. Chermette, *New J. Chem.*, 2014, **38**, 3717–3721.
170 F. A. Pasha, A. Bendjeriou-Sedjerari, E. Abou-Hamad, K.-W. Huang and J.-M. Basset, *Chem. Commun.*, 2016, **52**, 2577–2580.
171 Y. Musashi and S. Sakaki, *J. Am. Chem. Soc.*, 2000, **122**, 3867–3877.
172 G.-J. Xia, J. W. Liu and Z.-F. Liu, *Dalton Trans.*, 2016, **45**, 17329–17342.
173 F. Hutschka, A. Dedieu, M. Eichberger, R. Fornika and W. Leitner, *J. Am. Chem. Soc.*, 1997, **119**, 4432–4443.
174 I. Osadchuk, T. Tamm and M. S. G. Ahlquist, *Organometallics*, 2015, **34**, 4932–4940.
175 A. Barthel, Y. Saih, M. Gimenez, J. D. A. Pelletier, F. E. Kühn, V. D'Elia and J.-M. Basset, *Green Chem.*, 2016, **18**, 3116–3123.
176 M. J. Kelly, A. Barthel, C. Maheu, O. Sodpiban, F.-B. Dega, S. V. C. Vummaleti, E. Abou-Hamad, J. D. A. Pelletier, L. Cavallo, V. D'Elia and J.-M. Basset, *J. CO2 Util.*, 2017, **20**, 243–252.
177 S. J. Poland and D. J. Darensbourg, *Green Chem.*, 2017, **19**, 4990–5011.
178 H. Geerlings and R. Zevenhoven, *Annu. Rev. Chem. Biomol. Eng.*, 2013, **4**, 103–117.
179 C. Martín, G. Fiorani and A. W. Kleij, *ACS Catal.*, 2015, **5**, 1353–1370.
180 J. W. Comerford, I. D. V. Ingram, M. North and X. Wu, *Green Chem.*, 2015, **17**, 1966–1987.
181 H. Büttner, L. Longwitz, J. Steinbauer, C. Wulf and T. Werner, *Top. Curr. Chem.*, 2017, 375.
182 S. Arayachukiat, P. Yingcharoen, S. V. C. Vummaleti, L. Cavallo, A. Poater and V. D'Elia, *Mol. Catal.*, 2017, **443**, 280–285.
183 B. Schäffner, F. Schäffner, S. P. Verevkin and A. Börner, *Chem. Rev.*, 2010, **110**, 4554–4581.
184 S. Fukuoka, M. Kawamura, K. Komiya, M. Tojo, H. Hachiya, K. Hasegawa, M. Aminaka, H. Okamoto, I. Fukawa and S. Konno, *Green Chem.*, 2003, **5**, 497–507.
185 B. Schäffner, M. Blug, D. Kruse, M. Polyakov, A. Köckritz, A. Martin, P. Rajagopalan, U. Bentrup, A. Brückner, S. Jung, D. Agar, B. Rüngeler, A. Pfennig, K. Müller,

W. Arlt, B. Woldt, M. Graß and S. Buchholz, *ChemSusChem*, 2014, **7**, 1133–1139.
186 Z. Han, L. Rong, J. Wu, L. Zhang, Z. Wang and K. Ding, *Angew. Chem., Int. Ed.*, 2012, **51**, 13041–13045.
187 A. W. Kleij, M. North and A. Urakawa, *ChemSusChem*, 2017, **10**, 1036–1038.
188 V. D'Elia, J. D. A. Pelletier and J.-M. Basset, *ChemCatChem*, 2015, **7**, 1906–1917.
189 V. D'Elia, A. A. Ghani, A. Monassier, J. Sofack-Kreutzer, J. D. A. Pelletier, M. Drees, S. V. C. Vummaleti, A. Poater, L. Cavallo, M. Cokoja, J.-M. Basset and F. E. Kühn, *Chem. – Eur. J.*, 2014, **20**, 11870–11882.
190 R. M. Haak, S. J. Wezenberg and A. W. Kleij, *Chem. Commun.*, 2010, **46**, 2713.
191 M. I. Childers, A. K. Vitek, L. S. Morris, P. C. B. Widger, S. M. Ahmed, P. M. Zimmerman and G. W. Coates, *J. Am. Chem. Soc.*, 2017, **139**, 11048–11054.
192 A. Monassier, V. D'Elia, M. Cokoja, H. Dong, J. D. A. Pelletier, J.-M. Basset and F. E. Kühn, *ChemCatChem*, 2013, **5**, 1321–1324.
193 B. Dutta, J. Sofack-Kreutzer, A. A. Ghani, V. D'Elia, J. D. A. Pelletier, M. Cokoja, F. E. Kühn and J.-M. Basset, *Catal. Sci. Technol.*, 2014, **4**, 1534–1538.
194 F. Cavani and N. Ballarini, *Modern Heterogeneous Oxidation Catalysis: Design, Reactions and Characterization*, ed. N. Mizuno, Wiley, Weimhein, 2009, pp. 289–331.
195 R. Prins, A. Wang and X. Li, *Introduction to Heterogeneous Catalysis*, World Scientific Publishing, London, 2016, pp. 269–302.
196 F. Cavani and J. H. Teles, *ChemSusChem*, 2009, **2**, 508–534.
197 A. Gavriilidis, A. Constantinou, K. Hellgardt, K. K. Hii, G. J. Hutchings, G. L. Brett, S. Kuhn and S. P. Marsden, *React. Chem. Eng.*, 2016, **1**, 595–612.
198 R. Noyori, M. Aoki and K. Sato, *Chem. Commun.*, 2003, 1977–1986.
199 I. Carra, E. Ortega-Gómez, L. Santos-Juanes, J. L. Casas López and J. A. Sánchez Pérez, *Chem. Eng. J.*, 2013, **224**, 75–81.
200 S. Albonetti, L. Dal Pozzo and F. Trifirò, *Eurasian Chem.-Technol. J.*, 2017, **3**, 221.
201 J.-M. Brégeault, *Dalton Trans.*, 2003, 3289–3302.
202 C. W. Jones, *Applications of Hydrogen Peroxide and Derivatives*, Royal Society of Chemistry, London, 2007, pp. 65–72.
203 R. A. Sheldon and J. K. Kochi, *Metal-Catalyzed Oxidations of Organic Compounds, Mechanistic Principles and Synthetic Methodology Including Biochemical Processes*, Academic Press, London, 1981.
204 T. Tatsumi, M. Nakamura, S. Negishi and H.-o. Tominaga, *J. Chem. Soc., Chem. Commun.*, 1990, 476–477.
205 B. Notari, in *Adv. Catal.*, ed. D. D. Eley, W. O. Haag and B. Gates, Academic Press, San Diego (USA), 1996, vol. 41, pp. 253–334.
206 M. Clerici and P. Ingallina, *J. Catal.*, 1993, **140**, 71–83.
207 G. Bellussi and M. S. Rigutto, *Stud. Surf. Sci. Catal.*, 1994, **85**, 177–213.
208 P. Ratnasamy, D. Srinivas and H. Knözinger, *Adv. Catal.*, 2004, **48**, 1–169.
209 M. A. Mantegazza, A. Cesana and M. Pastori, *Top. Catal.*, 1996, **3**, 327–335.
210 T. Lu, J. Zou, Y. Zhan, X. Yang, Y. Wen, X. Wang, L. Zhou and J. Xu, *ACS Catal.*, 2018, **8**, 1287–1296.
211 J. Přech, *Catal. Rev.*, 2018, **60**, 71–131.
212 A. Tullo, *Chem. Eng. News*, 2005, **83**, 7.
213 T. A. Nijhuis, M. Makkee, J. A. Moulijn and B. M. Weckhuysen, *Ind. Eng. Chem. Res.*, 2006, **45**, 3447–3459.
214 M. Fukao and M. Oikawa, EP 1717222 A2, 2006.
215 M. G. Clerici and O. A. Kholdeeva, *Liquid Phase Oxidation via Heterogeneous Catalysis: Organic Synthesis and Industrial Applications*, Wiley, New Jersey, 2013.
216 R. Ugo, R. Psaro, G. M. Zanderighi, J. M. Basset, A. Theolier and A. K. Smith, *Fundamental Research in Homogeneous Catalysis*, ed. M. Tsutsui, Plenum Press, New York, NY, USA, 1979, vol. 3, pp. 579–601.
217 C. Copéret, M. Chabanas, R. Petroff Saint-Arroman and J.-M. Basset, *Angew. Chem., Int. Ed.*, 2003, **42**, 156–181.
218 J.-M. Basset, A. Baudouin, F. Bayard, J. Candy, C. Copéret, A. De Mallmann, G. Godard, E. Kuntz, F. Lefebvre, C. Lucas, S. Norsic, K. Pelzer, A. Quadrelli, C. Santini, D. Soulivong, F. Stoffelbach, M. Taoufik, C. Thieuleux, J. Thivolle-Cazat and L. Veyre, in *Modern Surface Organometallic Chemistry*, ed. R. P. J.-M. Basset, D. Roberto and R. Ugo, Wiley-VCH Verlag GmbH & Co KGaA, Weinheim, 2009, ch. 3, pp. 75–136.
219 F. Rascón, R. Wischert and C. Copéret, *Chem. Sci.*, 2011, **2**, 1449–1456.
220 Z. Shan, E. Gianotti, J. C. Jansen, J. A. Peters, L. Marchese and T. Maschmeyer, *Chem. – Eur. J.*, 2001, **7**, 1437–1443.
221 Z. Shan, J. C. Jansen, L. Marchese and T. Maschmeyer, *Microporous Mesoporous Mater.*, 2001, **48**, 181–187.
222 S. Gupta, C. P. Vinod and D. Jagadeesan, *RSC Adv.*, 2015, **5**, 92371–92377.
223 J. Chen, W. Fu, X. Yuan, H. Zeng and J. Wu, *Catal. Lett.*, 2017, **147**, 1263–1270.
224 M. Hamdy, O. Berg, J. Jansen, T. Maschmeyer, A. Arafat, J. Moulijn and G. Mul, *Catal. Today*, 2006, **117**, 337–342.
225 M. S. Hamdy and G. Mul, *Catal. Sci. Technol.*, 2012, **2**, 1894–1900.
226 Q. Yuan, A. Hagen and F. Roessner, *Appl. Catal., A*, 2006, **303**, 81–87.
227 W. S. Ahn, D. H. Lee, T. J. Kim, J. H. Kim, G. Seo and R. Ryoo, *Appl. Catal., A*, 1999, **181**, 39–49.
228 D. Shen, J. Liu, L. Gan, N. Huang and M. Long, *RSC Adv.*, 2017, **7**, 19237–19242.
229 Y.-C. Lin, C.-C. Chang, K.-H. Sung, J. F. Lee and S. Cheng, *Microporous Mesoporous Mater.*, 2018, **272**, 276–285.
230 S. Srinivasan, *J. Catal.*, 1994, **145**, 565–573.
231 A. O. Bouh, G. L. Rice and S. L. Scott, *J. Am. Chem. Soc.*, 1999, **121**, 7201–7210.
232 A. Tuel, *Microporous Mesoporous Mater.*, 1999, **27**, 151–169.
233 M. S. Morey, S. O'Brien, S. Schwarz and G. D. Stucky, *Chem. Mater.*, 2000, **12**, 898–911.
234 J. M. Fraile, J. I. García, J. A. Mayoral and E. Vispe, *J. Catal.*, 2000, **189**, 40–51.

235 Y. C. Hsu, C. Y. Tseng, P. S. Wu and H. C. Tsai, *US Pat.*, 15/218710, 2018.
236 P. Ferreira, I. S. Gonçalves, F. E. Kühn, M. Pillinger, J. Rocha, A. M. Santos and A. Thursfield, *Eur. J. Inorg. Chem.*, 2000, 551–557.
237 Y. Pérez, D. P. Quintanilla, M. Fajardo, I. Sierra and I. del Hierro, *J. Mol. Catal. A: Chem.*, 2007, **271**, 227–237.
238 J. M. Notestein, E. Iglesia and A. Katz, *J. Am. Chem. Soc.*, 2004, **126**, 16478–16486.
239 J. M. Notestein, L. R. Andrini, F. G. Requejo, A. Katz and E. Iglesia, *J. Am. Chem. Soc.*, 2007, **129**, 15585–15595.
240 Y. Guo, A. Solovyov, N. A. Grosso-Giordano, S.-J. Hwang and A. Katz, *ACS Catal.*, 2016, **6**, 7760–7768.
241 J. Jarupatrakorn and T. D. Tilley, *J. Am. Chem. Soc.*, 2002, **124**, 8380–8388.
242 K. L. Fujdala and T. D. Tilley, *J. Catal.*, 2003, **216**, 265–275.
243 I. Drake, K. Fujdala, A. Bell and T. Tilley, *J. Catal.*, 2005, **230**, 14–27.
244 A. T. Bell, *Science*, 2003, **299**, 1688–1691.
245 R. A. Sheldon and H. van Bekkum, in *Fine Chemicals through Heterogeneous Catalysis*, Wiley-VCH, Weimhein, 2007, ch. 9, pp. 473–551.
246 M. G. Clerici, Presented in part at the DGMK/SCI conference, Oxidation and functionalization: classical and alternative routes and sources, October 12-14 Milan, Italy, 2005.
247 O. A. Kholdeeva, I. D. Ivanchikova, N. V. Maksimchuk and I. Y. Skobelev, *Catal. Today*, 2018, DOI: 10.1016/j.cattod.2018.04.002.
248 P. Jiménez-Lozano, I. Y. Skobelev, O. A. Kholdeeva, J. M. Poblet and J. J. Carbó, *Inorg. Chem.*, 2016, **55**, 6080–6084.
249 M. Fujiwara, H. Wessel, P. Hyung-Suh and H. W. Roesky, *Tetrahedron*, 2002, **58**, 239–243.
250 V. Dal Santo, M. Guidotti, R. Psaro, L. Marchese, F. Carniato and C. Bisio, *Proc. R. Soc. A*, 2012, **468**, 1904–1926.
251 J. M. Fraile, J. I. García, J. A. Mayoral and E. Vispe, *J. Catal.*, 2001, **204**, 146–156.
252 F. Quignard, A. Choplin and R. Teissier, *J. Mol. Catal. A: Chem.*, 1997, **120**, L27–L31.
253 C. Cativiela, J. Fraile, J. García and J. Mayoral, *J. Mol. Catal. A: Chem.*, 1996, **112**, 259–267.
254 J. M. Fraile, J. I. García, J. A. Mayoral and E. Vispe, *Appl. Catal., A*, 2003, **245**, 363–376.
255 M. Fadhli, I. Khedher and J. M. Fraile, *C. R. Chim*, 2017, **20**, 827–832.
256 M. Fadhli, I. Khedher and J. M. Fraile, *J. Mol. Catal. A: Chem.*, 2016, **420**, 282–289.
257 T. Maschmeyer, F. Rey, G. Sankar and J. M. Thomas, *Nature*, 1995, **378**, 159.
258 R. D. Oldroyd, J. M. Thomas, T. Maschmeyer, P. A. MacFaul, D. W. Snelgrove, K. U. Ingold and D. D. M. Wayner, *Angew. Chem., Int. Ed.*, 1996, **35**, 2787–2790.
259 M. Guidotti, C. Pirovano, N. Ravasio, B. Lazaro, J. M. Fraile, J. A. Mayoral, B. Coq and A. Galarneau, *Green Chem.*, 2009, **11**, 1421–1427.
260 L. Y. Chen, G. K. Chuah and S. Jaenicke, *Catal. Lett.*, 1998, **50**, 107–114.
261 M. Guidotti, N. Ravasio, R. Psaro, E. Gianotti, S. Coluccia and L. Marchese, *J. Mol. Catal. A: Chem.*, 2006, **250**, 218–225.
262 C. Berlini, M. Guidotti, G. Moretti, R. Psaro and N. Ravasio, *Catal. Today*, 2000, **60**, 219–225.
263 M. Guidotti, L. Conti, A. Fusi, N. Ravasio and R. Psaro, *J. Mol. Catal. A: Chem.*, 2002, (182–183), 151–156.
264 M. Fukuda, N. Tsunoji, Y. Yagenji, Y. Ide, S. Hayakawa, M. Sadakane and T. Sano, *J. Mater. Chem. A*, 2015, **3**, 15280–15291.
265 J. M. Fraile, J. I. García, J. A. Mayoral and E. Vispe, *Appl. Catal., A*, 2004, **276**, 113–122.
266 C. Palumbo, C. Tiozzo, N. Ravasio, R. Psaro, F. Carniato, C. Bisio and M. Guidotti, *Catal. Sci. Technol.*, 2016, **6**, 3832–3839.
267 V. Smeets, L. Ben Mustapha, J. Schnee, E. M. Gaigneaux and D. P. Debecker, *Mol. Catal.*, 2018, **452**, 123–128.
268 M. Guidotti, N. Ravasio, R. Psaro, E. Gianotti, L. Marchese and S. Coluccia, *Green Chem.*, 2003, **5**, 421–424.
269 E. Gianotti, C. Bisio, L. Marchese, M. Guidotti, N. Ravasio, R. Psaro and S. Coluccia, *J. Phys. Chem. C*, 2007, **111**, 5083–5089.
270 M. Guidotti, R. Psaro, N. Ravasio, M. Sgobba, E. Gianotti and S. Grinberg, *Catal. Lett.*, 2008, **122**, 53–56.
271 J. Vernimmen, M. Guidotti, J. Silvestre-Albero, E. O. Jardim, M. Mertens, O. I. Lebedev, G. Van Tendeloo, R. Psaro, F. Rodríguez-Reinoso, V. Meynen and P. Cool, *Langmuir*, 2011, **27**, 3618–3625.
272 N. E. Thornburg, A. B. Thompson and J. M. Notestein, *ACS Catal.*, 2015, **5**, 5077–5088.
273 D. T. Bregante, N. E. Thornburg, J. M. Notestein and D. W. Flaherty, *ACS Catal.*, 2018, **8**, 2995–3010.
274 T. R. Eaton, A. M. Boston, A. B. Thompson, K. A. Gray and J. M. Notestein, *ChemCatChem*, 2014, **6**, 3215–3222.
275 I. J. Shannon, T. Maschmeyer, R. D. Oldroyd, G. Sankar, J. M. Thomas, H. Pernot, J.-P. Balikdjian and M. Che, *J. Chem. Soc., Faraday Trans.*, 1998, **94**, 1495–1499.
276 J. M. Thomas and R. Raja, *Stud. Surf. Sci. Catal.*, 2004, **148**, 163–211.
277 A. Sakthivel, J. Zhao and F. E. Kühn, *Catal. Lett.*, 2005, **102**, 115–119.
278 A. Ramanathan and B. Subramaniam, *Molecules*, 2018, **23**, 263.
279 N. Morlanés and J. M. Notestein, *J. Catal.*, 2010, **275**, 191–201.
280 N. E. Thornburg, S. L. Nauert, A. B. Thompson and J. M. Notestein, *ACS Catal.*, 2016, **6**, 6124–6134.
281 R. L. Brutchey, C. G. Lugmair, L. O. Schebaum and T. D. Tilley, *J. Catal.*, 2005, **229**, 72–81.
282 D. A. Ruddy and T. D. Tilley, *Chem. Commun.*, 2007, 3350–3352.
283 D. A. Ruddy and T. D. Tilley, *J. Am. Chem. Soc.*, 2008, **130**, 11088–11096.
284 P. J. Cordeiro and T. D. Tilley, *Langmuir*, 2011, **27**, 6295–6304.
285 J. Jarupatrakorn, M. P. Coles and T. D. Tilley, *Chem. Mater.*, 2005, **17**, 1818–1828.

286 Q. Yang, C. Coperet, C. Li and J.-M. Basset, *New J. Chem.*, 2003, **27**, 319–323.
287 C. Nozaki, C. G. Lugmair, A. T. Bell and T. D. Tilley, *J. Am. Chem. Soc.*, 2002, **124**, 13194–13203.
288 C. Roukoss, S. Fiddy, A. de Mallmann, N. Rendon, J.-M. Basset, E. Kuntz and C. Coperet, *Dalton Trans.*, 2007, 5546–5548.
289 K. L. Fujdala, R. L. Brutchey and T. D. Tilley, in *Topics in Organometallic Chemistry*, ed. C. Coperet and B. Chaudret, Springer-Verlag, New York, 2005, vol. 16, pp. 69–116.
290 P. Guillo, M. I. Lipschutz, M. E. Fasulo and T. D. Tilley, *ACS Catal.*, 2017, 7, 2303–2312.
291 N. Morlanes and J. M. Notestein, *Appl. Catal., A*, 2010, **387**, 45–54.
292 N. E. Thornburg and J. M. Notestein, *ChemCatChem*, 2017, **9**, 3714–3724.
293 C. Tiozzo, C. Bisio, F. Carniato, A. Gallo, S. L. Scott, R. Psaro and M. Guidotti, *Phys. Chem. Chem. Phys.*, 2013, **15**, 13354–13362.
294 A. Gallo, C. Tiozzo, R. Psaro, F. Carniato and M. Guidotti, *J. Catal.*, 2013, **298**, 77–83.
295 R. Turco, R. Vitiello, R. Tesser, A. Vergara, S. Andini and M. Di Serio, *Top. Catal.*, 2017, **60**, 1054–1061.
296 S. Dworakowska, C. Tiozzo, M. Niemczyk-Wrzeszcz, P. Michorczyk, N. Ravasio, R. Psaro, D. Bogdał and M. Guidotti, *J. Cleaner Prod.*, 2017, **166**, 901–909.
297 C. Tiozzo, C. Bisio, F. Carniato and M. Guidotti, *Catal. Today*, 2014, **235**, 49–57.
298 I. D. Ivanchikova, I. Y. Skobelev, N. V. Maksimchuk, E. A. Paukshtis, M. V. Shashkov and O. A. Kholdeeva, *J. Catal.*, 2017, **356**, 85–99.
299 M. Boronat, P. Concepción, A. Corma and M. Renz, *Catal. Today*, 2007, **121**, 39–44.
300 T. Blasco, M. A. Camblor, A. Corma, P. Esteve, J. M. Guil, A. Martínez, J. A. Perdigón-Melón and S. Valencia, *J. Phys. Chem. B*, 1998, **102**, 75–88.
301 A. Corma, L. T. Nemeth, M. Renz and S. Valencia, *Nature*, 2001, **412**, 423–425.
302 F.-F. Guan, T.-T. Ma, X. Yuan, H.-Y. Zeng and J. Wu, *Catal. Lett.*, 2018, **148**, 443–453.
303 A. Corma, M. a. T. Navarro and M. Renz, *J. Catal.*, 2003, **219**, 242–246.
304 A. Corma, S. Iborra, M. A. Mifsud and M. Renz, *ARKIVOC*, 2005, 124–132.
305 M. Boronat, P. Concepcion, A. Corma, M. T. Navarro, M. Renz and S. Valencia, *Phys. Chem. Chem. Phys.*, 2009, **11**, 2876–2884.
306 J. Přech, M. A. Carretero and J. Čejka, *ChemCatChem*, 2017, **9**, 3063–3072.
307 R. P. Saint-Arroman, B. Didillon, A. de Mallmann, J. M. Basset and F. Lefebvre, *Appl. Catal., A*, 2008, **337**, 78–85.
308 E. Spier, U. Neuenschwander and I. Hermans, *Angew. Chem., Int. Ed.*, 2013, **52**, 1581–1585.
309 M. S. Hamdy, A. Ramanathan, T. Maschmeyer, U. Hanefeld and J. C. Jansen, *Chem. – Eur. J.*, 2006, **12**, 1782–1789.
310 I. Hermans, P. A. Jacobs and J. Peeters, *J. Mol. Catal. A: Chem.*, 2006, **251**, 221–228.
311 I. Hermans, T. L. Nguyen, P. A. Jacobs and J. Peeters, *ChemPhysChem*, 2005, **6**, 637–645.
312 J. D. Chen, J. Dakka and R. A. Sheldon, *Appl. Catal., A*, 1994, **108**, L1–L6.
313 R. P. Saint-Arroman, J.-M. Basset, F. Lefebvre and B. Didillon, *Appl. Catal., A*, 2005, **290**, 181–190.
314 Z. Sun, J. Xu, Z. Du and W. Zhang, *Appl. Catal., A*, 2007, **323**, 119–125.
315 B. P. C. Hereijgers, R. F. Parton and B. M. Weckhuysen, *ACS Catal.*, 2011, **1**, 1183–1192.
316 E. Fache, F. Igersheim, D. Bonnet, J. M. Basset, F. Lefebvre and R. P. Saint-Arroman, *PCT Int. Appl.*, WO2002085826 A2, 2002.
317 O. A. Kholdeeva, M. S. Mel'gunov, A. N. Shmakov, N. N. Trukhan, V. V. Kriventsov, V. I. Zaikovskii, M. E. Malyshev and V. N. Romannikov, *Catal. Today*, 2004, **91–92**, 205–209.
318 K. K. Kang and W. S. Ahn, *J. Mol. Catal. A: Chem.*, 2000, **159**, 403–410.
319 N.-K. Kim, G.-J. Kim and W.-S. Ahn, *React. Kinet. Catal. Lett.*, 2000, **71**, 273–279.
320 S. Gontier and A. Tuel, *Appl. Catal., A*, 1996, **143**, 125–135.
321 O. A. Kholdeeva, I. D. Ivanchikova, M. Guidotti and N. Ravasio, *Green Chem.*, 2007, **9**, 731–733.
322 O. A. Kholdeeva, I. D. Ivanchikova, M. Guidotti, C. Pirovano, N. Ravasio, M. V. Barmatova and Y. A. Chesalov, *Adv. Synth. Catal.*, 2009, **351**, 1877–1889.
323 O. A. Kholdeeva, I. D. Ivanchikova, N. V. Maksimchuk, M. S. Mel'gunov, J.-S. Chang, M. Guidotti, A. A. Shutilov and V. I. Zaikovskii, *Top. Catal.*, 2014, **57**, 1377–1384.
324 O. A. Kholdeeva, I. D. Ivanchikova, M. Guidotti, N. Ravasio, M. Sgobba and M. V. Barmatova, *Catal. Today*, 2009, **141**, 330–336.
325 M. Selvaraj, *Catal. Sci. Technol.*, 2014, **4**, 2674–2684.